香港科技大學
THE HONG KONG UNIVERSITY OF SCIENCE AND TECHNOLOGY

Recent Advances in Centrifuge Modelling at HKUST

Charles W.W. Ng

Hong Kong University of Science and Technology (HKUST)

Contents

1. Introduction - International Society for Soil Mechanics and Geotechnical Engineering (ISSMGE)
2. The Geotechnical Centrifuge Facility at HKUST
3. Forensic engineering – the collapse of 13-storey building in Shanghai, China
4. 3D interaction between multiple tunnels of different shapes (horse-shoe shaped versus circular tunnels) using “donuts”
5. The serviceability of energy piles in clay and sand
6. The impact mechanisms and performance of barriers subject to debris flows
7. The effects of root geometry on slope stability
8. Future developments in HKUST

International Society for Soil Mechanics and Geotechnical Engineering (ISSMGE)

www.issmge.org

1936 - First Int. Conf., USA (20 countries, 206 delegates)

Terzaghi is the first President

1957 - ISSMGE is more formally organized (Skempton)

2019 – 92 member societies and 20,000 individual members (the largest geo-related society in the world)

ISSMGE Presidents

1936–1957	K. Terzaghi	Austria, USA
1957–1961	A. W. Skempton	UK
1961–1965	A. Casagrande	USA, Austria
1965–1969	L. Bjerrum	Norway
1969–1973	R. B. Peck	USA
1973–1977	J. Kerisel	France
1977–1981	M. Fukuoka	Japan
1981–1985	V. F. B. de Mello	Brazil
1985–1989	B. B. Broms	Sweden
1989–1994	N. R. Morgenstern	Canada
1994–1997	M. Jamiolkowski	Italy
1997–2001	K. Ishihara	Japan
2001-2005	W. Van Impe	Belgium
2005-2009	P.S. Sêco e Pinto	Portugal
2009-2013	J.-L. Briaud	USA
2013-2017	R. Frank	France
2017-2021	Charles Ng	HKSAR

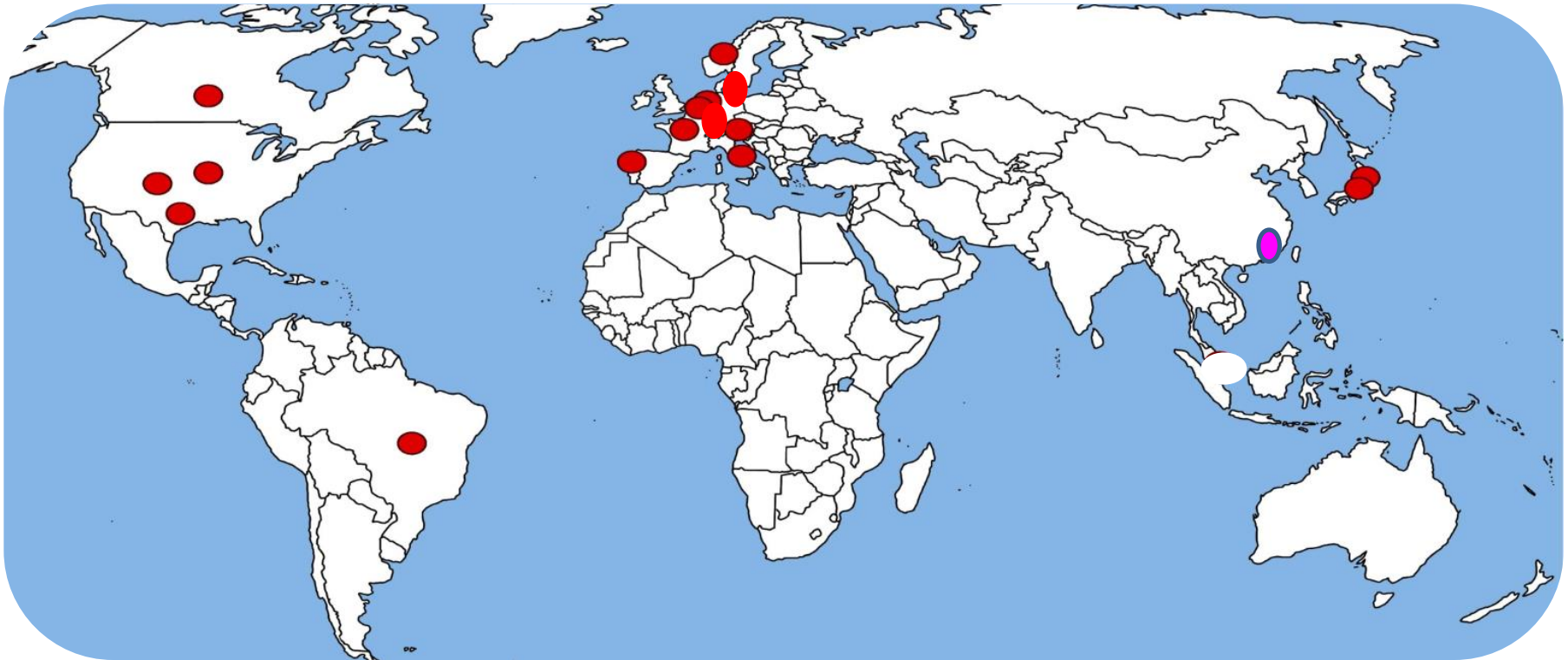

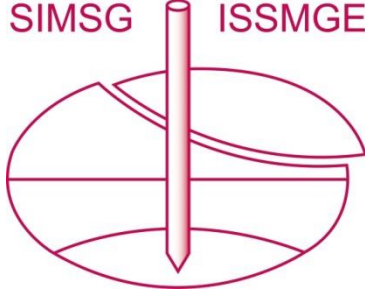

The ISSMGE Board (2017-2021)

ISSMGE President	**Charles W.W. Ng (Hong Kong SAR)**
Immediate Past President ISSMGE	**Roger Frank (France)**
ISSMGE Vice President (Africa)	**Marcelin Kana (Cameroon)**
ISSMGE Vice President (Asia)	**Eun Chul Shin (South Korea)**
ISSMGE Vice President (Australasia)	**Gavin Alexander (New Zealand)**
ISSMGE Vice President (Europe)	**Mario Manassero (Italy)**
ISSMGE Vice-President (North America)	**Timothy Newson (Canada)**
ISSMGE Vice President (South America)	**Alejo Sfriso (Argentina)**
Appointed Board Member	**Mounir Bouassida (Tunisia)**
Appointed Board Member	**Kok Kwang Phoon (Singapore)**
Appointed Board Member	**Pedro Sêco E Pinto (Portugal)**
Secretary General	**R Neil Taylor (UK)**

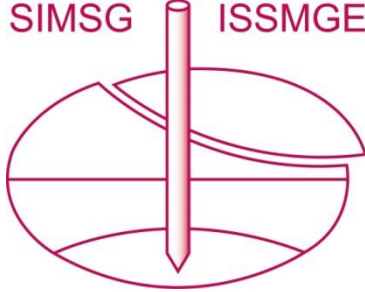

Education, Innovation, Diversity
Éducation, Innovation, Diversité

1. "ISSMGE virtual university" – to provide a series of free online postgraduate courses – 6 new courses formed: Risk-Mitigation, monitoring & Observational methods, In-situ Testing, Earthquake Engineering, Foundations, Soil Characterisation, Unsaturated Soil Mechanics…….more to come
2. "ISSMGE virtual library" – all ISSMGE related publications/ honours lectures/videos etc (e.g., 19th ICSMGE, 7th Unsat2018) and ISSMGE publisher (e.g., ISC'6 in Budapest 2020)
3. New technical committees: TC219 – System Performance of Geotechnical Structures, TC220 – Field Measurement in Geomechanics, TC309 - Machine Learning and Big Data
4. Boasting Corporate Associates to narrow the gap between academics and practioners (4 new CAs + Contractor and Consultant's forum)
5. Reviewing all awards and honours lectures, and promoting more young and upcoming keynote lecturers (more than 8 Bright Spark lectures given)

The Geotechnical Centrifuge Facility at HKUST

The Hong Kong University of Science & Technology (HKUST)

Established in 1991, 4 schools, 9500 UGs and 4300 PGs

Geotechnical group: about 60 PhDs and 20 M.Phil students

East

NE

SW

Young but Globally Recognized

Source	Ranking
QS Top 50 Under 50, 2018	2
Times Higher Education World University Rankings Top 150 Under 50, 2018	1
QS Asian University Rankings, 2018	3
Times Higher Education World University Rankings, 2018 (Engineering & Technology)	18
EMBA program by Financial Times (For 8 years)	1
Global Employability University Ranking, 2018	15

The Geotechnical Centrifuge Facility at Hong Kong University of Science and Technology

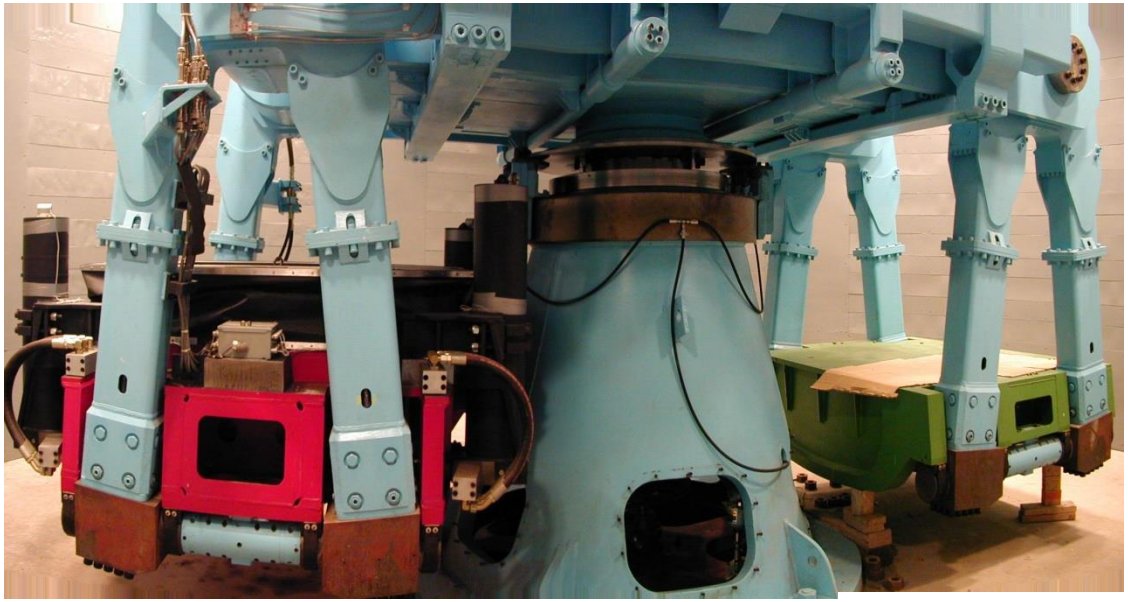

- Diameter: 8.4m
- Maximum g-level: 150g
- Maximum payload: 400g-ton (design)
- Real-time monitoring and viewing via internet
- Operated in 2001

The world first 2D Hydraulic In-flight Shaking Table

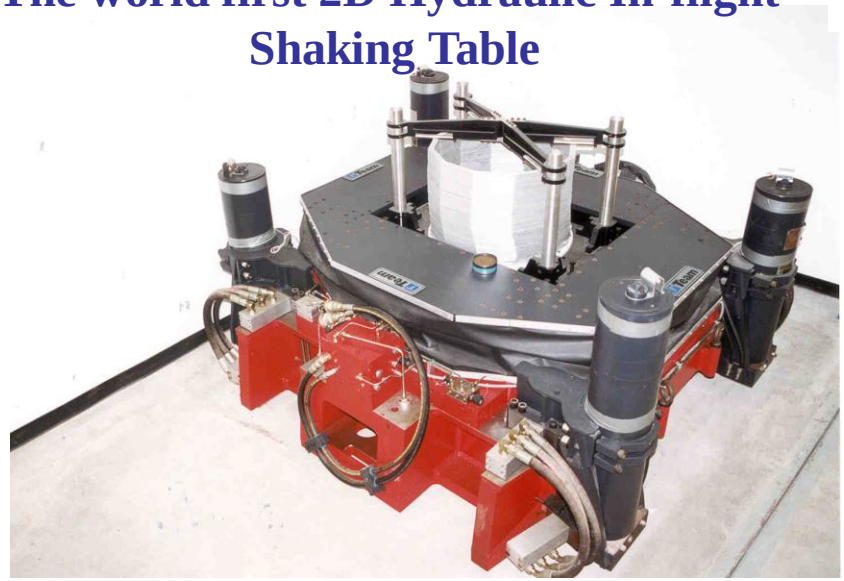

The world 2nd Four-Axis Robotic Manipulator

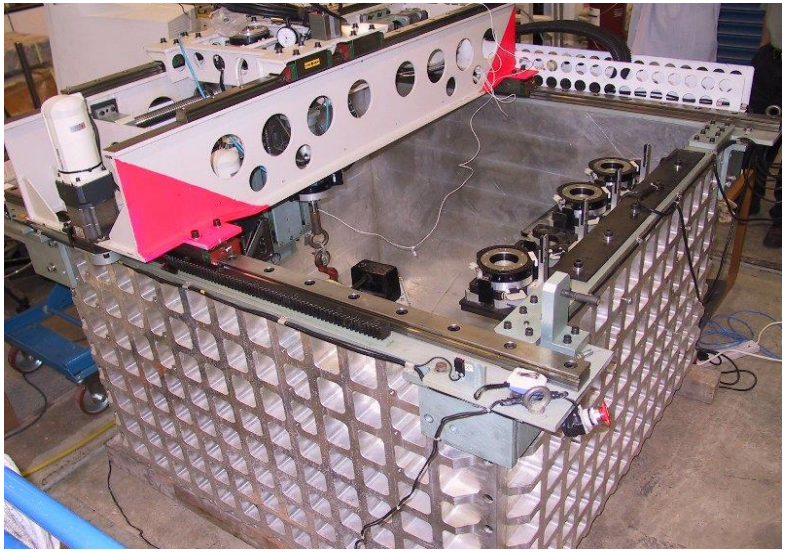

4-axis robotic manipulator and sand hopper

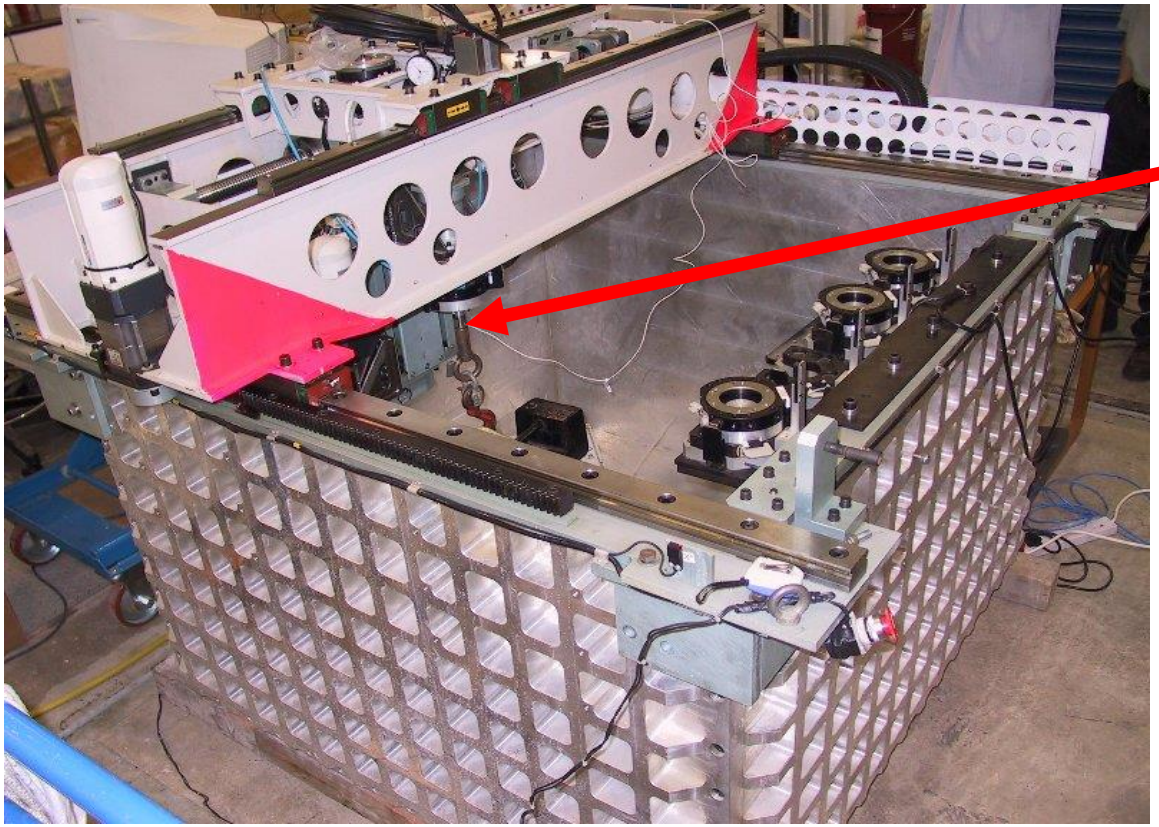

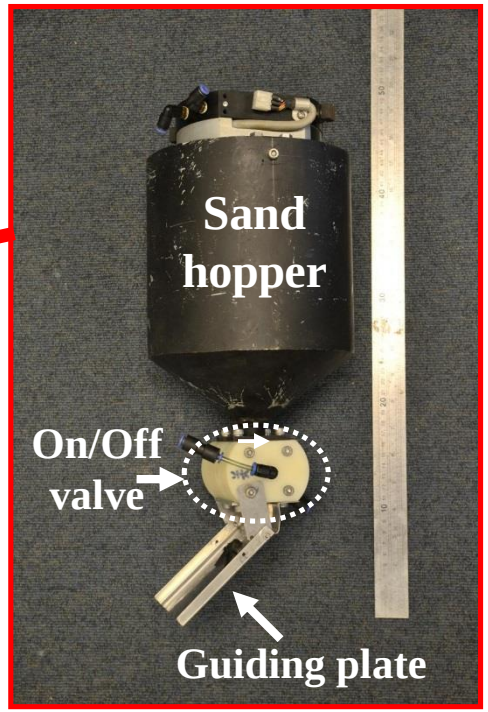

Chinese patent application (invention). **吴宏伟, 洪义** (2014). **用于土工离心机中模**拟高速公**路建造的装置及方法**. (专利申请号为：CN201410745332.2).

In-flight simulation of embankment construction

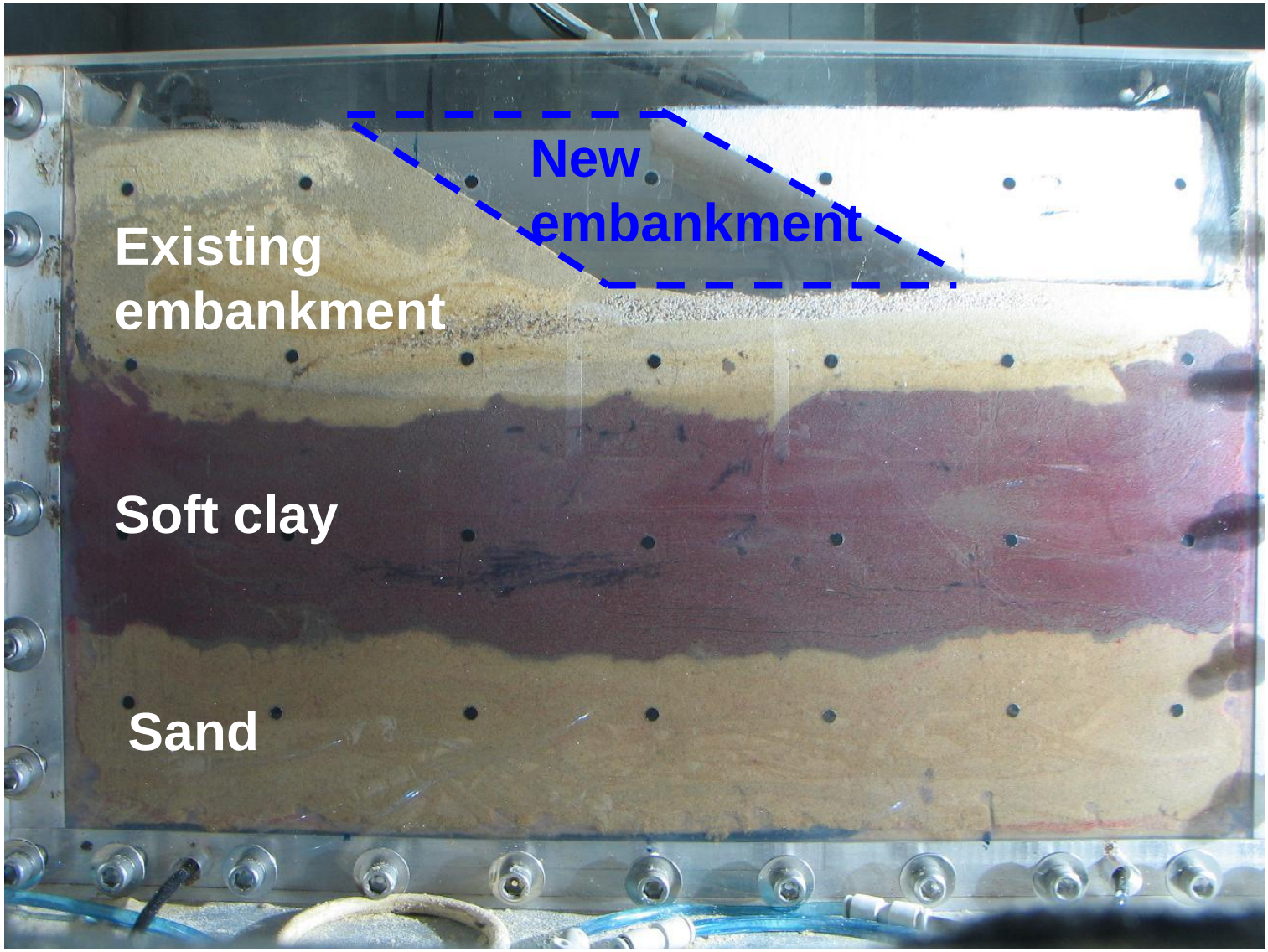

Current research students, RAPs and post-docs (with 17 different nationalities)

Exchange scholarship (PGs): CAN$ 1,700 per month

Scholarships for full-time research student: CAN$ 2,850 - 4,800 per month

Dual PhD degree programmes

Five projects

1. Forensic engineering – the collapse of 13-storey building in Shanghai, China
2. 3D Interaction between multiple tunnels of different shapes (horse-shoe shaped versus circular tunnels) using “donuts”
3. The serviceability of energy piles in clay and sand
4. The impact mechanisms and performance of barriers subject to debris flows
5. The effects of root geometry on slope stability

(i) Forensic Engineering: Collapse of Building in Shanghai

Client: East China Architectural Design & Research Institute Co. Ltd (华东建筑设计研究院) and Shanghai Municipal Government

香港科技大學
THE HONG KONG UNIVERSITY OF SCIENCE AND TECHNOLOGY

On 3rd July 2009 for a 13-Storey Building Collapse in Shanghai

Wang, W.D., Ng, C.W.W., Hong, Y., Hu, Y. & Li, Q. (2019). Forensic study on the collapse of a high-rise building in Shanghai: 3D centrifuge and numerical modelling. *Géotechnique*, https://doi.org/10.1680/jgeot.16.P.315.

Field observations on the collapsed building 7 (Wang *et al*., 2017)

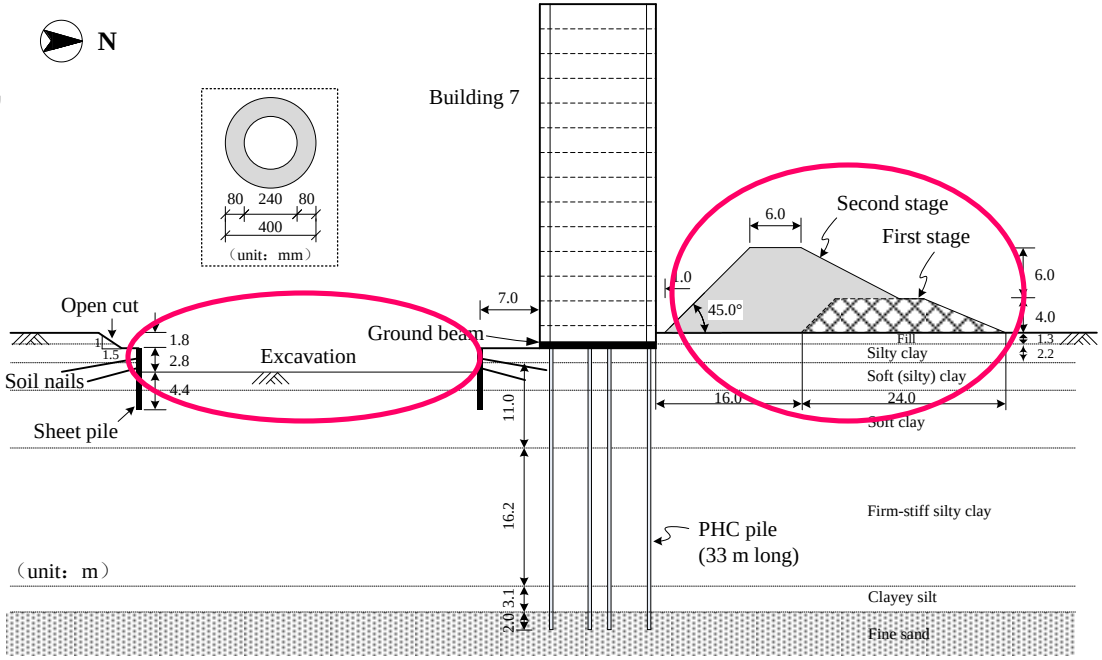

The construction status at the time of the collapse (Wang *et al*., 2017)

Comparisons of field and simulated shear strength cu profiles (prototype)

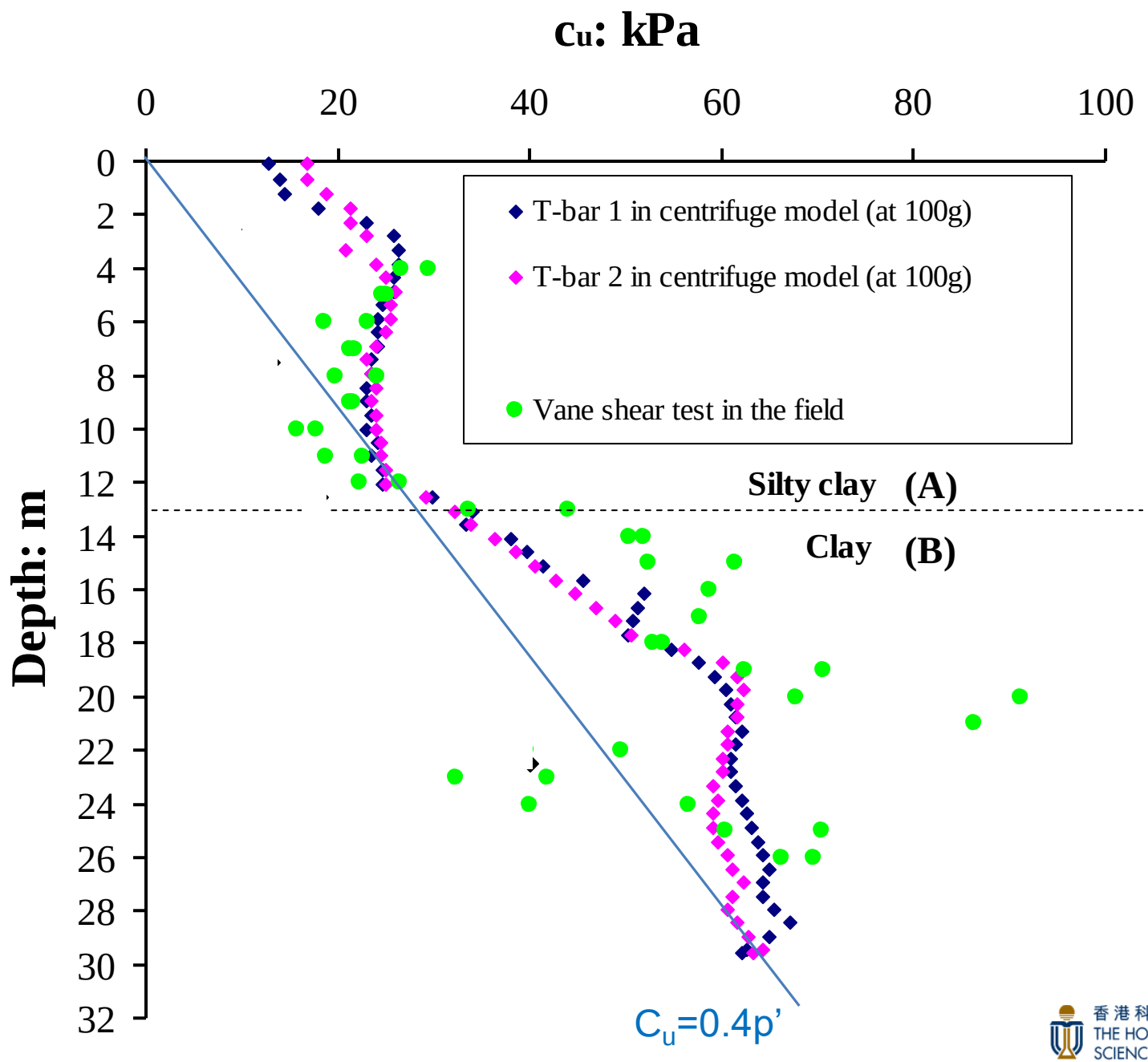

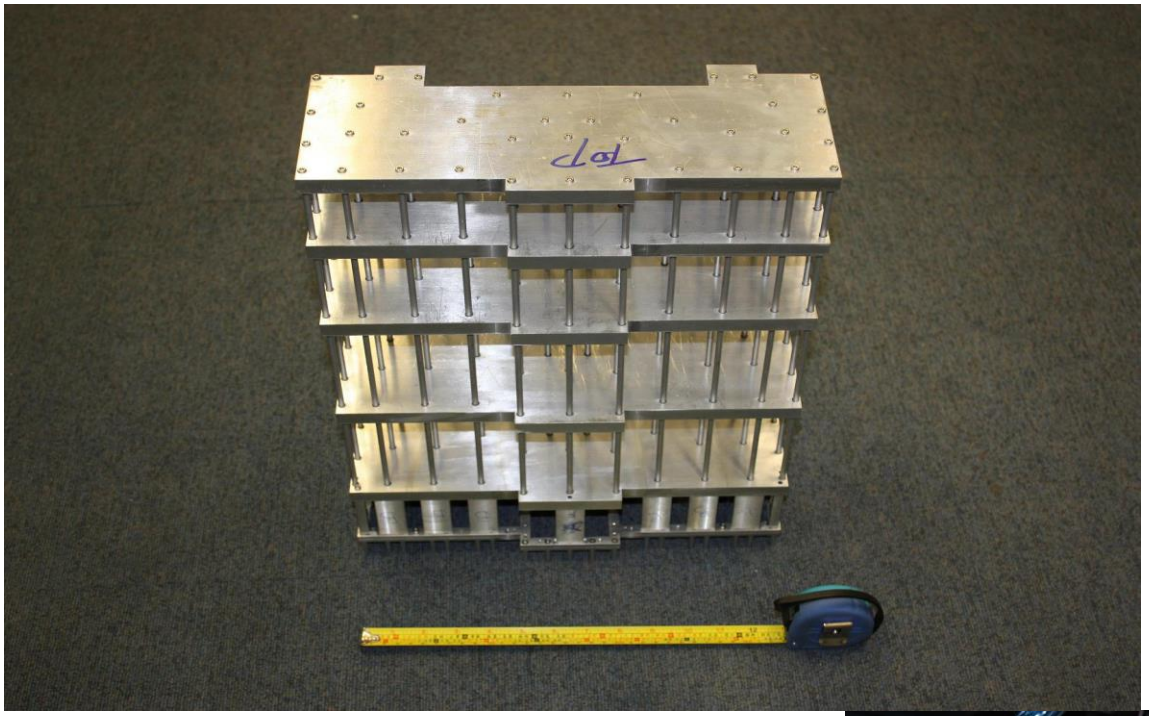

A fully assembled building

Installation of model building

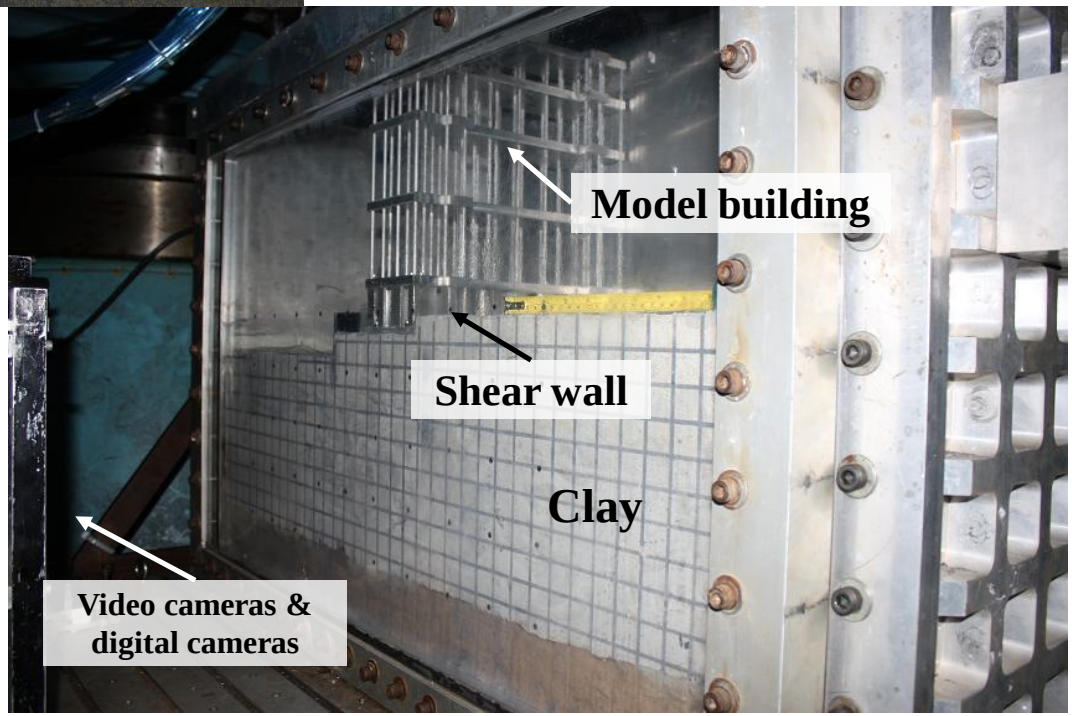

Comparison of model and prototype

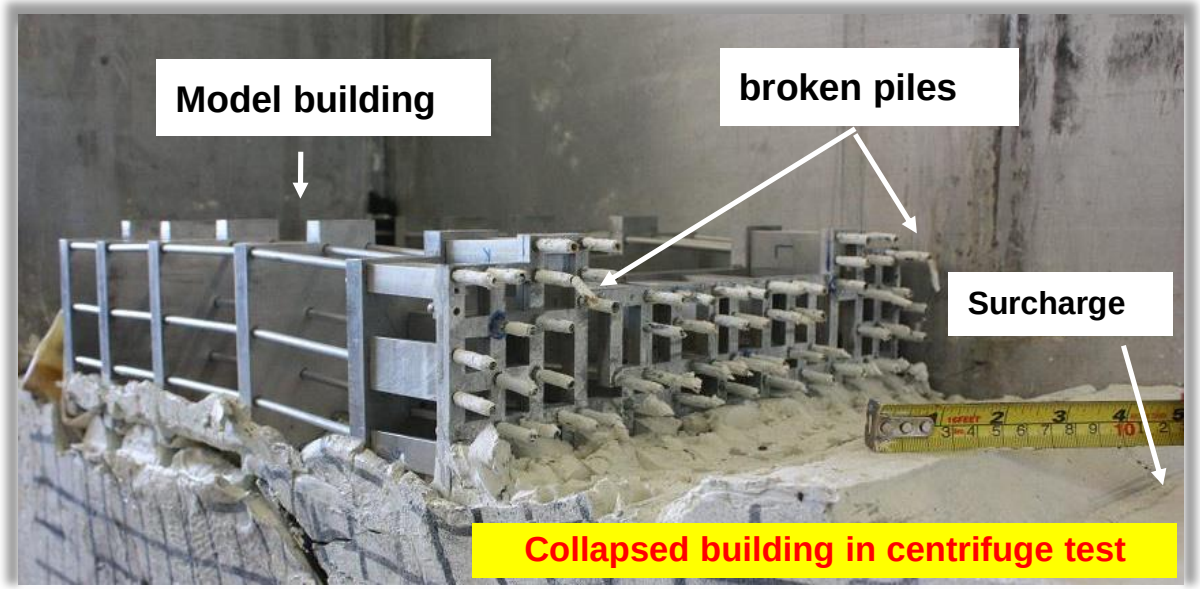

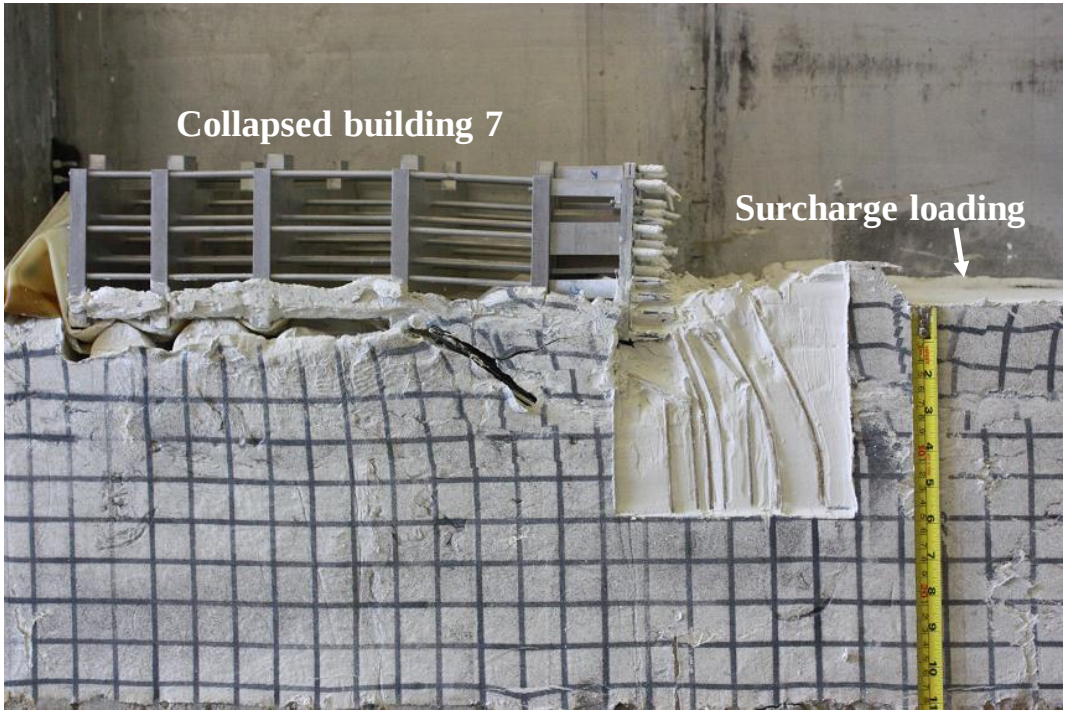
Collapsed building 7
Surcharge loading

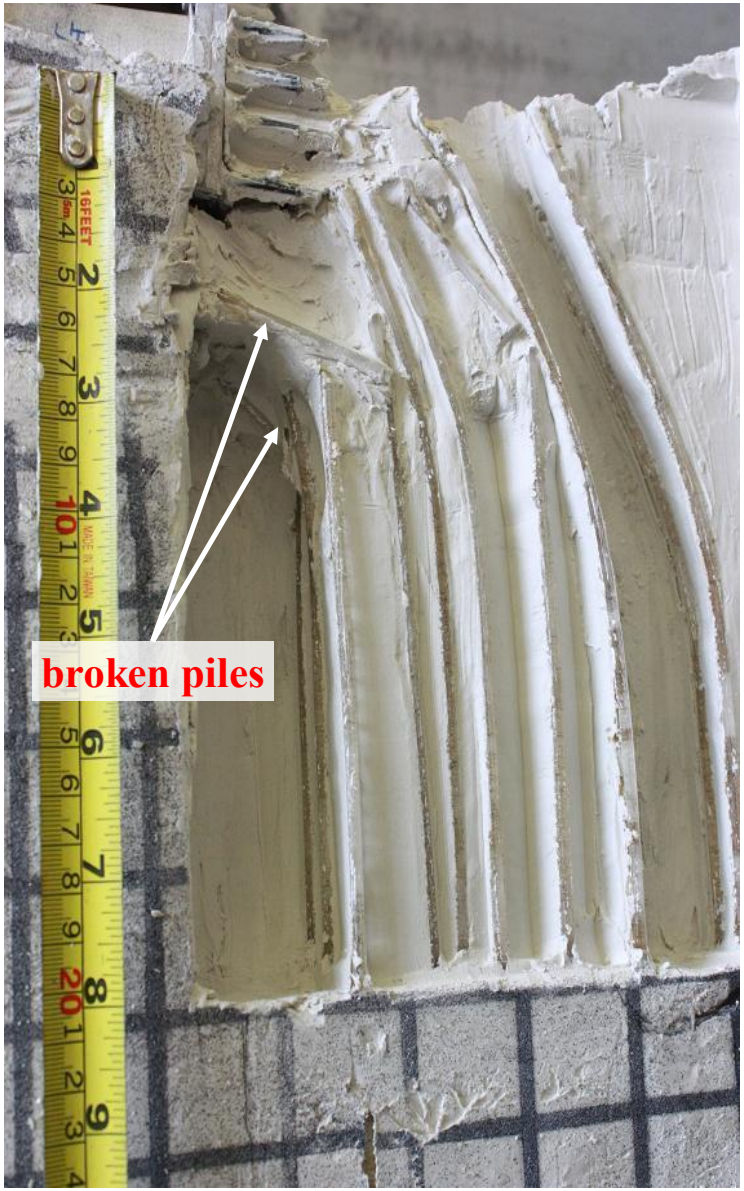
broken piles


Typical broken piles

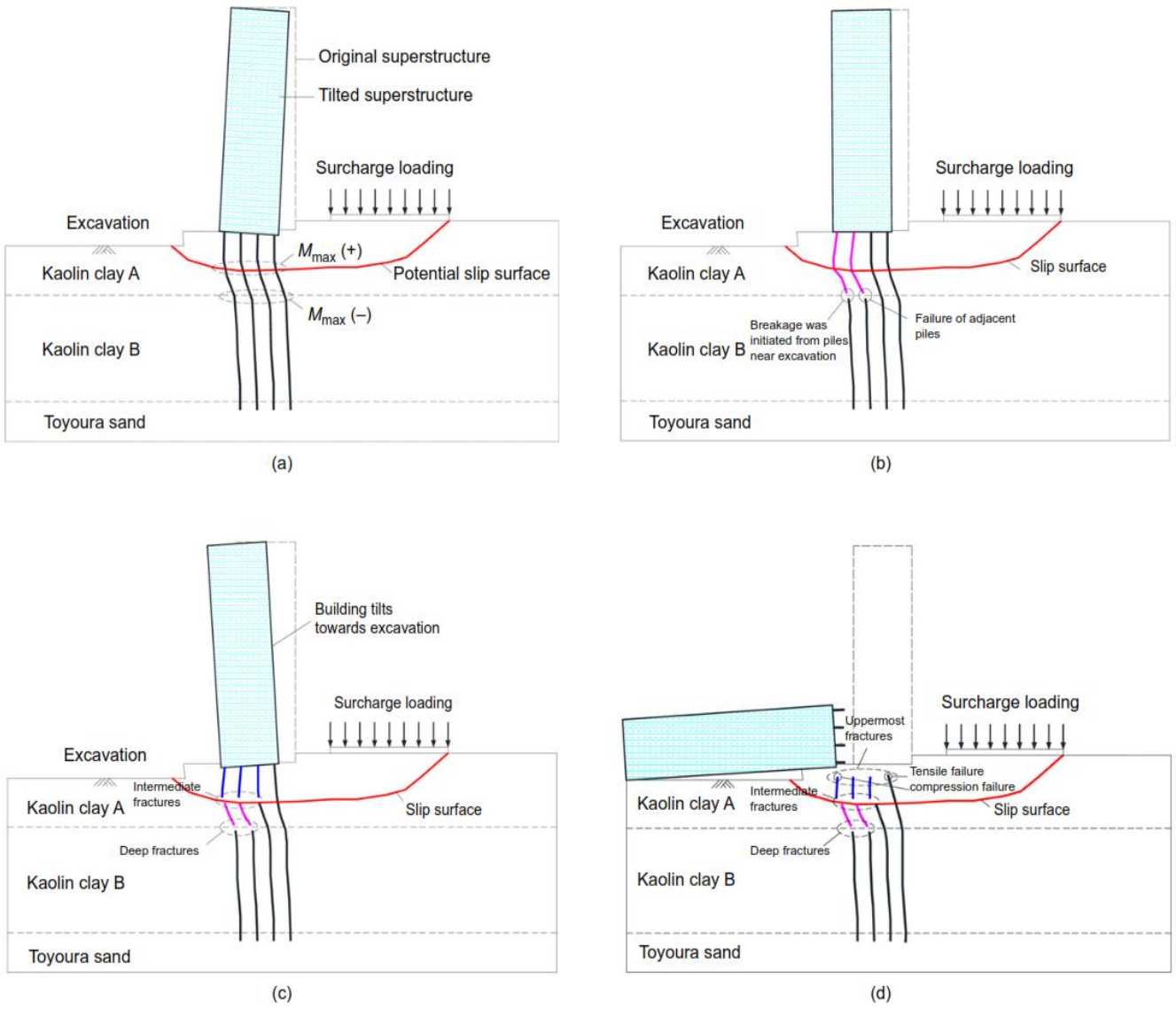

Proposed mechanism: (a) slip surface developed due to surcharge loading; (b) piles broke at inter-layer boundary; (c) piles broke at location of maximum bending moment and building tilted; (d) building collapsed towards excavation (Wang et al., 2019)

(ii) 3D Interaction between multiple tunnels of different shapes (horse-shoe shaped versus circular tunnels) using “donuts”

香港科技大學
THE HONG KONG UNIVERSITY OF SCIENCE AND TECHNOLOGY

Wuhan-Guangzhou high speed railway - Changsha Metro Line 3

- New Changsha Metro Line 3 (twin tunnel) will be constructed undercrossing the existing Liuyang River tunnel.
- Deformation and stress control is vital to ensure the safety and serviceability of Wuhan-Guangzhou high speed railway that inside the Liuyang River tunnel.

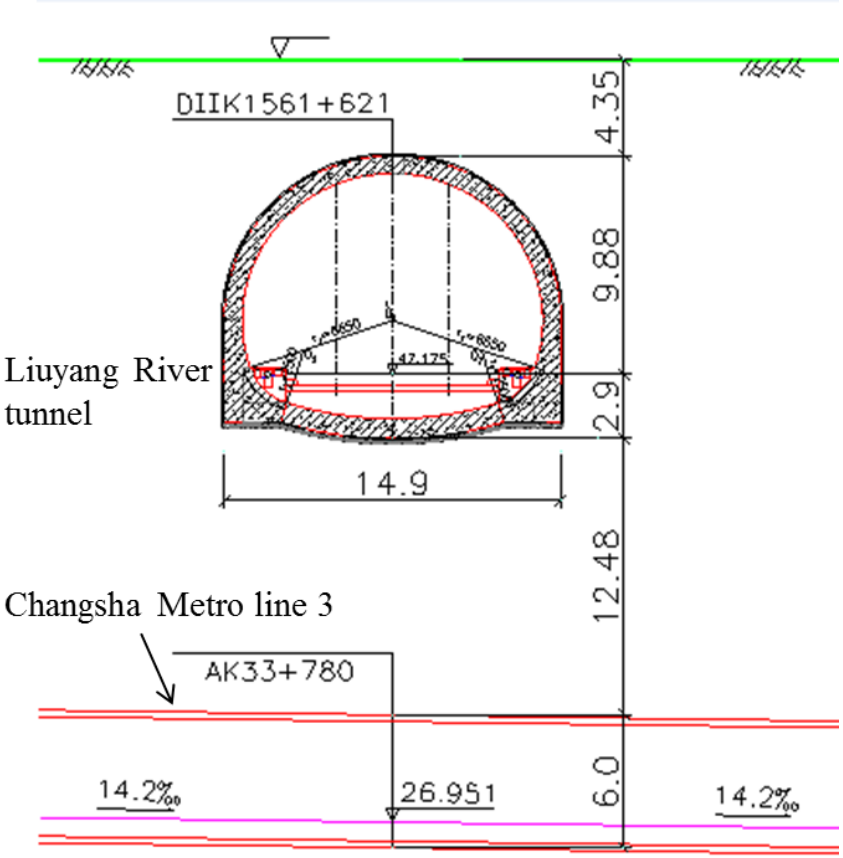

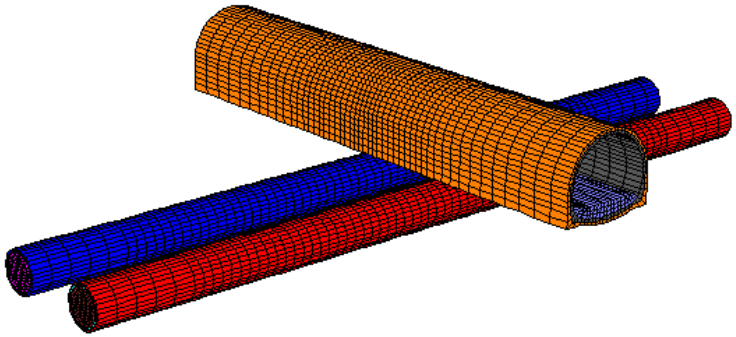

1. Correct horse-shoe shaped tunnel
2. Advancement of twin tunnels three-dimensionally
3. Effects of volume and weight losses

Instrumentation of existing horse-shoe shaped tunnel

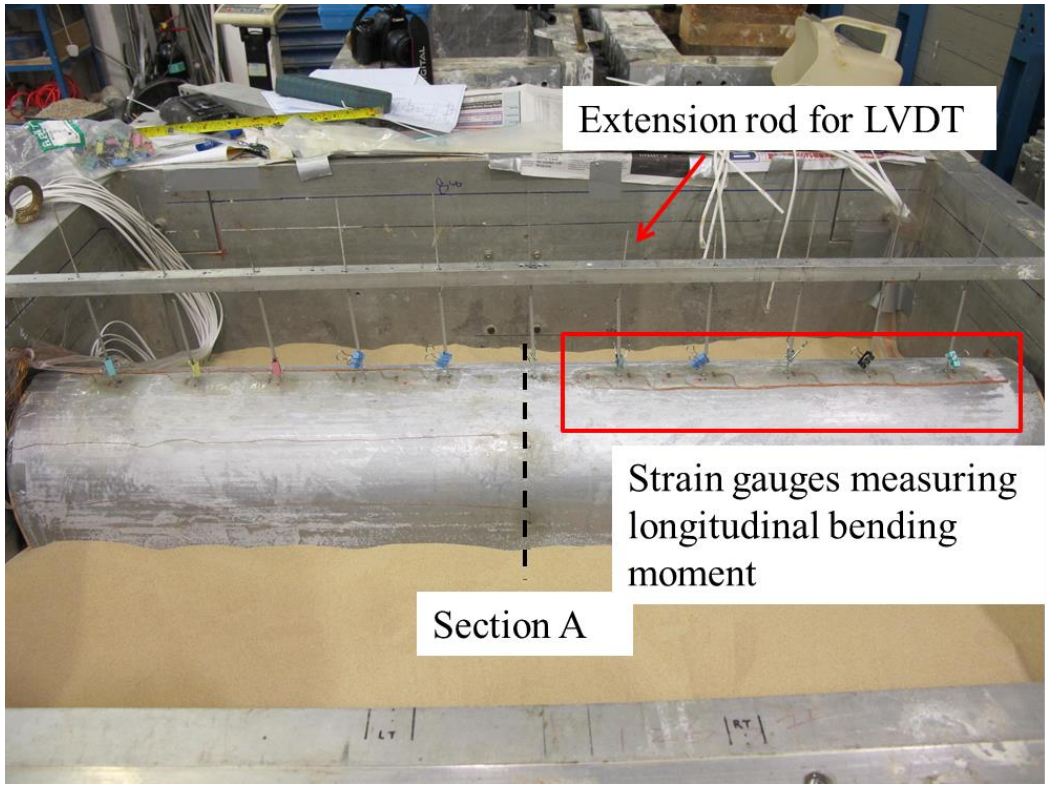

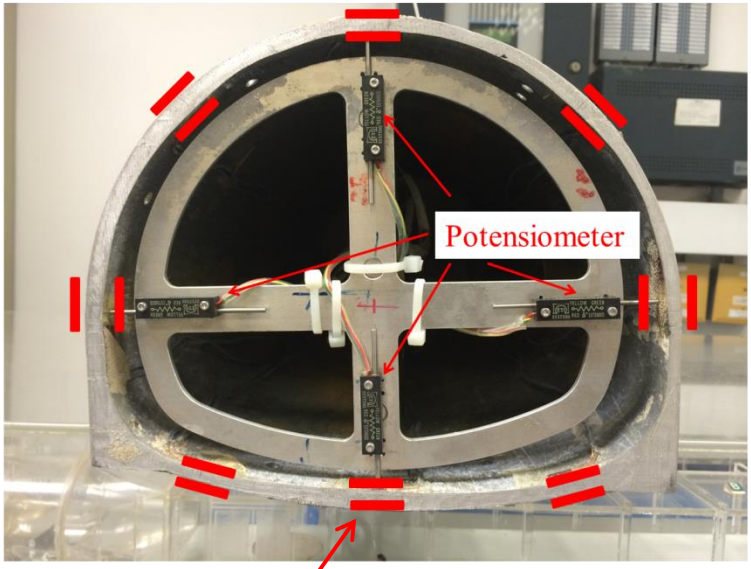

Strain gauges measuring transverse bending moment (every 45°)

Jiang, B., Chen, L., Yang, J.S., Wang, S. & Ng, C.W.W. (2017). Effects of twin-tunnel excavation on an existing horseshoe-shaped tunnel considering the influence of a settlement joint. *Canadian Geotechnical Journal* 54, No. 9, 1346-1355

Modeling of tunnel advancement and advancing sequences

(effects of volume loss (1%, 2%...) and weight loss)

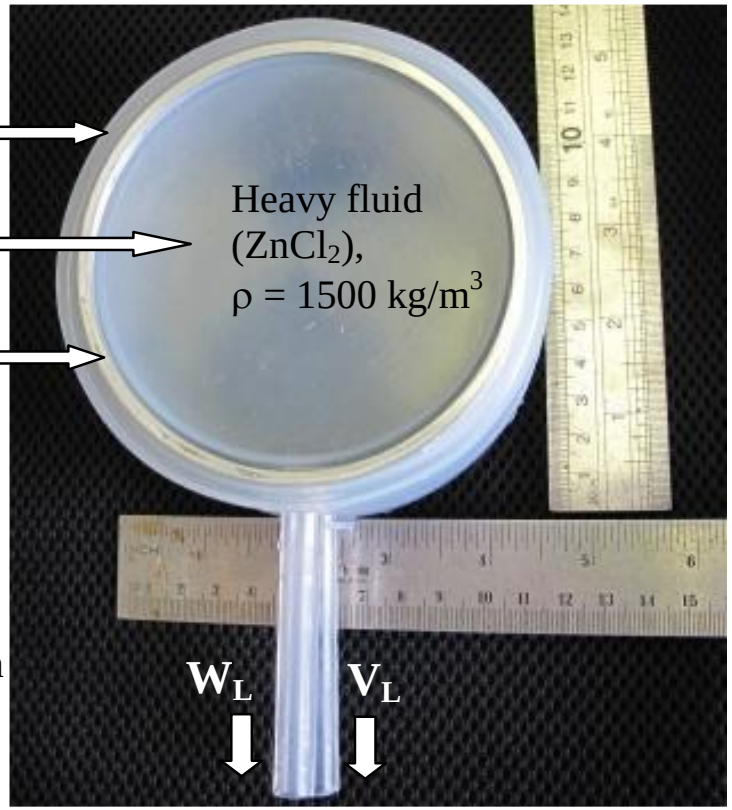

(a) "Donut" for simulating volume loss and weight loss during tunnel advancement

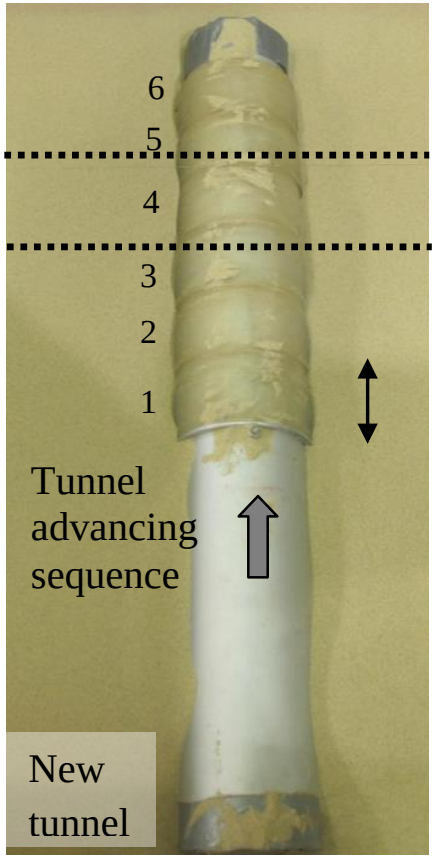

(b) Tunnel advancing sequence in centrifuge

Ng, C.W.W., Boonyarak, T. & Mašín, D. (2015). Effects of pillar depth and shielding on the interaction of crossing multitunnels. *Journal of Geotechnical and Geoenvironmental Engineering* , ASCE, 141, No. 6, 04015021. https://doi.org/10.1061/(ASCE)GT.1943-5606.0001293.

Tunnel excavation sequences of twin tunnels (control volume loss (1%, 2%...) and weight loss)

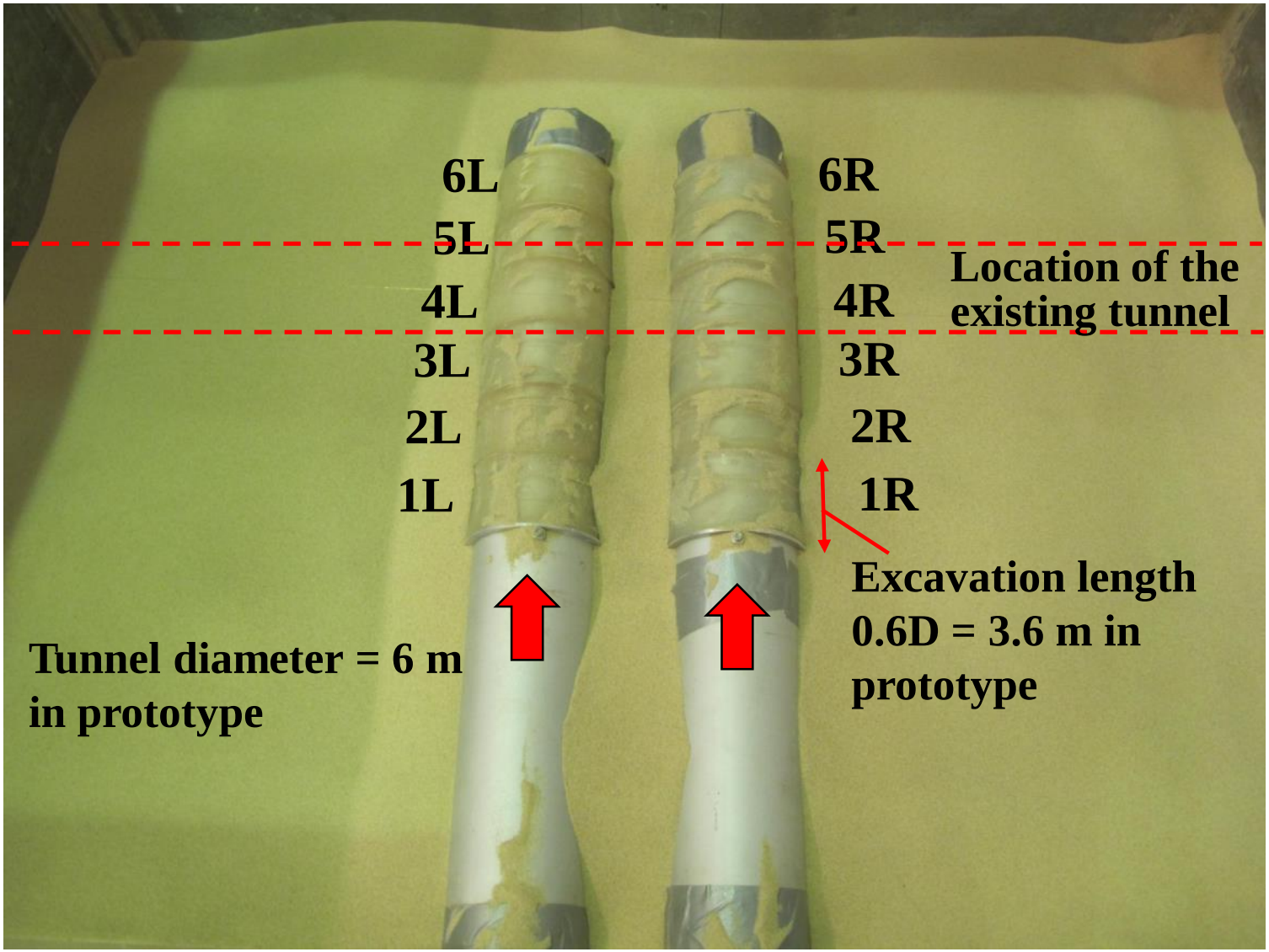

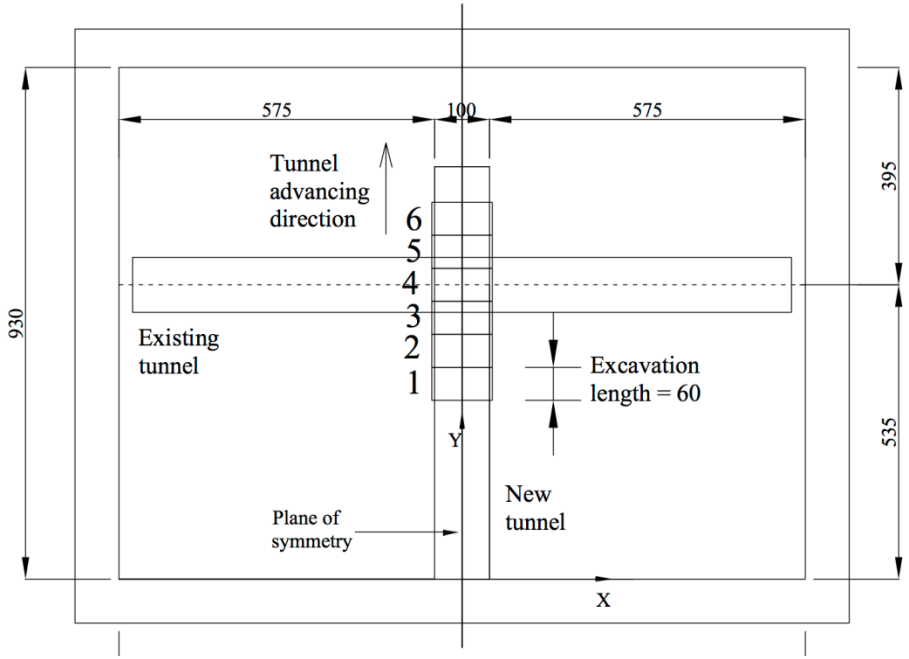

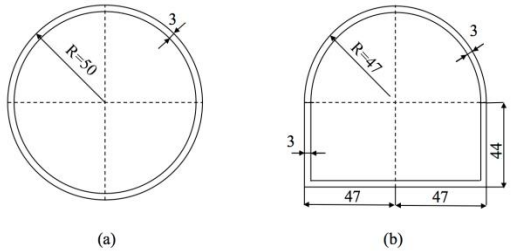

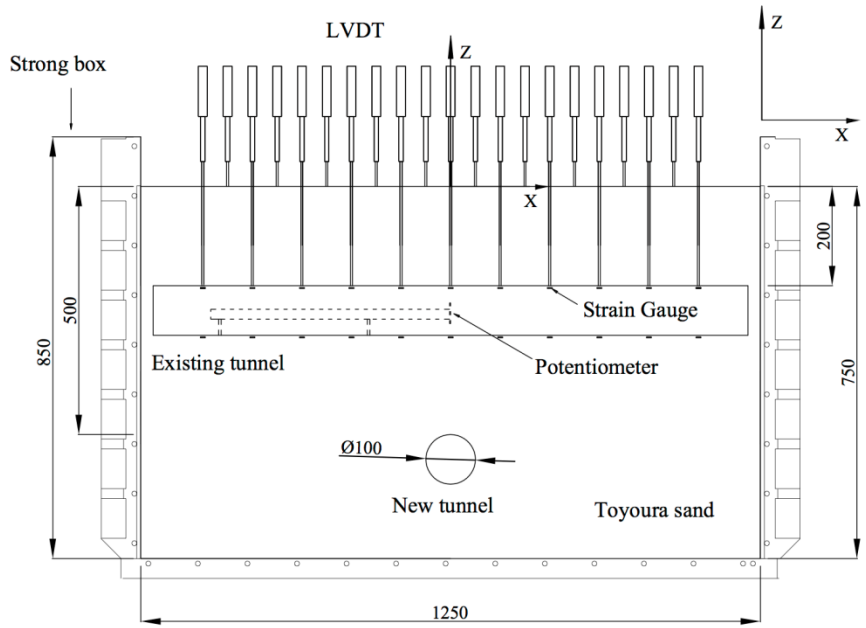

Ng, C.W.W., Wang, R. & Boonyarak, T. (2016). A comparative study of different responses of circular and horseshoe-shaped tunnels to an advancing tunnel underneath. *Géotechnique Letters,* 6, No.2, 168–175.

Deformations of existing horse-shoe shaped and circular tunnels due to new twin tunnel construction (mm)

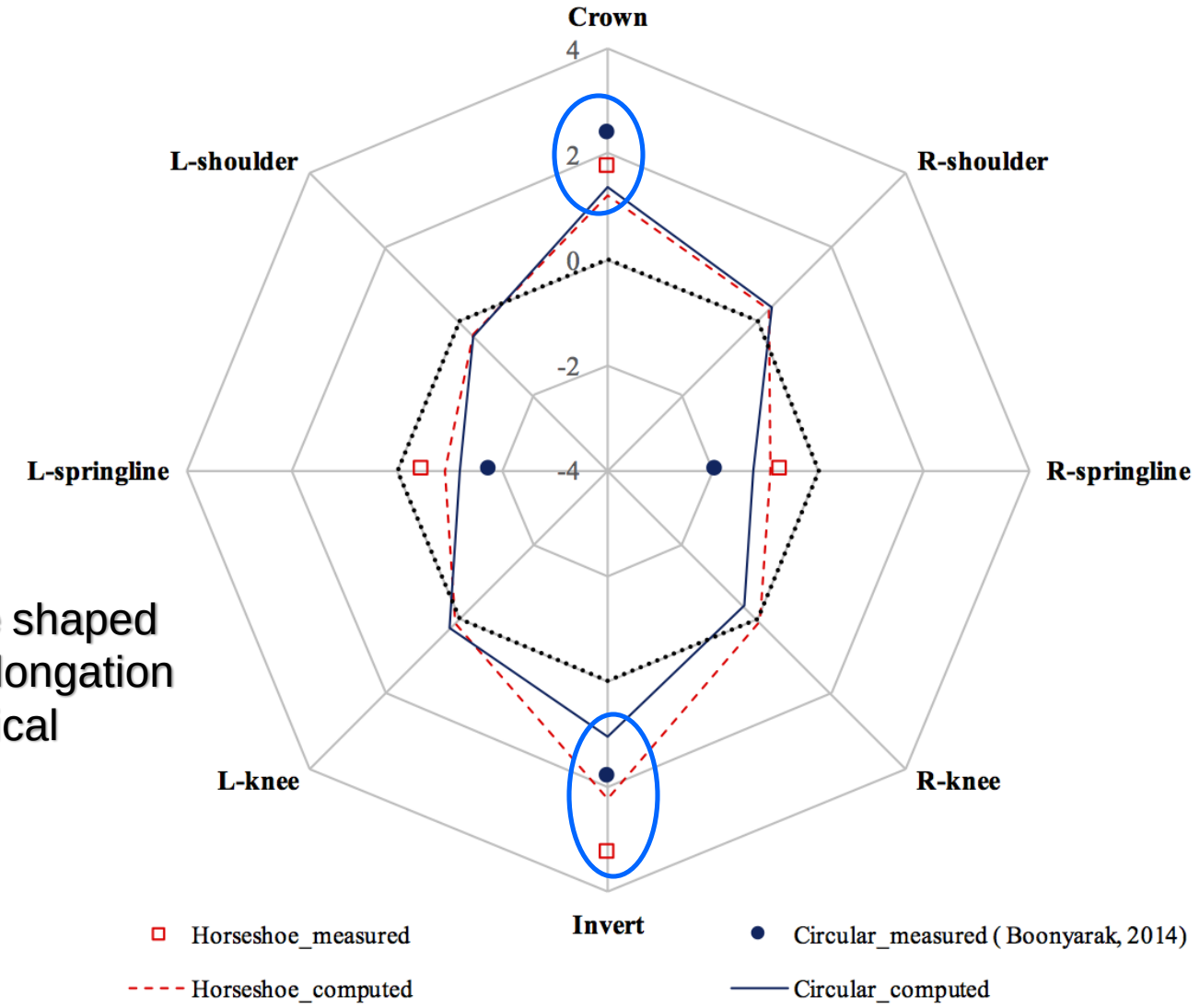

Horse-shoe shaped
20% more elongation
in vertical

(iii) The Serviceability of Energy Floating Piles in Sand and Clay

香港科技大學
THE HONG KONG UNIVERSITY OF SCIENCE AND TECHNOLOGY

Working Principle and Scientific Challenges of Energy Piles

Working Principle

Winter Summer

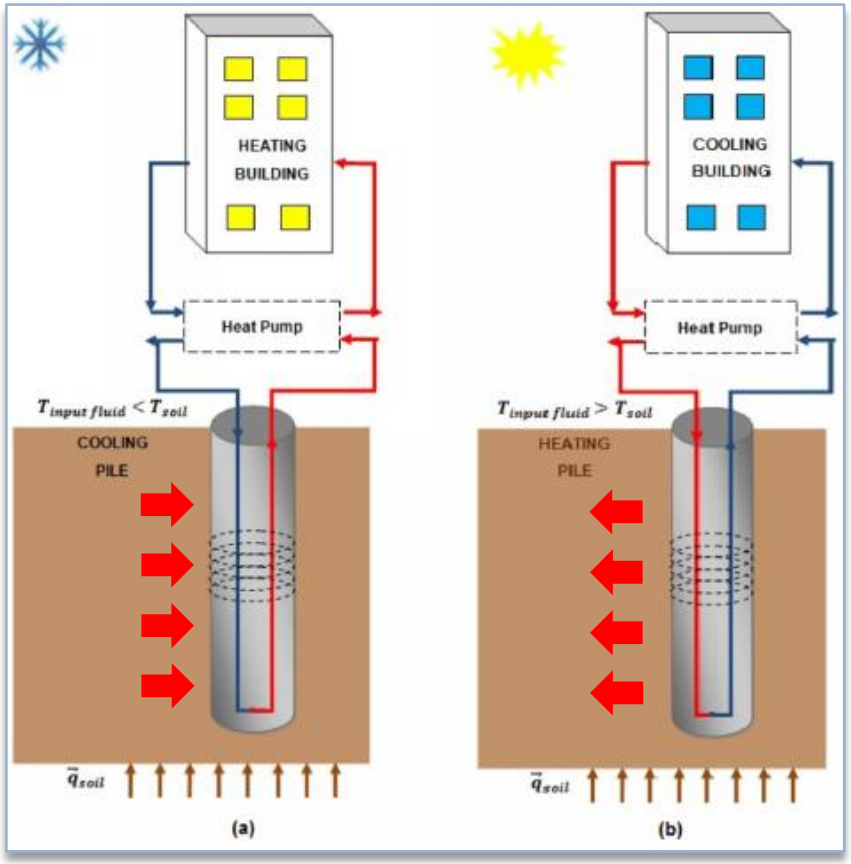

(Suryatriyastuti et al., 2012)

Energy pile

- Heat transfer medium
- Constant ground temperature at 10~15m below the ground (Adam & Markiewics, 2009)
- Extract heat in winter and discharge heat in summer
- Save up to 75% of electricity (Brandl, 2006)

Design uncertainties

- Long-term serviceability (floating piles in particular) (Bourne-Webb et al., 2009; GSHPA, 2012)

Scientific/design Challenges : Temperature effects on axially loaded piles

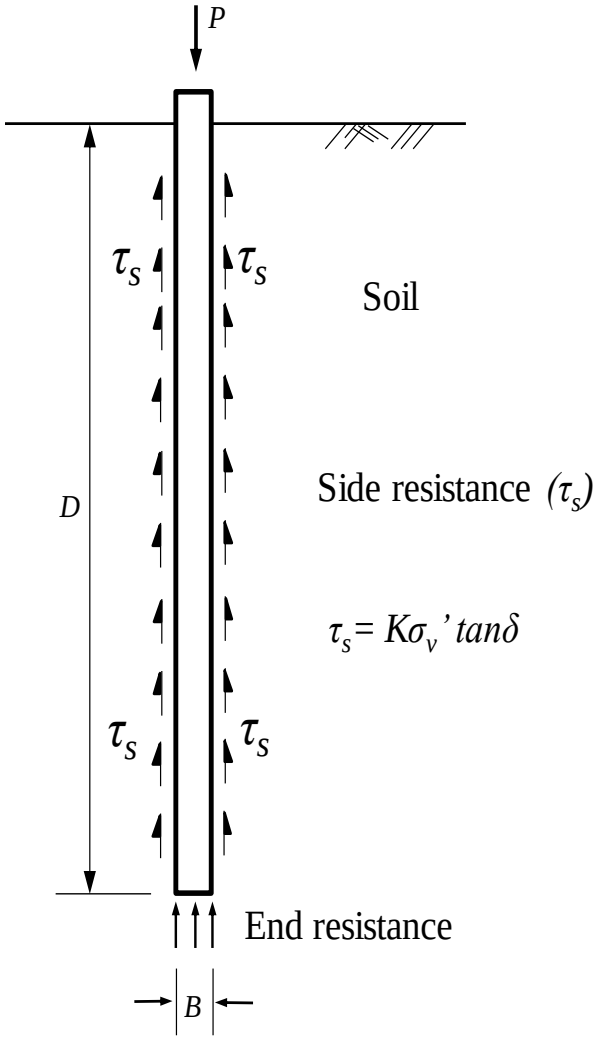

Governing mechanism:
$\tau_s = (\sigma'_n +/- \Delta\sigma'_n) \tan\delta$

1. Soil, which is temperature sensitive, has different responses under different temperatures

2. Temperature change may induce contractive or dilative response on soil, affecting the confining stress on pile, ultimately its carrying capacity and settlement/heave

3. Higher temperature reduces apparent preconsolidation pressure and hence encourage soil yielding in clays

4. Effects of thermal cycles on soil stiffness

$$\Delta\sigma_h = \frac{4 \cdot \delta_h \cdot E_s}{D}$$ (Boulon & Foray, 1986)

5. Pile lateral expansion and contraction (compression and extension), longitudinal elongation and shortening of pile (induce soil shearing) can affect lateral stress acting on the soil-pile interface, hence pile capacity and settlement

Volume changes of saturated loess (low plasticity clay)

under cyclic thermal load and vertical stress of 50 kPa in oedometer

Reconstituted

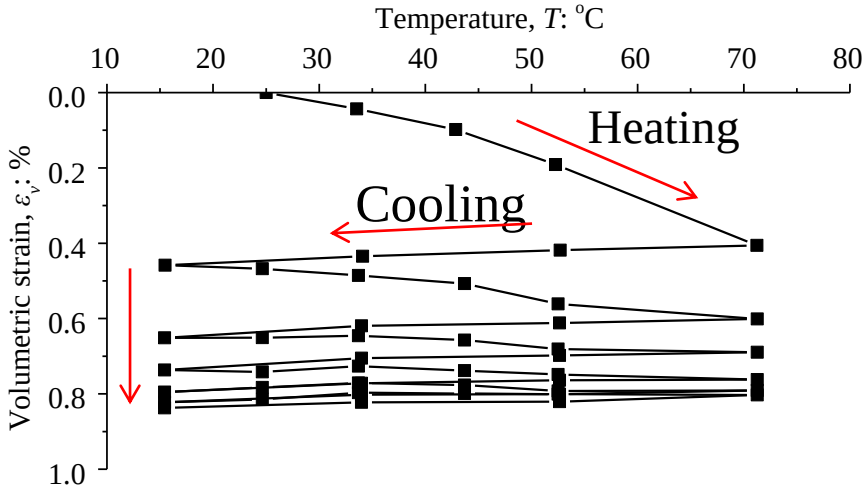

Recompacted

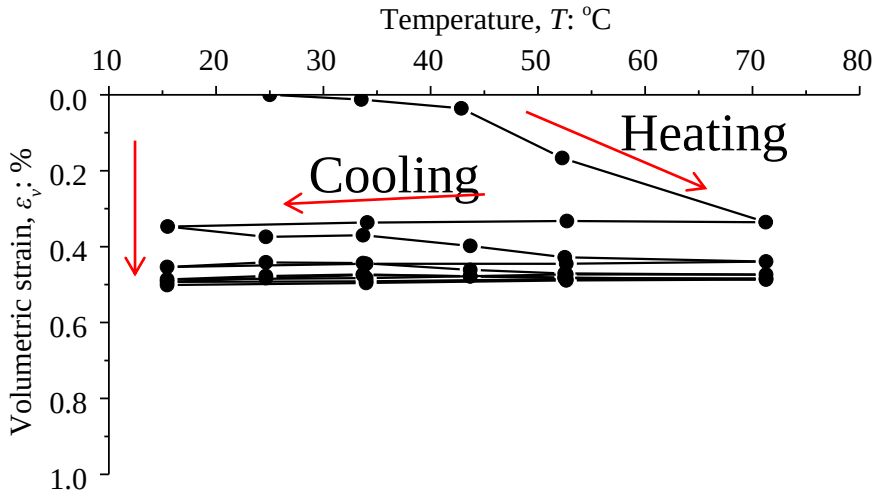

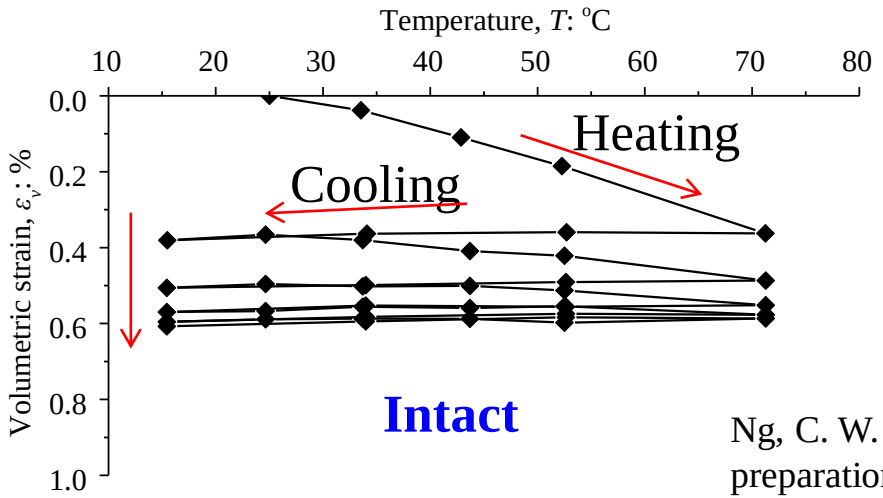

Intact

- All specimens show accumulated contraction
- Accumulated plastic strain can not be captured by existing models

Ng, C. W. W., Mu, Q. Y., and Zhou, C. (2018). Effects of specimen preparation method on volume changes of clay under cyclic thermal loads. *Géotechnique. Published online. doi.org/10.1680/jgeot.16.P.293*

Comparisons between model predictions and experimental results

Cyclic behaviour: thermal effects on stiffness at zero suction (silt (ML)

T = 20°C

T = 40°C

T = 60°C

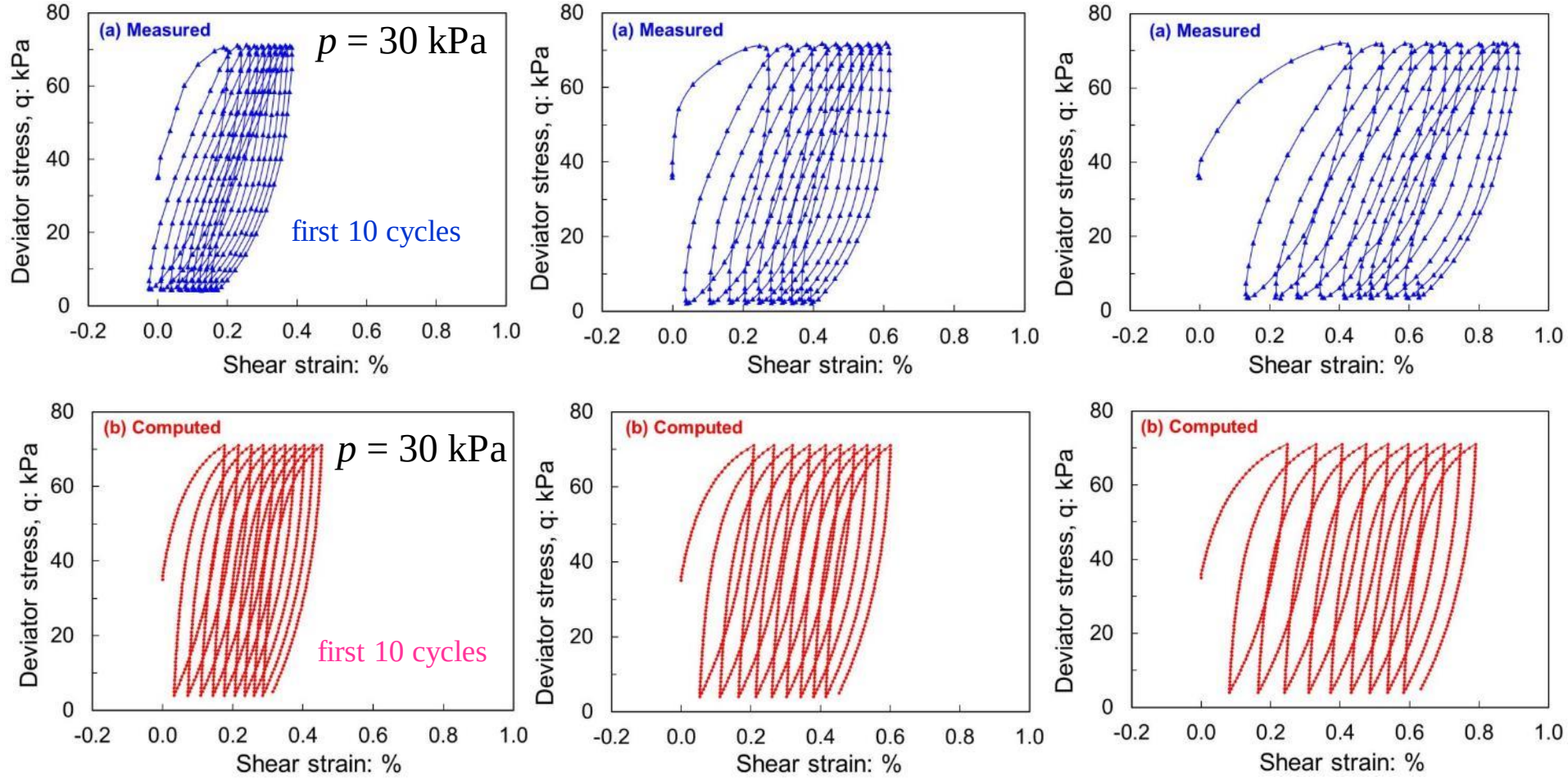

Zhou, C. and Ng, C. W. W. (2016). Simulating the cyclic behaviour of unsaturated soil at various temperatures using a bounding surface model. *Géotechnique*, 66(4): 344-350.

Test Plan

- Replacement Floating Energy Piles Subjected to Heating and Cooling Cycles in Saturated Clays (OCR=1.7 and 4.7) – serviceability limit state
- Replacement and Displacement Floating Energy Piles due to Heating and Cooling Cycles in Saturated Sand – serviceability limit state

Scaling Laws

Parameter	Scale (prototype / model)
Time (diffusion)	n^2
Temperature	1
Temperature gradient	n
Density	1
Length	n
Stress	1
Strain	1

Large scaling factor ($\mathbf{n^2}$) to minimize duration of testing for problem dealing with diffusion processes (conduction, convection and consolidation)

*where n is a factor of increase in g-level as compared with 1-***g** condition (Taylor, 2004)

- For in-flight test on heat conduction problems for 2 hours at 40***g***, on prototype scale = 40^2 x 2 hrs = 4.4 months

香港科技大學
THE HONG KONG UNIVERSITY OF SCIENCE AND TECHNOLOGY

Floating Replacement Energy Piles Subjected to Thermal Cycles in NC & OC Clays

A Typical Diagram of Centrifuge Model Package

Overconsolidated kaolin clay (OCR = 4.7 at toe)

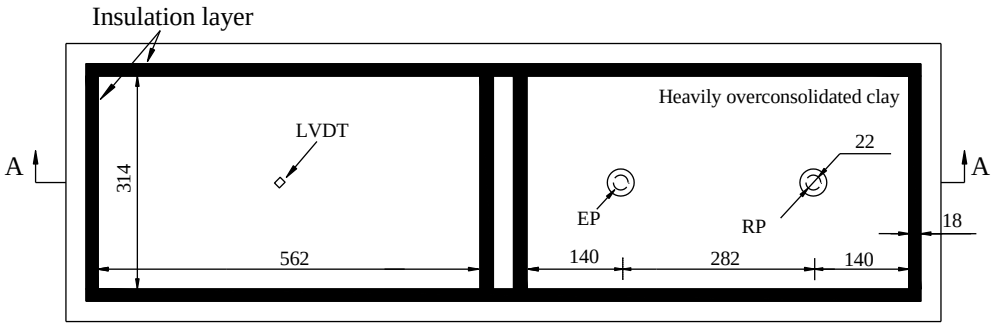

(a)

g - level: 40g

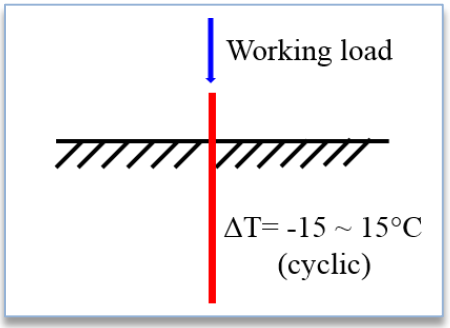

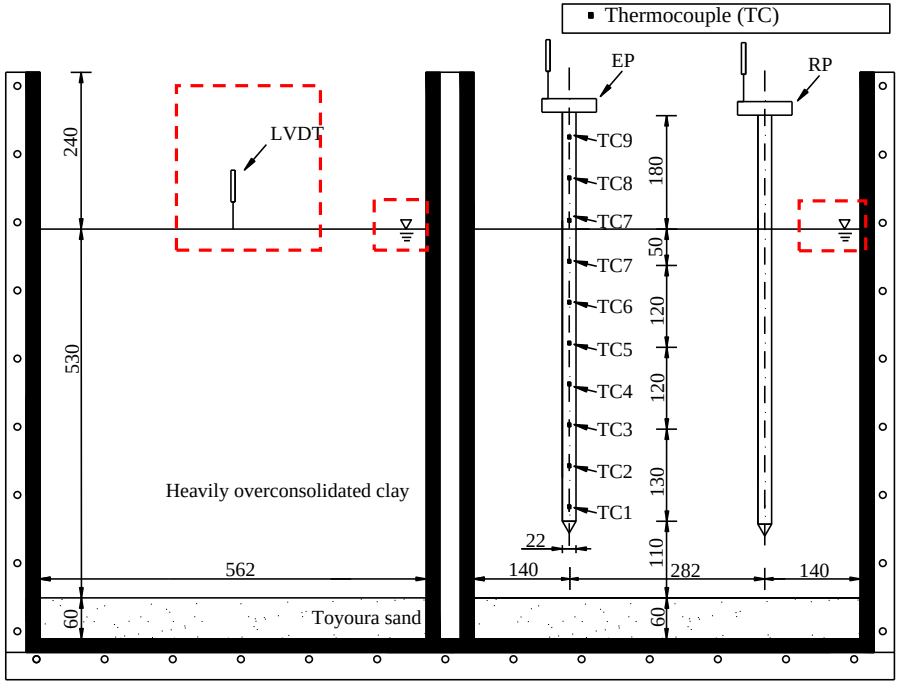

(b)

- Two identical clay beds
- Monitoring of ground settlement
- Pile diameter
  D_p = 0.88 m (prototype) at 40g
- Pile length
  L_p= 16.8 m (prototype) at 40g
- OCR = **4.7** close to pile toe

Energy Pile

Inlet and outlet heat-exchange pipes mounted on reinforcement cage of a bored pile

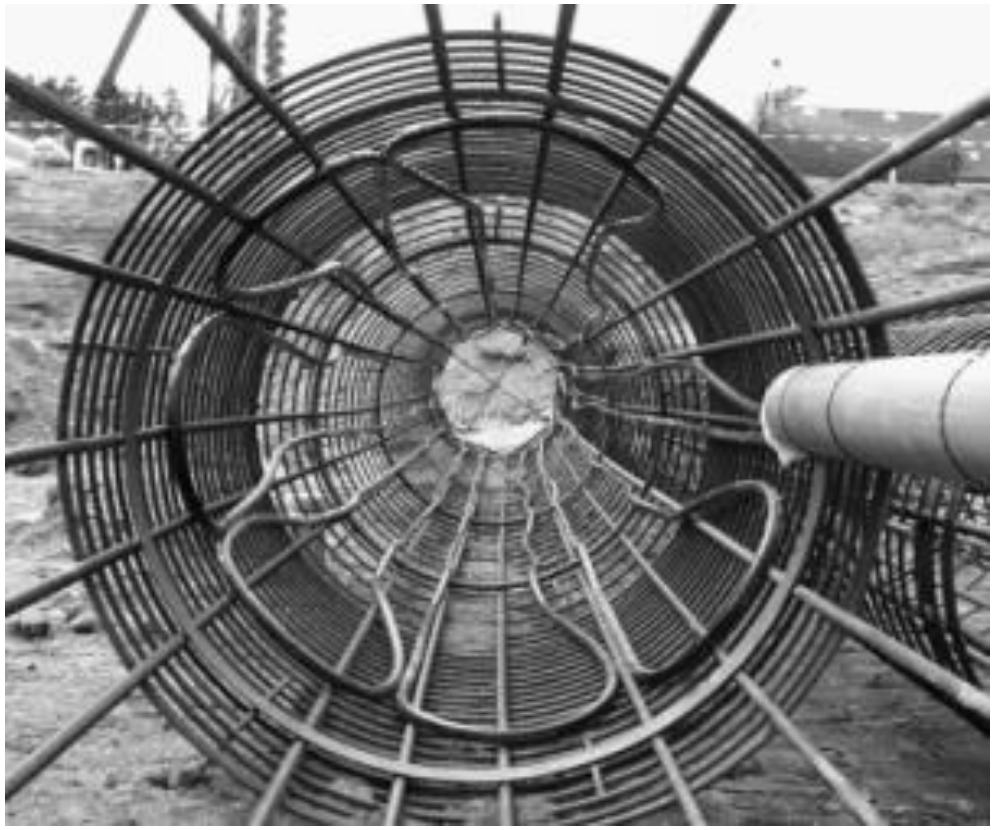

Brandl (2006)

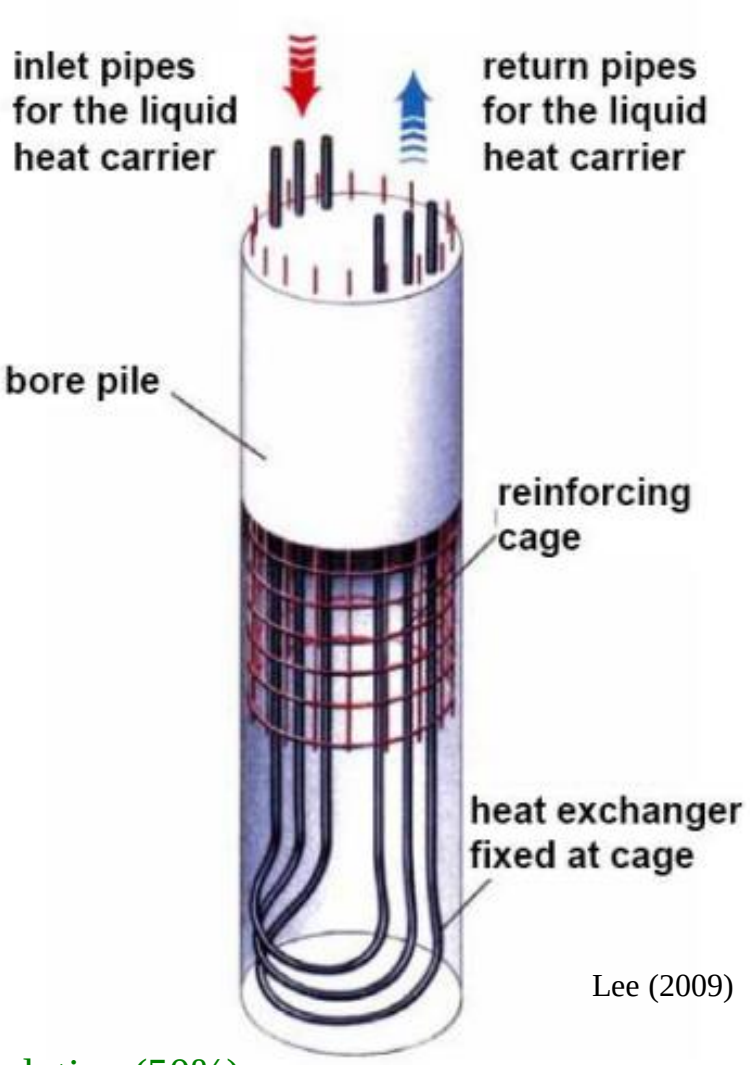

Lee (2009)

Heat exchange fluids: water, salt water, or ethylene glycol solution (50%)

Model Energy Pile

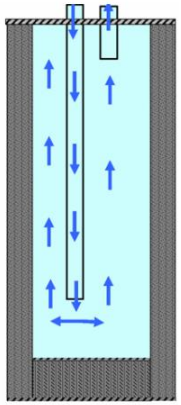

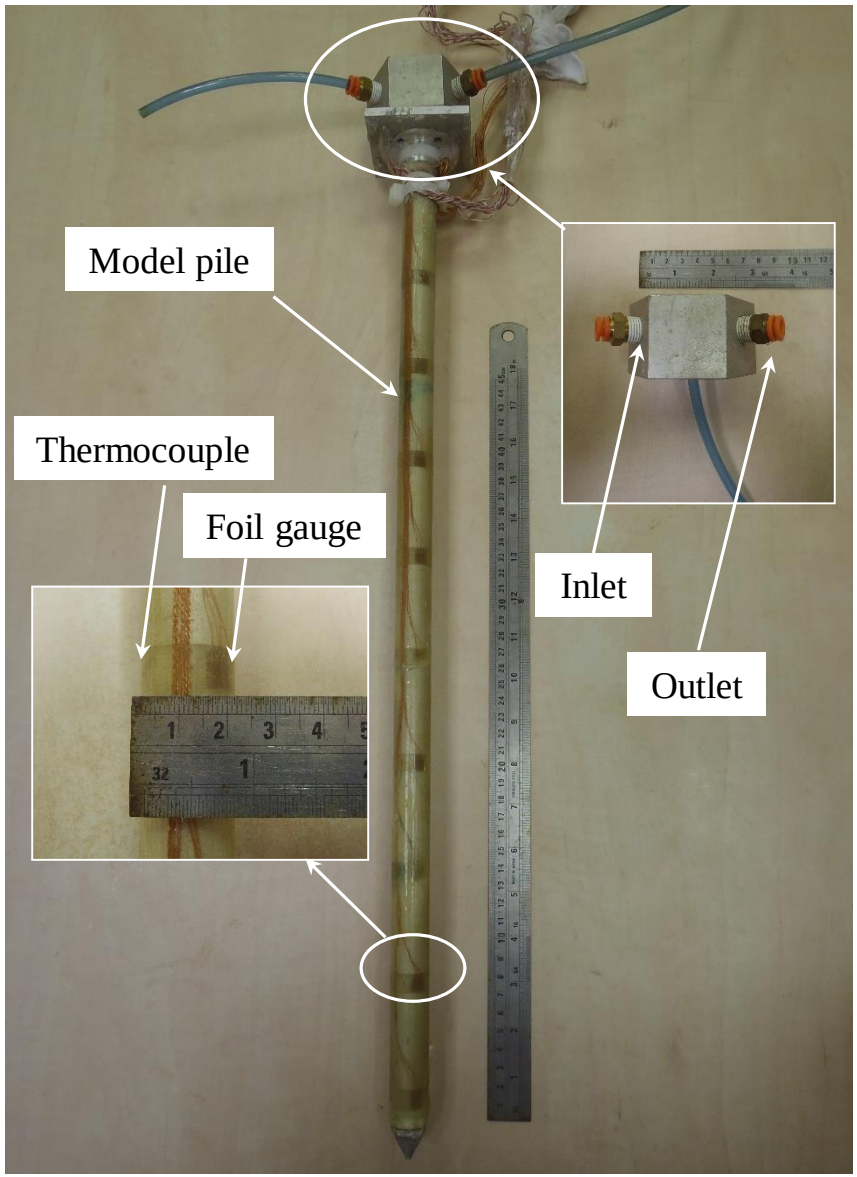

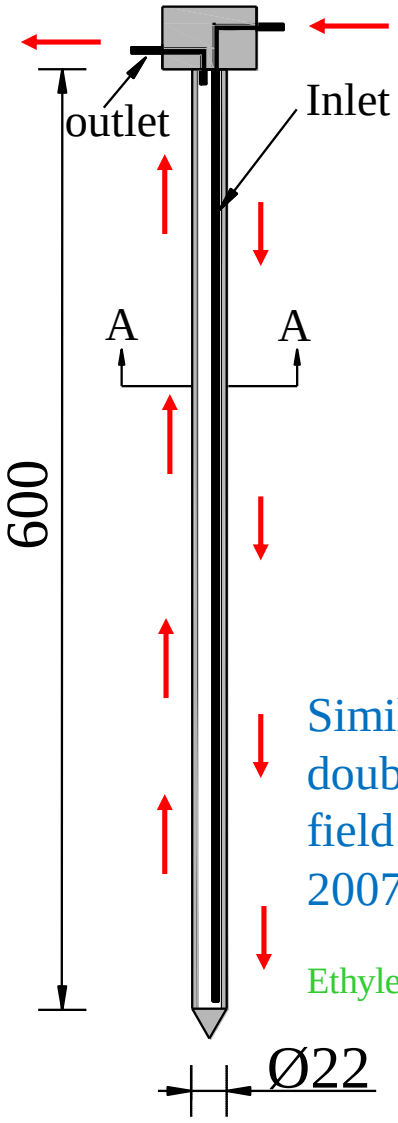

A-A section

Similar to that of direct double pipe type in the field (Hamada et al. 2007)

Ethylene Glycol Solution (50%)

All dimensions are in model scale (mm)

Overall view of heating and cooling system

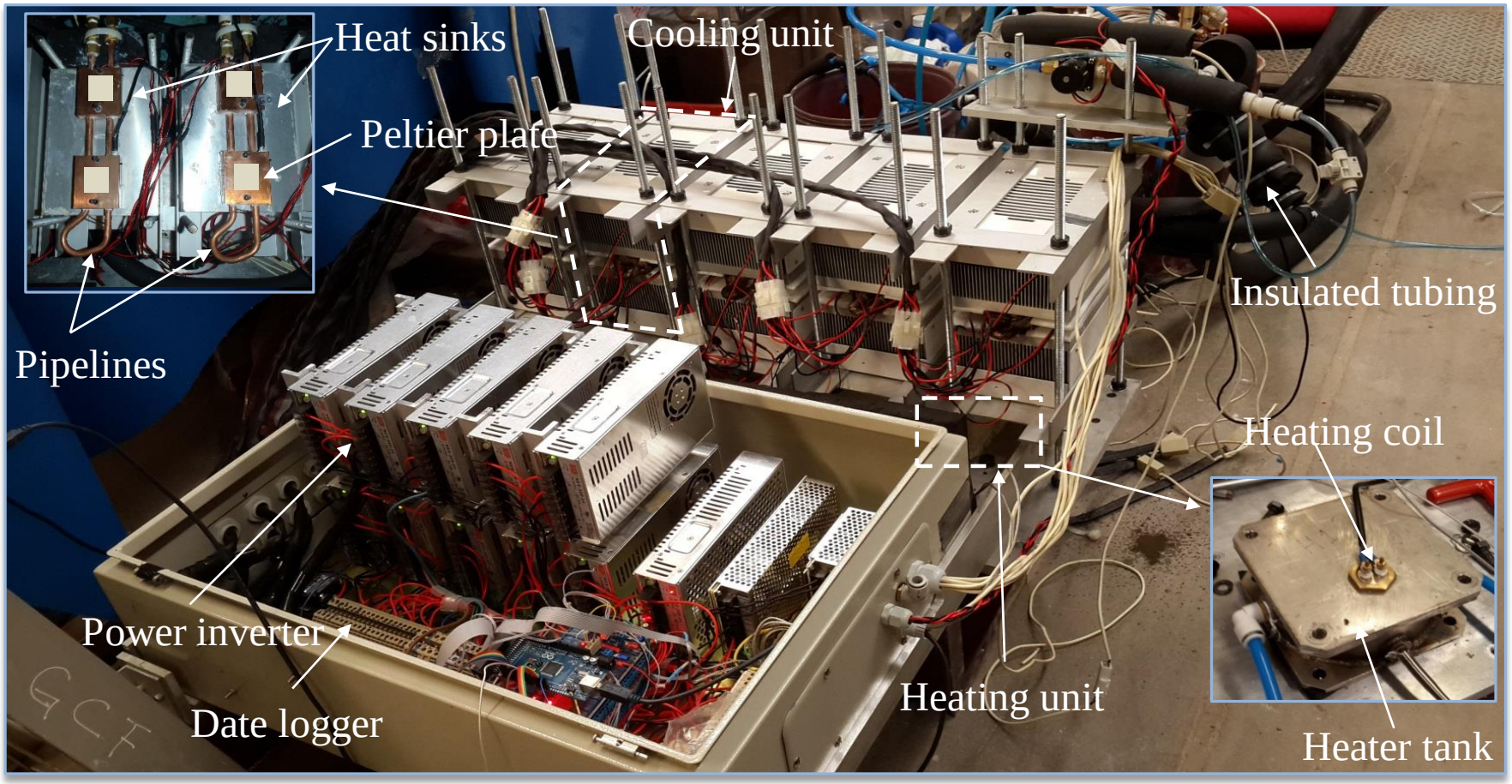

(1) group of heating units, (2) cooling units, (3) pneumatic pump and (4) insulated piping

Heating and Cooling system

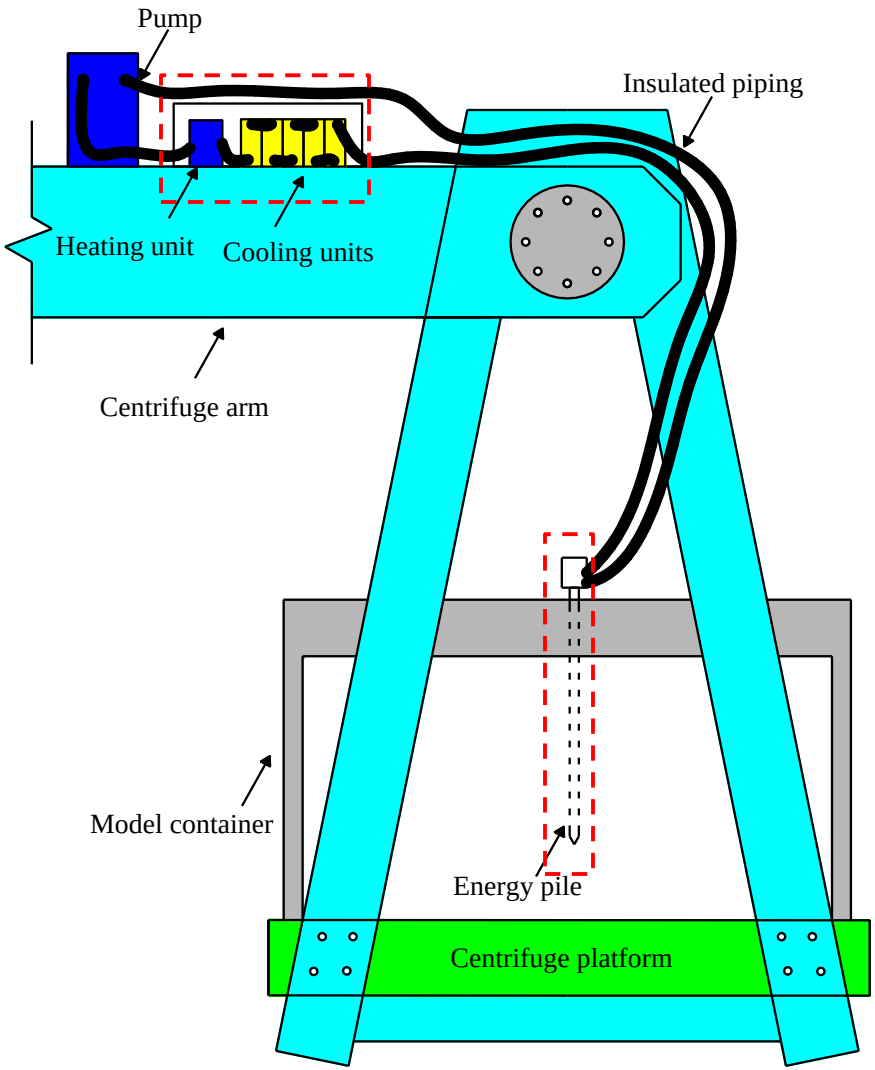

Schematic diagram of temperature control system

- ❖ Heating unit

One cartridge heater with a total power of 2500W

- ❖ Cooling units

Ten thermoelectric coolers (TECs) with a total power of 1000W

- ❖ Fluid (coolant - glycol)

Working temperature: -18° C ~ 123° C (3 to 90° tested for pile)

- ❖ Pump

Max operation pressure of 8.3 bar

- ❖ Piping

Insulated plastic tubes (D=6 mm)

Typical Measured Temperature History at EP-C1

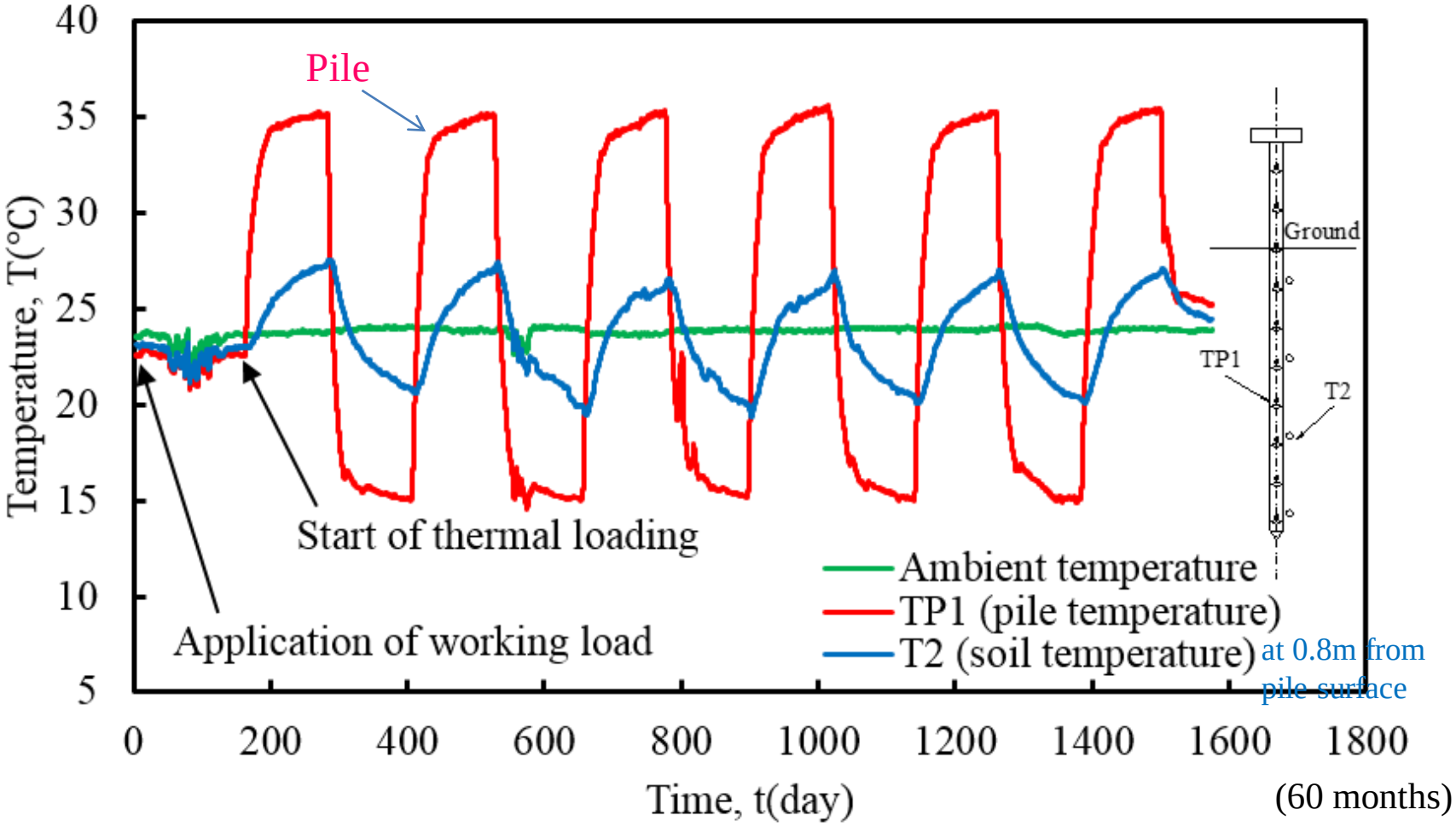

- After sustaining a working load 4.4 months (130 days), 5 heating and cooling cycles initiated
- Measured minimum and maximum temperature in the pile is 14 ºC and 36 ºC, respectively
- Each heating and cooling process lasted 4 months, 8 months per cycle for 5 cycles
- Similar temperature history was recorded for EP-C2

Measure Pile Head Displacement of EP-C1 (OCR=1.7)

(corrected for consolidation and creep of clay)

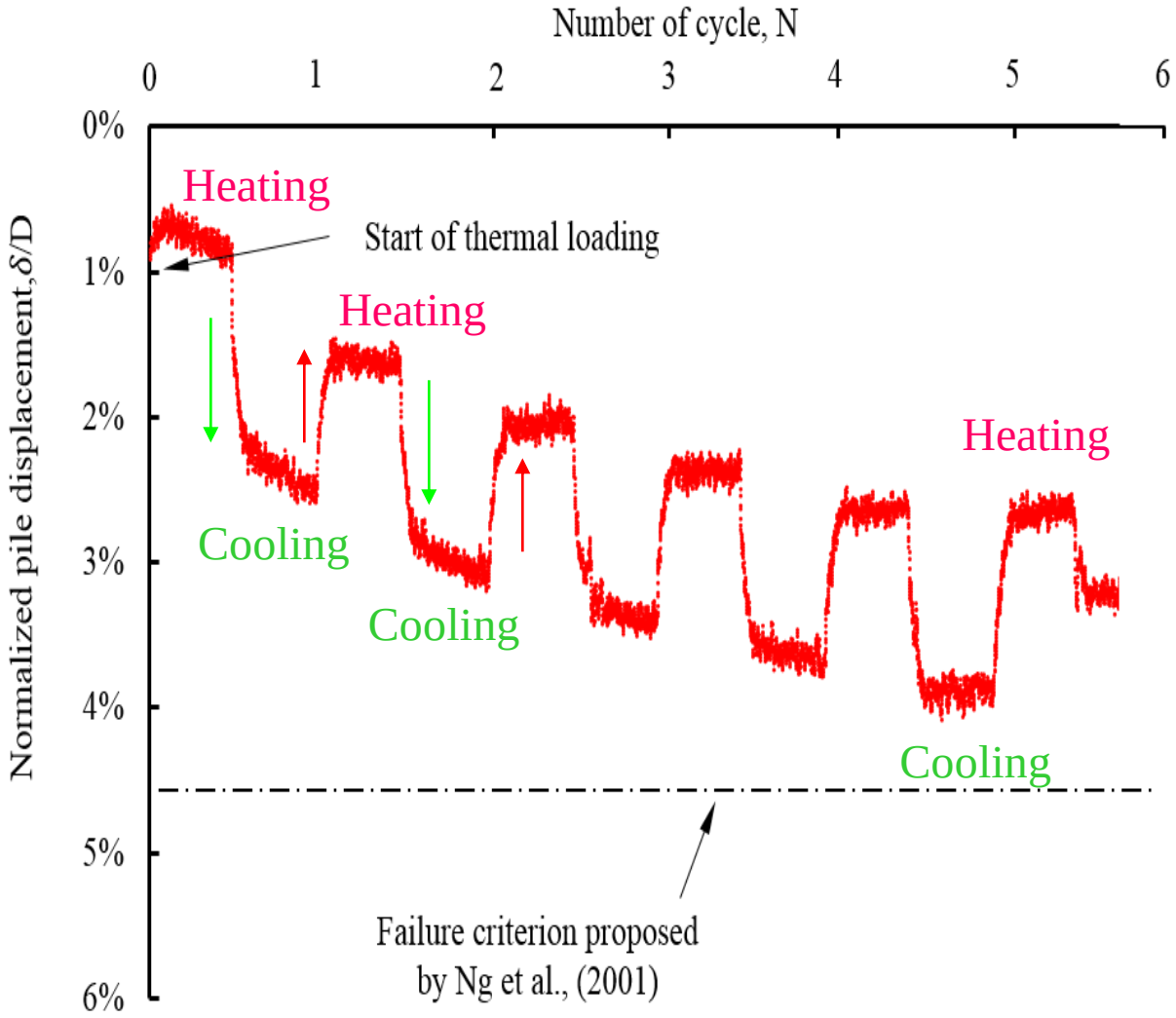

- Working load of 96 kN (FOS = 2.5)
- Ratcheting displacement mechanism
- Failure criterion (Ng et al. 2001):

$$\Delta_M \cong 0.045D + \frac{1}{2}\frac{PL}{EA}$$

- Creep under a sustained working load:

$$\frac{\delta}{D} = a \cdot t^b$$

(Edil and Mochtar, 1988)

Comparisons of Pile Head Displacements between EP-C1 and EP-C2 (corrected for consolidation and creep of clay)

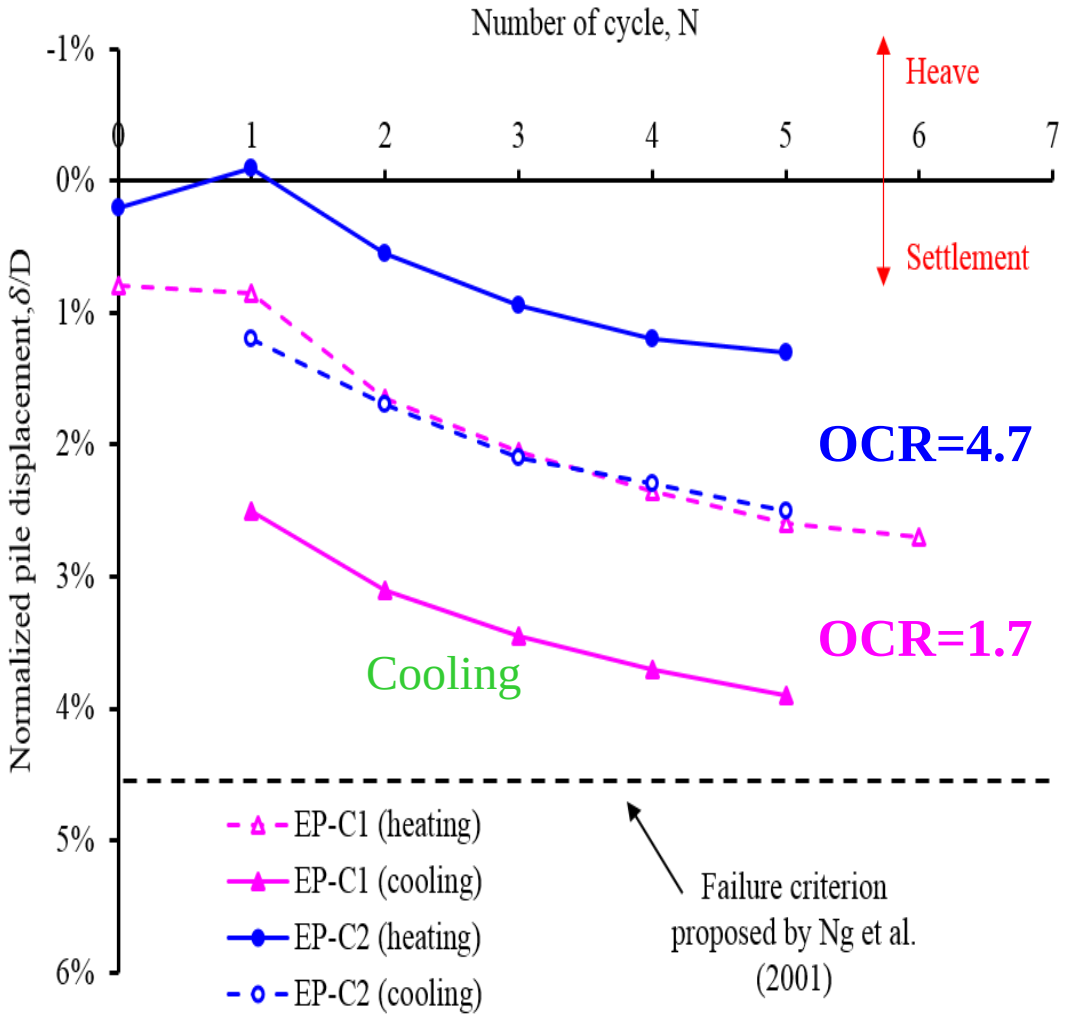

- Displacement measured at the *end* of each heating and cooling process plotted
- Settlement of pile in lightly overconsolidated clay was *more severe* than that in heavily overconsolidated clay
- Due to thermally induced *shear creep of clay* ???
- *Thermally induced plastic contraction* (irreversible thermal contraction) of lightly overconsolidated clay (Cekerevac & Laloui, 2004; Ng et al., 2018) ???
- *Thermally accelerated creep* (Akrouch et al. 2014) ???

Replacement versus Displacement Energy Piles in Saturated Sand

Model Replacement and Displacement Floating Energy Piles in Sand

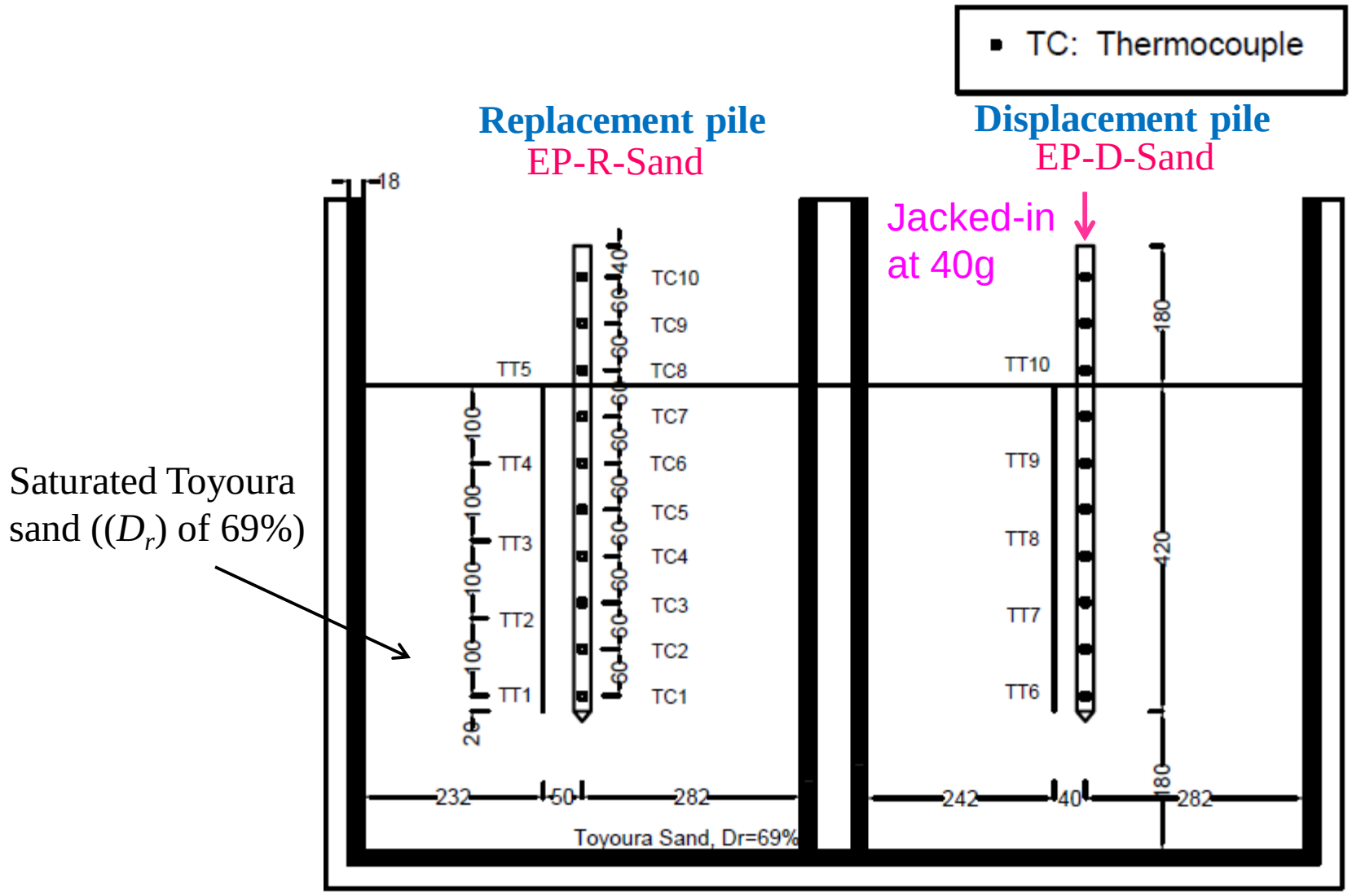

Typical Temperature History of Energy Pile

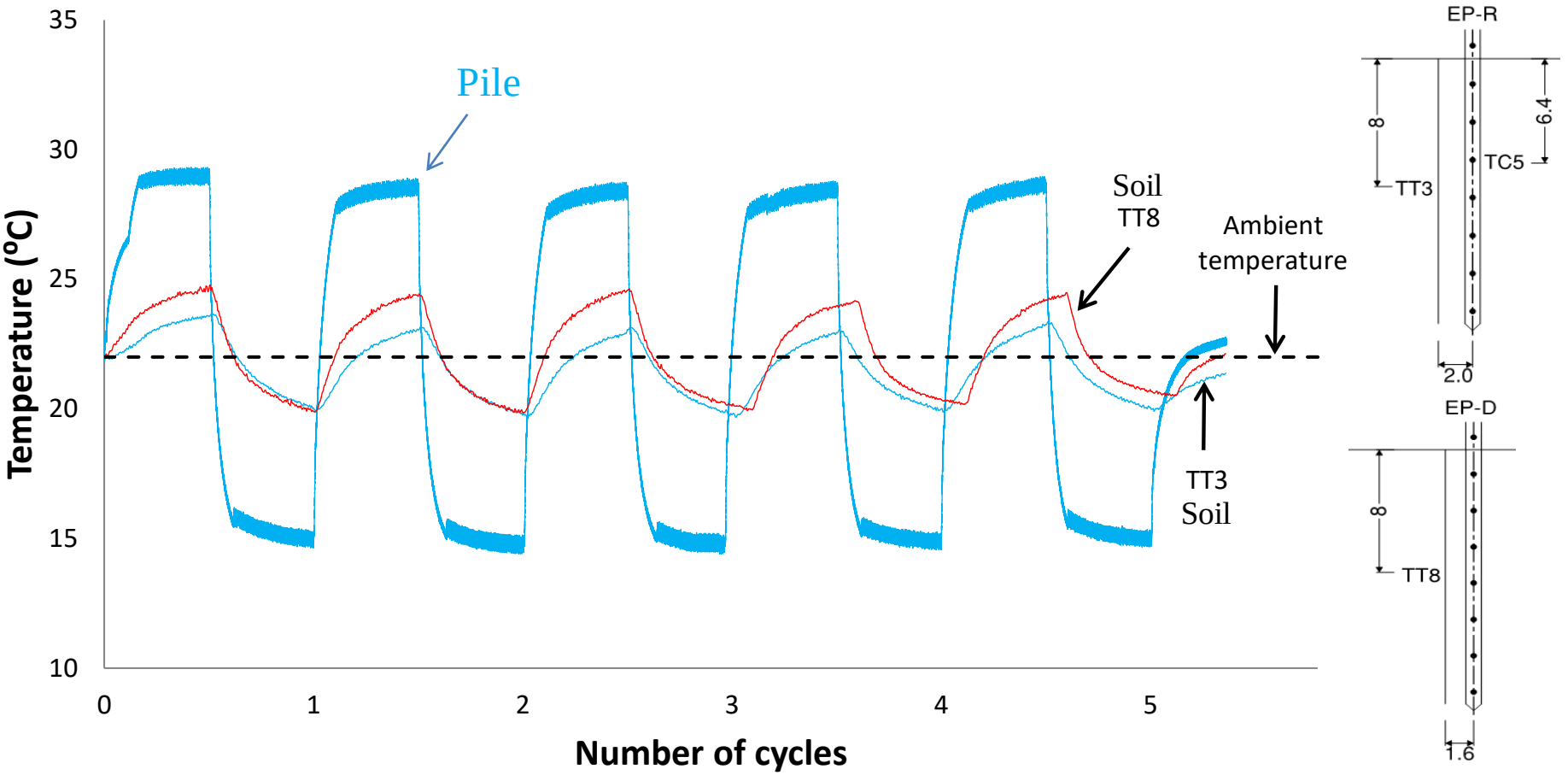

- After sustaining a working load (FoS = 2) for 4.4 months (130 days), 5 heating and cooling cycles initiated
- Measured minimum and maximum temperature in the pile is 15 ºC and 30 ºC, respectively
- Each heating and cooling process lasted 4 months, 8 months per cycle for 5 cycles

Measured Pile Head Displacements Under Working Load

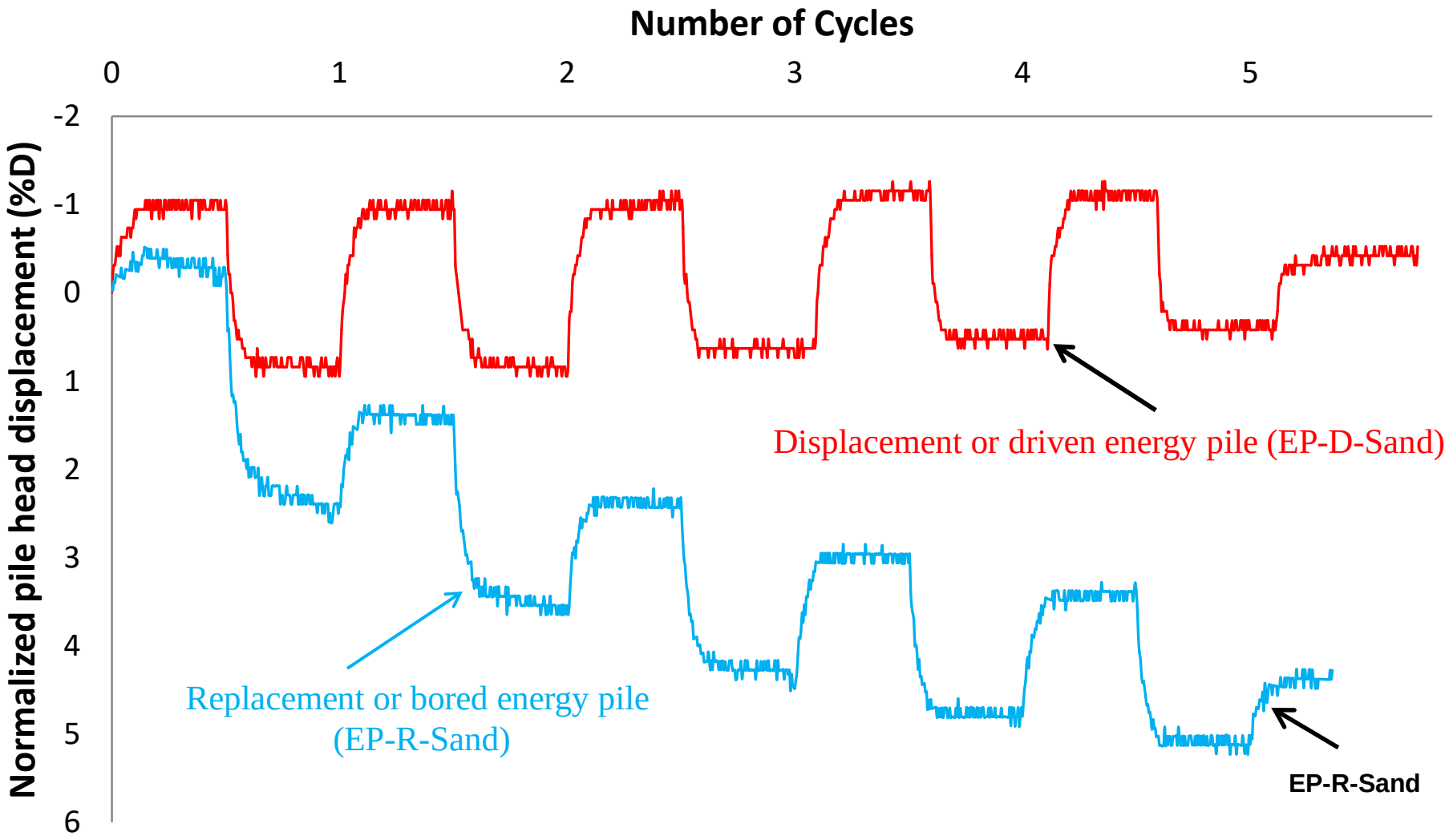

- Ratcheting settlement but at reducing rate for replacement energy pile (EP-R-Sand)
  - Due to thermal contraction of sand, loss of confining stress, hence loss of shaft resistance
- Slight heave for displacement energy pile (EP-D-Sand)
  - Densification effect due to jacking of pile, dilative response from further shearing (temperature induced shear)

(iii) The Serviceability of Energy Floating Piles in Sand and Clay

- Ng, C.W.W., Gunawan, A., Shi, C., Ma, Q.J. & Liu, H.L. (2016). Centrifuge modelling of displacement and replacement energy piles constructed in saturated sand: a comparative study. *Géotechnique Letters*. Vol. 6, 34-38.
- Ng, C.W.W., Shi, C., Gunawan, A., Laloui, L. & Liu, H.L. (2015). Centrifuge modelling of heating effects on energy pile performance in saturated sand. *Canadian Geotechnical Journal,* Vol. 52, No. 8, 1045-1057.
- Ng, C.W.W., Shi, C., Gunawan, A. & Laloui, L. (2014). Centrifuge modelling of energy piles subjected to heating and cooling cycles in clay. *Géotechnique Letters*, Vol. 4, 310-315.

(iv) The impact mechanisms and performance of barriers subject to debris flows

香港科技大學
THE HONG KONG UNIVERSITY OF SCIENCE AND TECHNOLOGY

Video shows – three debris flows in Korea, Taiwan and HK

Canada (BC): Johnsons Landing
Vancouver Outskirts

How do we mitigate debris flow hazards?

Rigid barrier (GEO, Lantau Island, Hong Kong)

Flexible barrier (GEOBRUGG, Lorch, Germany)

Slit structure (ELB, Germany)

Deflector (GEO, Hin Tin, Hong Komg)

- Debris flows have **poor temporal predictability**
  - **impact mechanisms** of geophysical flows against structural countermeasures not revealed and understood fully
- Current practice relies on **empiricism** or **prescriptive approach**

What is debris flow and composition ?

Triggered by earthquake and/or rainfall

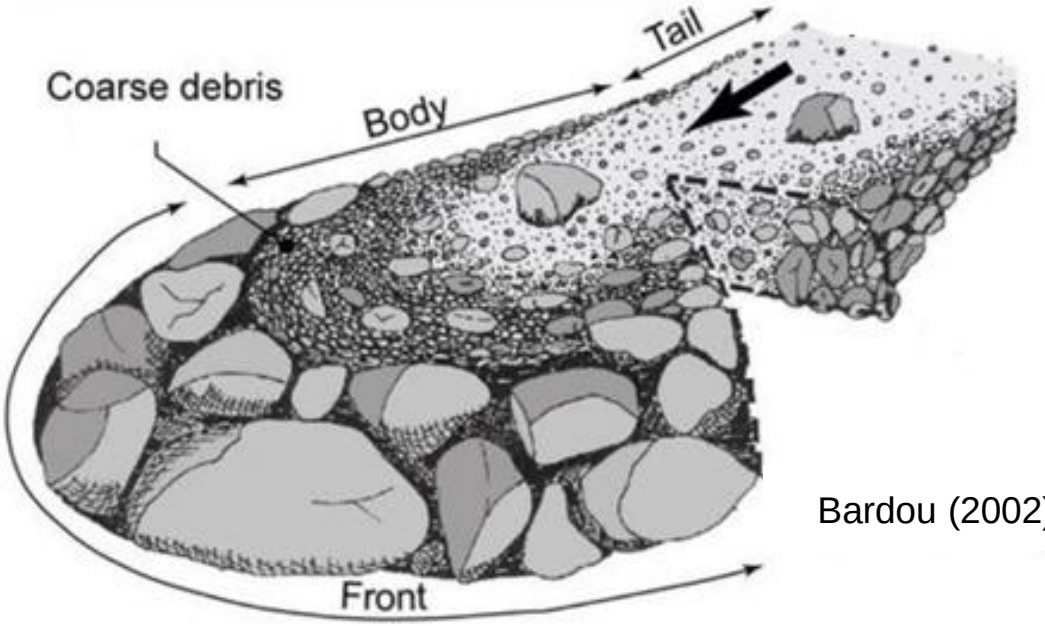

Bardou (2002)

(AGU)

(courtesy of Dr. Zhou, IMHE)

Hertz equation (GEO report 2012)

$$F = K_c 4000 v^{1.2} r^2$$

where F = impact force of a single boulder (in kN)

K_c = load reduction factor

v = boulder impact velocity normal to the barrier (in m/s)

r = radius of boulder (in m)

Hydro-dynamic equation (GEO report 2012)

Force $F = \alpha \rho v^2 \sin\beta h w$ **Pressure** $P = \alpha \rho v^2$

where α = dynamic pressure coefficient

ρ = density of debris flow (in kg/m^3)

v = debris velocity at impact (in m/s)

h = debris thickness (in m)

w = debris width (in m)

β = angle between impact face of barrier and debris motion direction

α is hydrodynamic pressure coefficient, 2.5 for rigid barrier and 2.0 for flexible barrier in HK

Gravity- and Scale-dependency

Geophysical flows are scale-dependent phenomena (Iverson 1997; 2015)

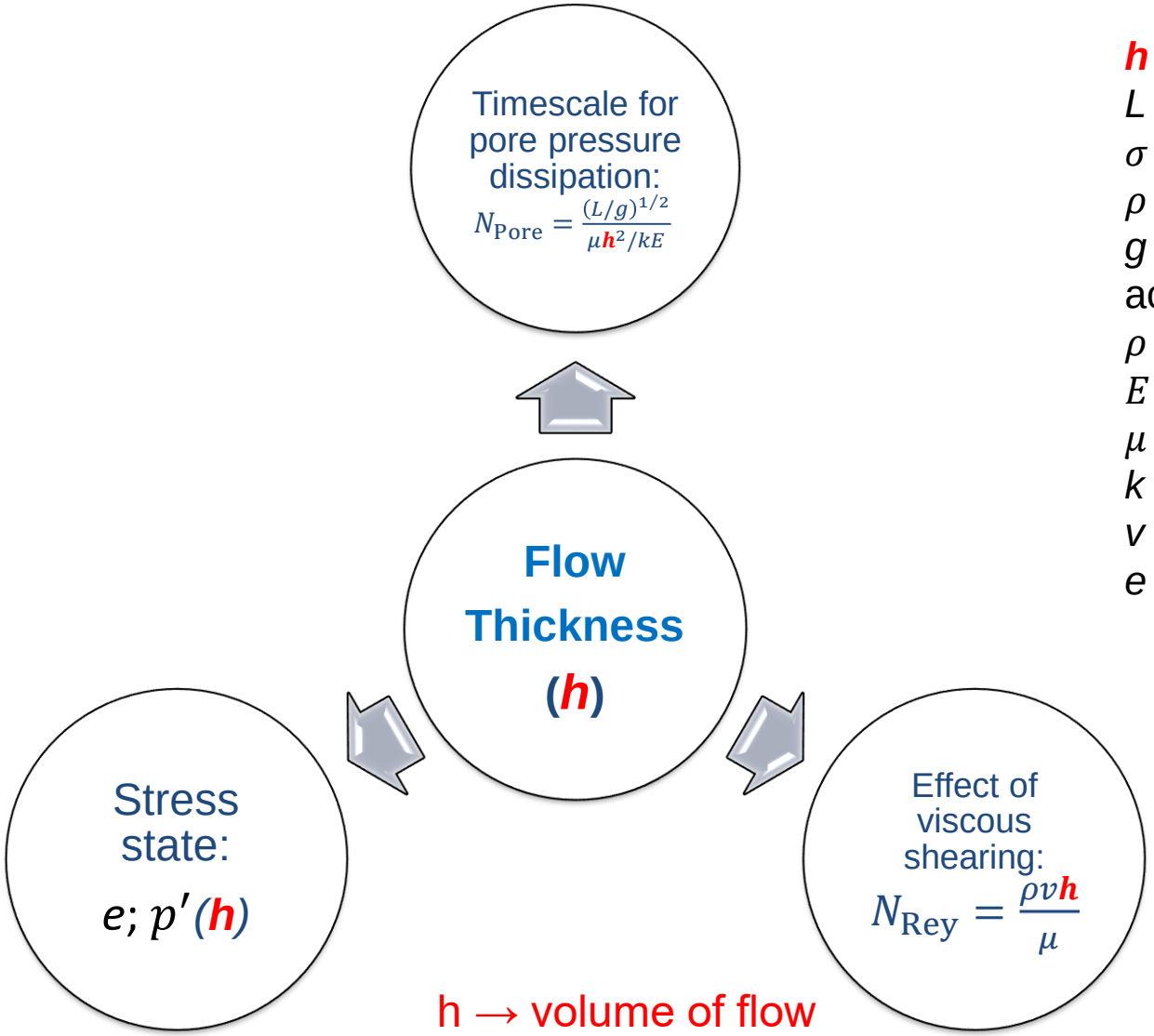

h is the flow thickness
L is the length of flow path
σ is the internal stress
ρ is bulk density
g is gravitational acceleration
ρ is the solid density
E is bulk mixture stiffness
μ viscosity of the fluid phase
k hydraulic permeability
v flow velocity
e void ratio

h → volume of flow

Multi-scale physical modelling

Model	Length (m)	Width (m)	Volume (m^3)	Advantages	Disadvantages
6-m long flume	6	0.2	0.1	• Cost effective • Time efficient • Ideal for parametric studies • Repeatable	• Limited range
28-m long flume	28	2	10	• Captures typical small-scale events in Hong Kong • Long-term debris flow facility for Hong Kong • Perspex along one side to study flow-structure interaction along entire channel • Designed for steeper 30º • Repeatable	• Costly • Time consuming
Geotechnical centrifuge	22	5	170	• Replicates prototype volumes and impact energies • Ideal for parametric studies • Cost effective • Time efficient • Repeatable	• Limited channel length
172-m long flume	172	6	500	• Captures typical large-scale events in Hong Kong • Repeatable	• Costly • Time consuming
Pendulum	A 6-m tall frame suspending a 1.1-m diameter concrete ball with a mass of 2000 kg model boulder impact into a cushioning layer shielding an instrumented rigid barrier			• Enables the investigation of a wide range of cushion materials at up to 70 kJ • Repeatable	• Only models concentrated loading from boulders

Summary of dimensionless numbers

Name	Parameter	Physical meaning	Values for natural and large-scale debris flows
Froude number (*Fr*)	$\frac{v}{\sqrt{gh\cos\theta}}$	Ratio of inertial to gravitational forces	0.5 to 5.9 [a]
Pore pressure number (N_{Pore})	$\frac{\sqrt{l/g}}{\mu h^2/kE}$	Ratio of bulk inertial forces to pore fluid pressure diffusional time scales	10^{-4} to 10^{-10} [b]
Reynolds number (N_{Rey})	$\frac{\rho h\sqrt{gl}}{\mu}$	Ratio of bulk inertial forces to fluid viscous effects	1×10^{7} to 2×10^{9} [b]
Savage number (N_{Sav})	$\frac{\rho_s \dot{\gamma}^2 \delta^2}{(\rho_s - \rho_f) g\, h \tan\phi}$	Ratio of stress associated with grain collisions to stress associated with grain friction (≥ 0.1 is collisional; ≤ 0.1 is frictional)	1×10^{-7} to 2×10^{-4} [b]
Bagnold number (N_{Bag})	$\frac{\upsilon_s}{1-\upsilon_s}\frac{\rho_s \delta^2 \dot{\gamma}}{\mu}$	Ratio of stress associated with grain collisions to viscous shear stress	0.2 to 4 [b]
Friction number (N_{Fric})	$\frac{\upsilon_s}{1-\upsilon_s}\frac{N(\rho_s - \rho_f) g\delta \tan\phi}{\dot{\gamma}\mu}$	Ratio of contact grain stress to viscous effects	2×10^{3} to 4×10^{5}

v: velocity of the flow; *g*: gravitational acceleration; *h*: depth of the flow; *θ*: channel inclination; *γ*: shear rate; *ρ*: bulk debris density; ρ_s: solid density; *δ*: characteristic grain diameter; ρ_f: fluid density; *∅*: bulk friction angle; υ_s: volume fraction of solids ($\upsilon_s+\upsilon_f$ =1) for two-phase mixtures; *μ*: fluid dynamic viscosity; *k:* hydraulic permeability of mixture; *E*: bulk stiffness; *l* flow length; *N* number of grains above slip surface; [a] Hübl *et al*. (2009); [b] Iverson (1997)

Novel centrifuge flexible barrier model

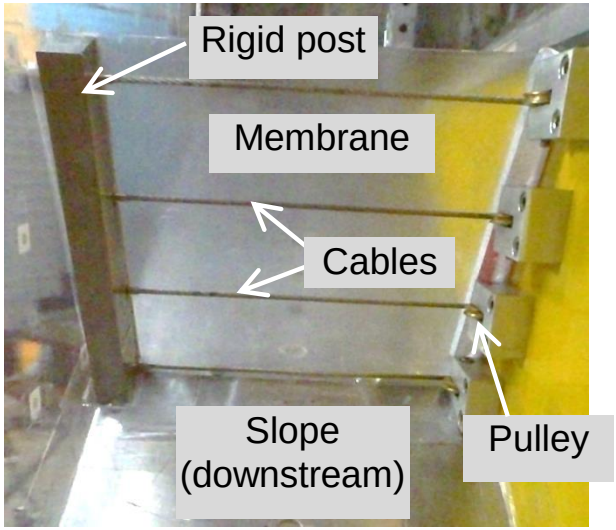

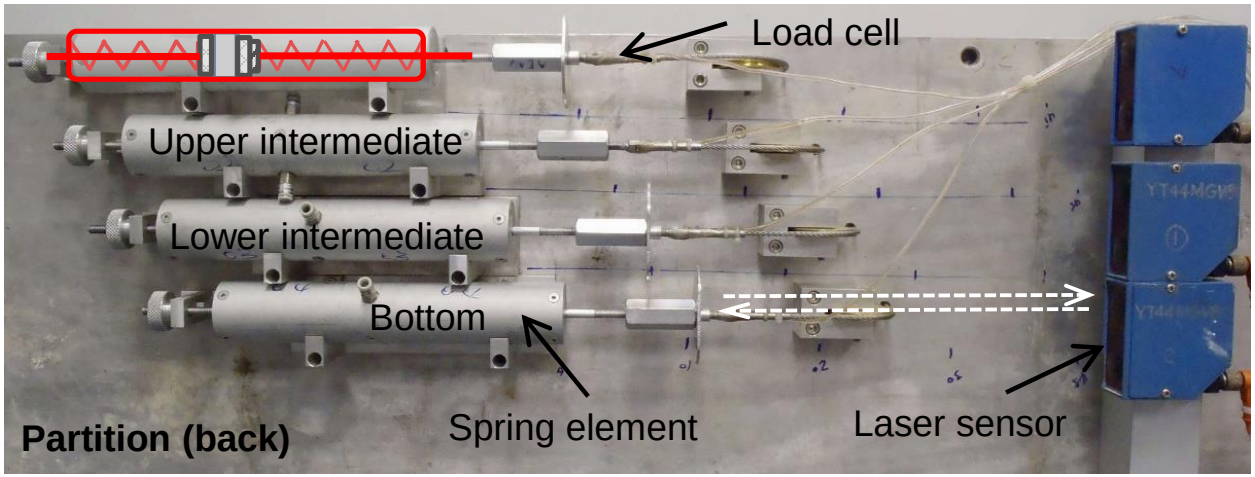

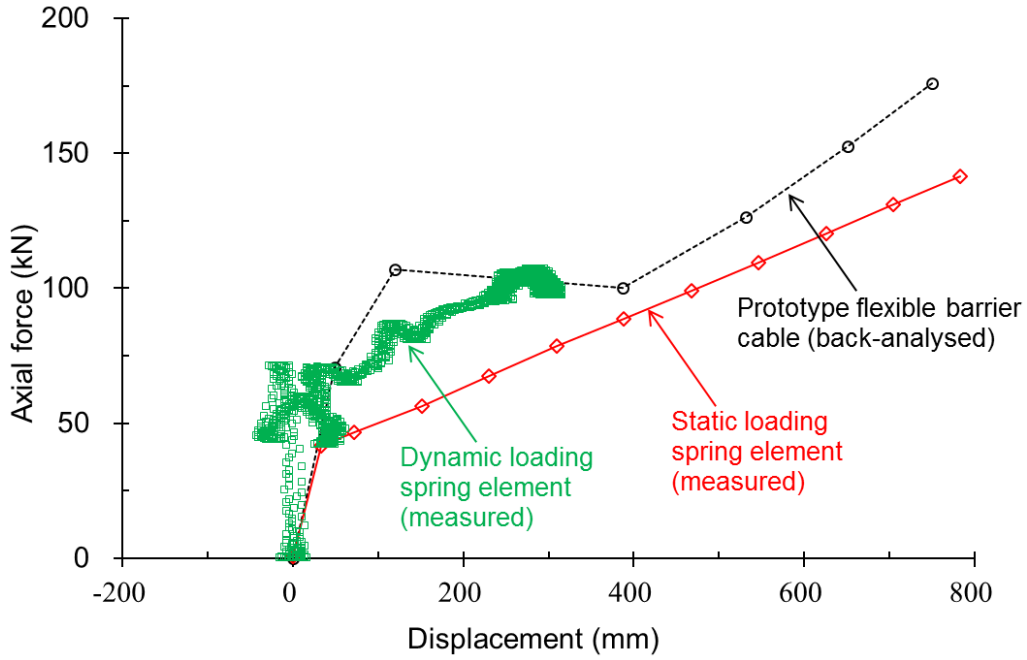

Ng, C.W.W., Song, D., Choi, C.E., Koo, C. H. & Kwan, J. S. H. (2017). A novel flexible barrier for landslide impact in centrifuge. *Géotechnique Letters*. Vol. 6, No. 3, 221–225.

US patent (Provisional application no. 62/387,524) and Chinese patent (Provisional application no. PCT/CN2017/070127) are currently pending for the core component of the model, "*a new bi-linear energy dissipating and shock absorbing device for cable under tension*".

New flexible barrier model for centrifuge tests

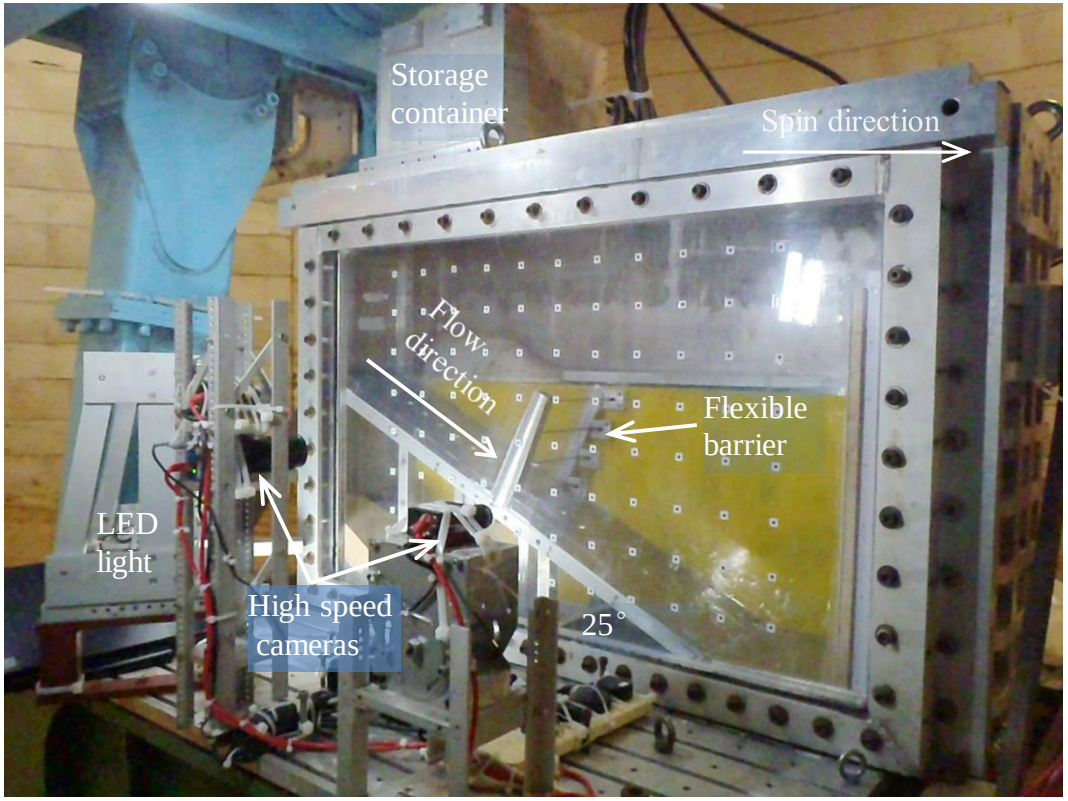

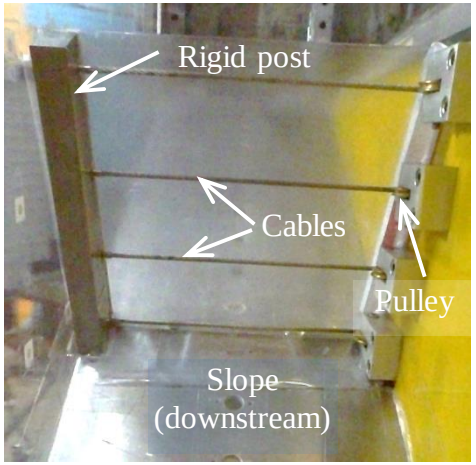

- Barrier: height 200 mm (prototype 4.5 m), width 203 mm (prototype 4.5 m)
- Full retention of the debris material
- High speed camera: 1312×1600 pixel, 640 fps

Effects of solid-fluid fraction on flexible barrier interaction

Viscous liquid

0.022 Pas (model)

0.5 Pas (prototype)
500 times of that of water

Sand

0.6 mm (model)

13 mm (prototype)

Flexible barrier impact mechanism

Viscous liquid

0.022 Pas (model)

0.5 Pas (prototype)
500 times of that of water

Sand

0.6 mm (model)

13 mm (prototype)

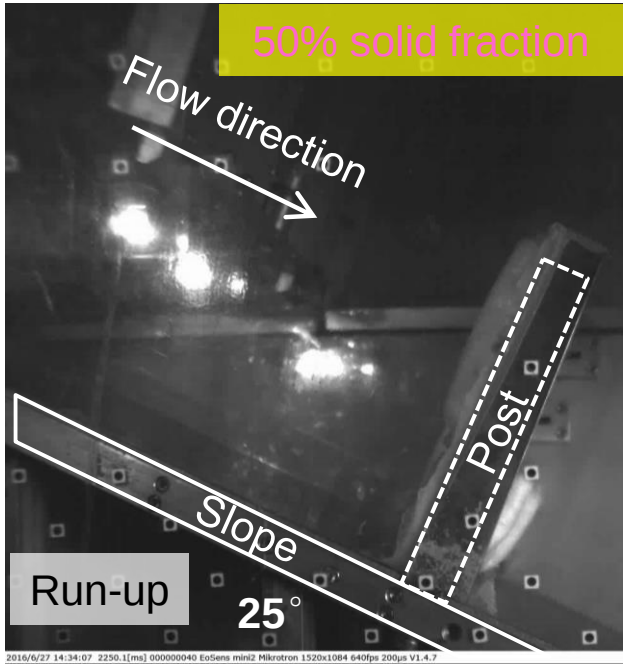

Test	Kinetic energy (kJ)	Absorbed energy (kJ)	Ratio
20% solid fraction	2270	342	0.15
40% solid fraction	2834	332	0.12
50% solid fraction	3115	360	0.12
Dry sand	2612	73	0.03

→ α much smaller than 2

Measured cable force and elongation - Test FL

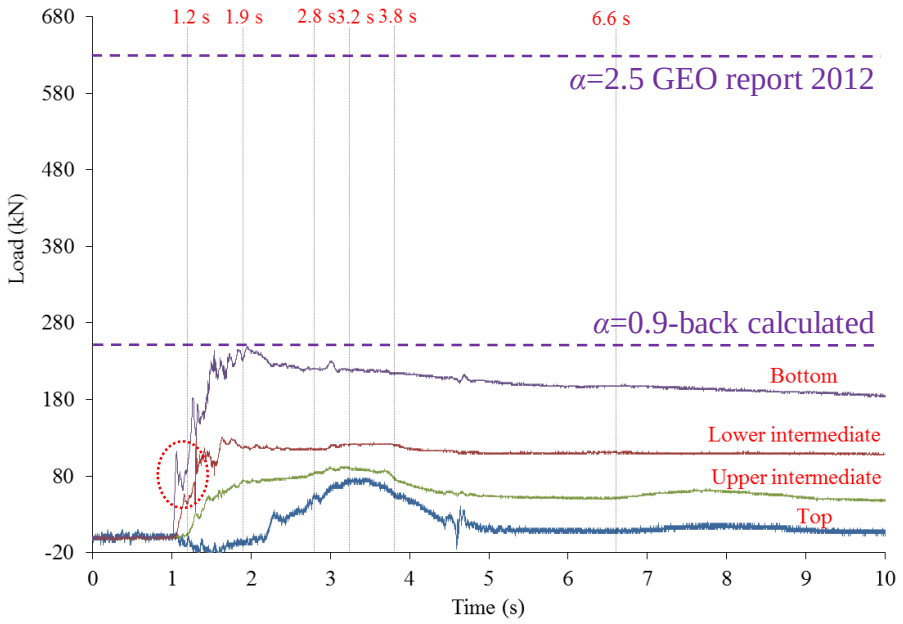

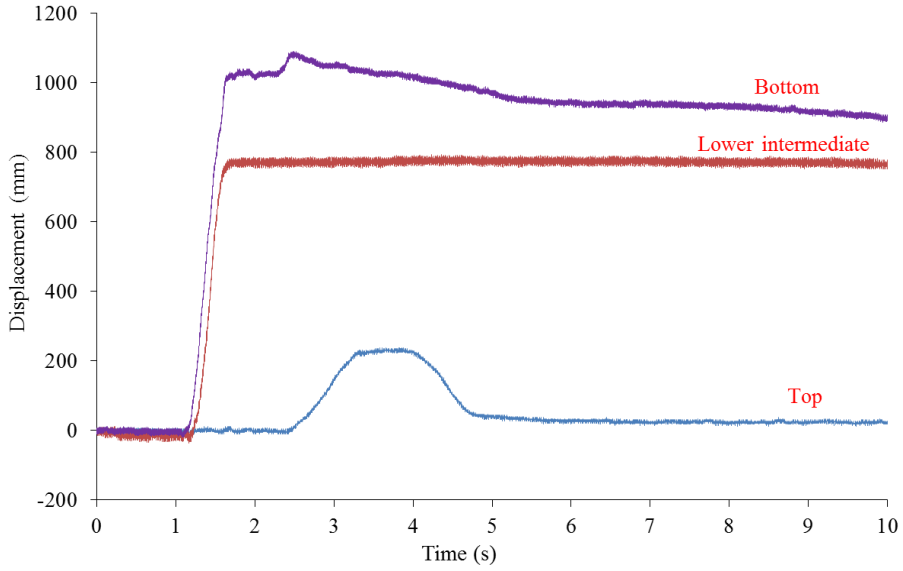

$$P = \alpha \rho v^2$$

α is hydrodynamic pressure coefficient, 2.5 for rigid barrier and 2.0 for flexible barrier in HK

- Prototype simulated = 250 m^3
- Instant load pick up
- Slope change: inflection point of the bilinear behavior
- Back-calculated α=0.9
- Max. elongation 1090 mm at bottom cable

Effects of boulder size on impact mechanism of **rigid** and **flexible** barriers

Novel centrifuge package for studying debris flow impact on rigid barrier

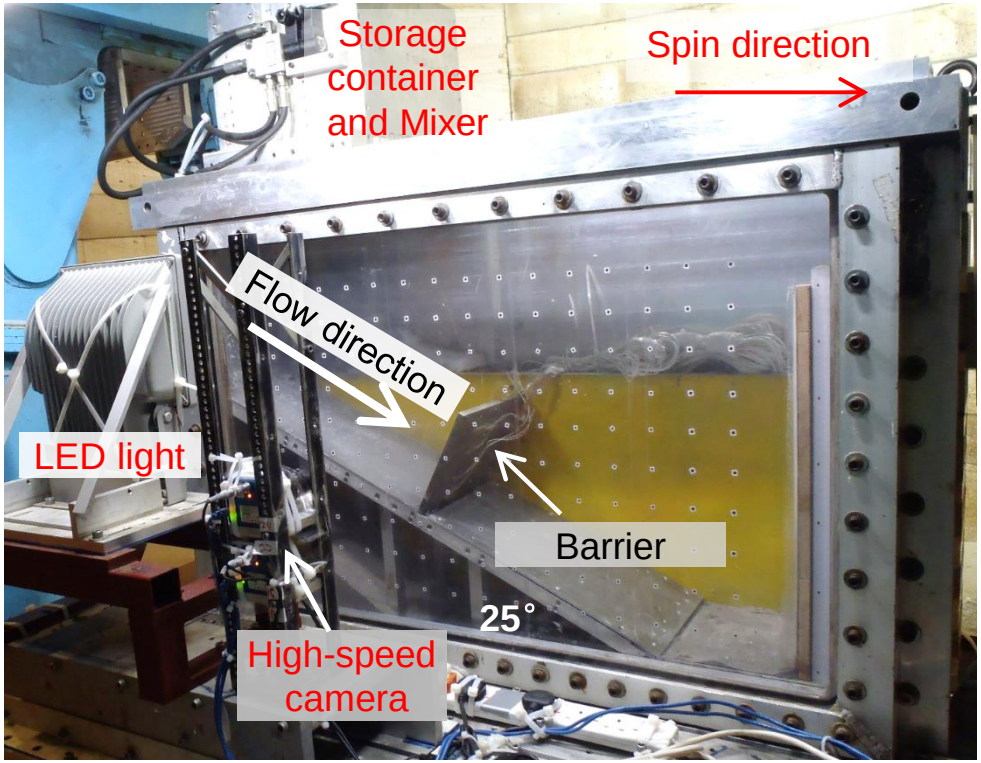

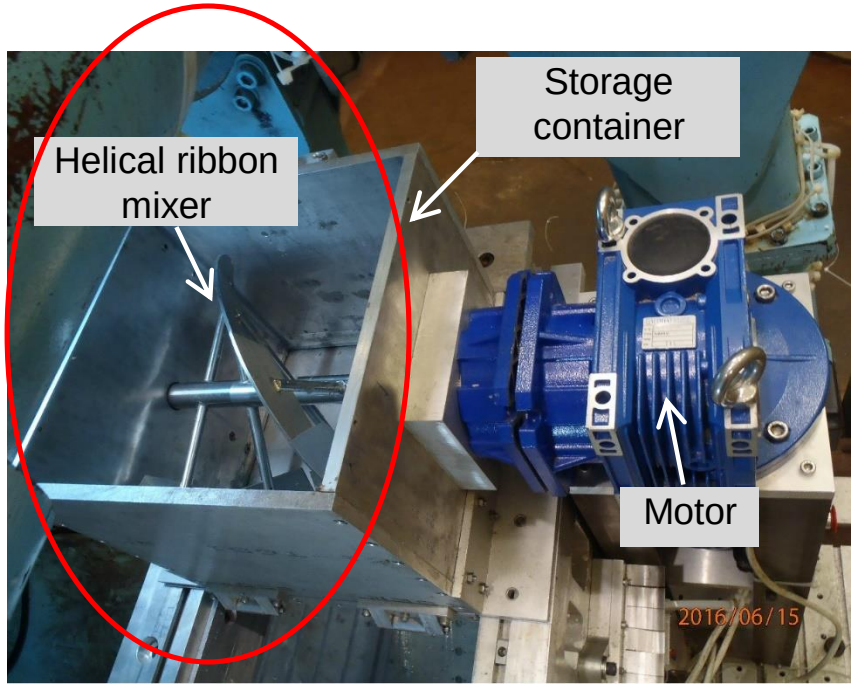

Scaled model materials in centrifuge tests

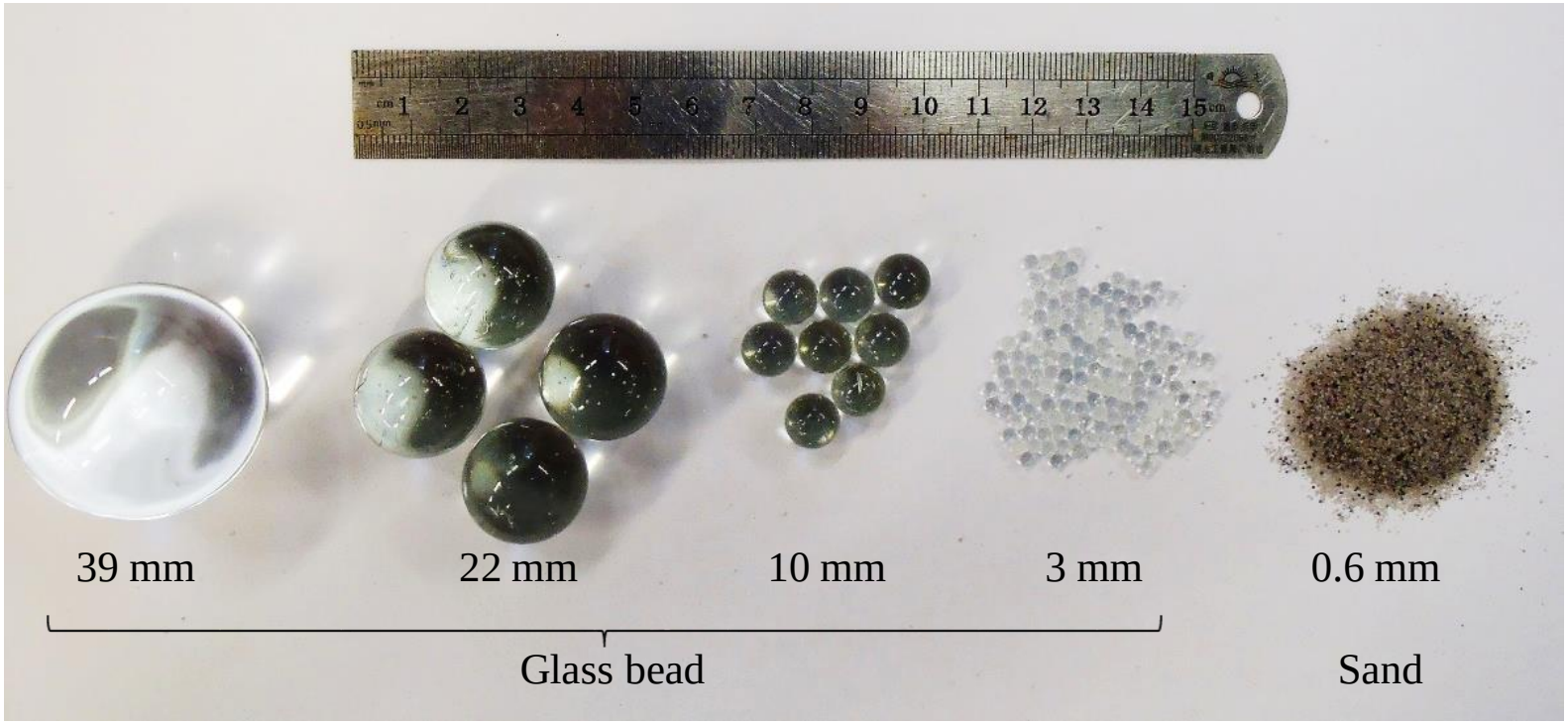

870 mm 490 mm 220 mm 70 mm 13 mm in *prototype*

Material	**Young's modulus *E* (GPa)**	**Poisson ratio *v***
Boulder (granite)	30-60	0.20-0.30
Concrete wall	26-38	0.30
Glass	60	0.25
Magnesium alloy	40	0.30

Influence of boulder size impacting **rigid** barrier

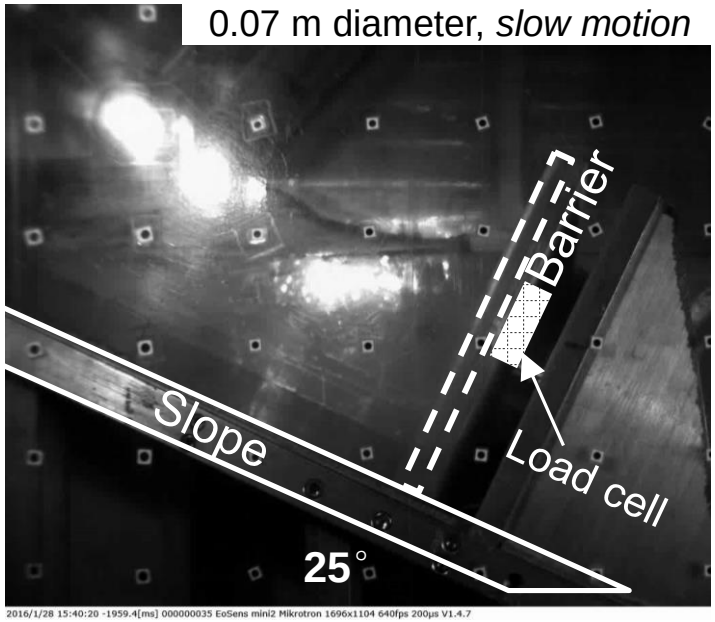

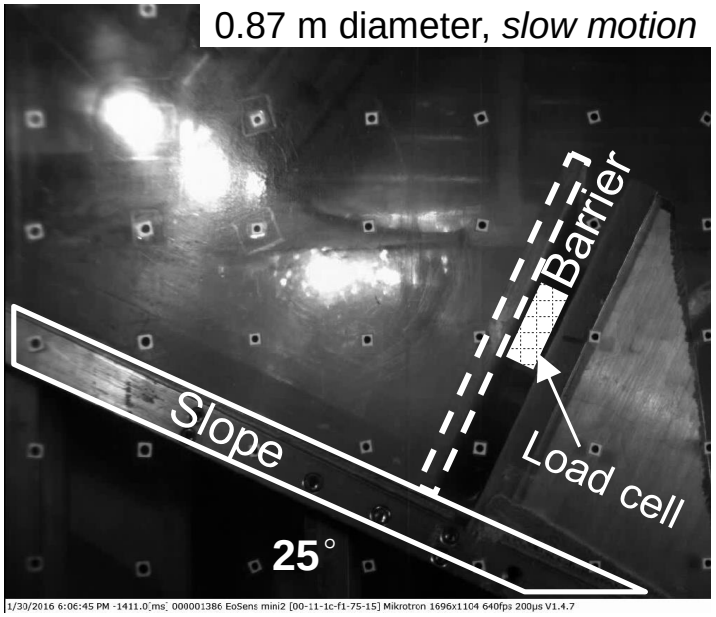

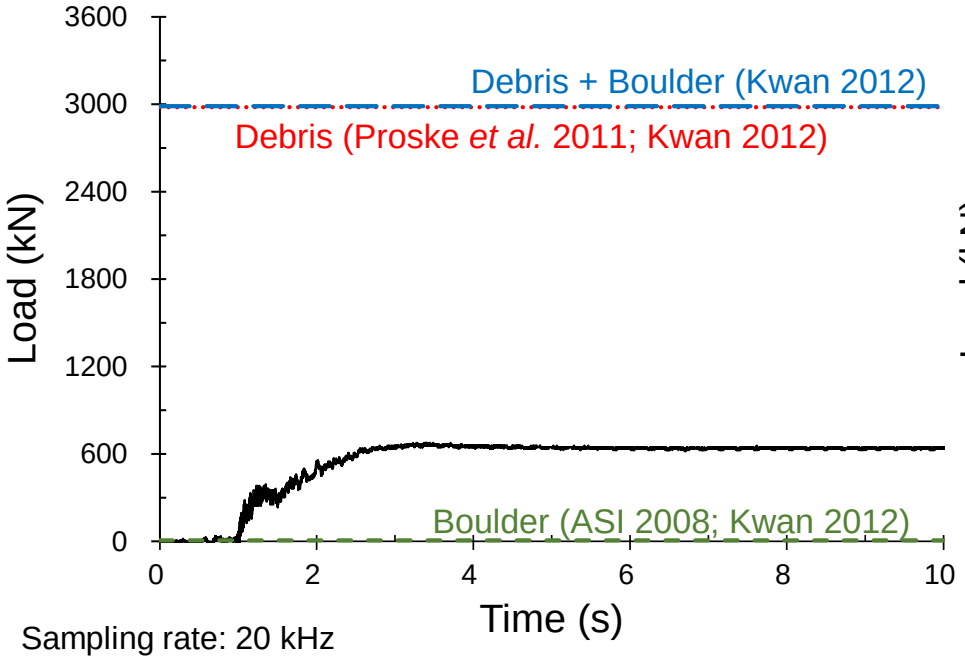

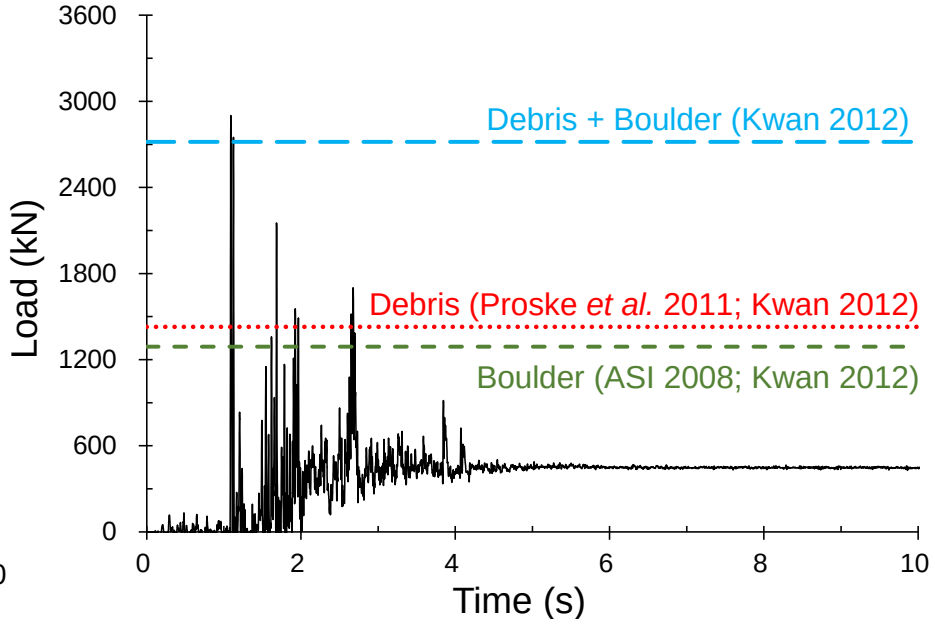

Sampling rate: 20 kHz

Boulders impacting **flexible** barrier

0.87 m diameter, *slow motion*

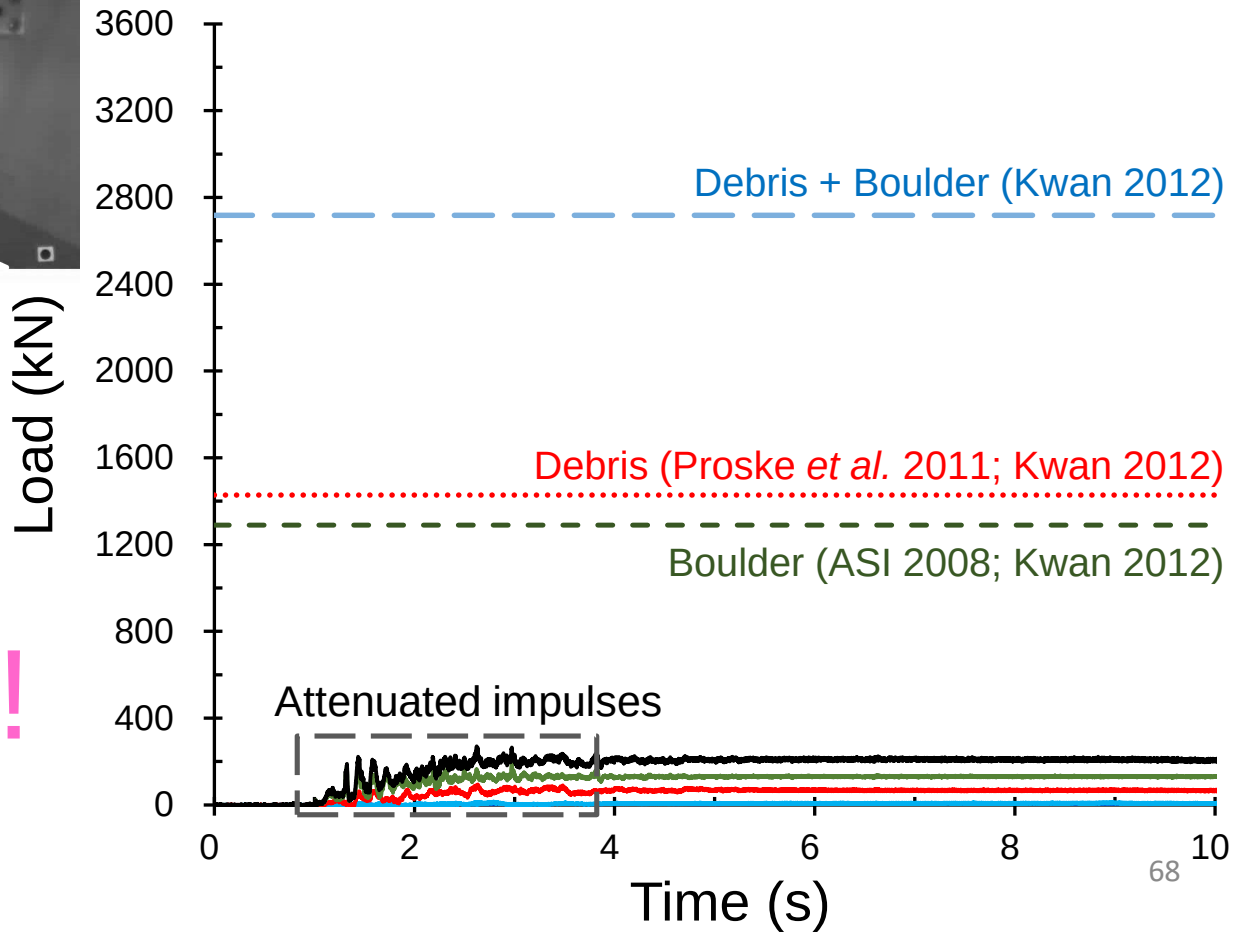

No Worry !

Effects of boulder size: dynamic response of rigid barrier

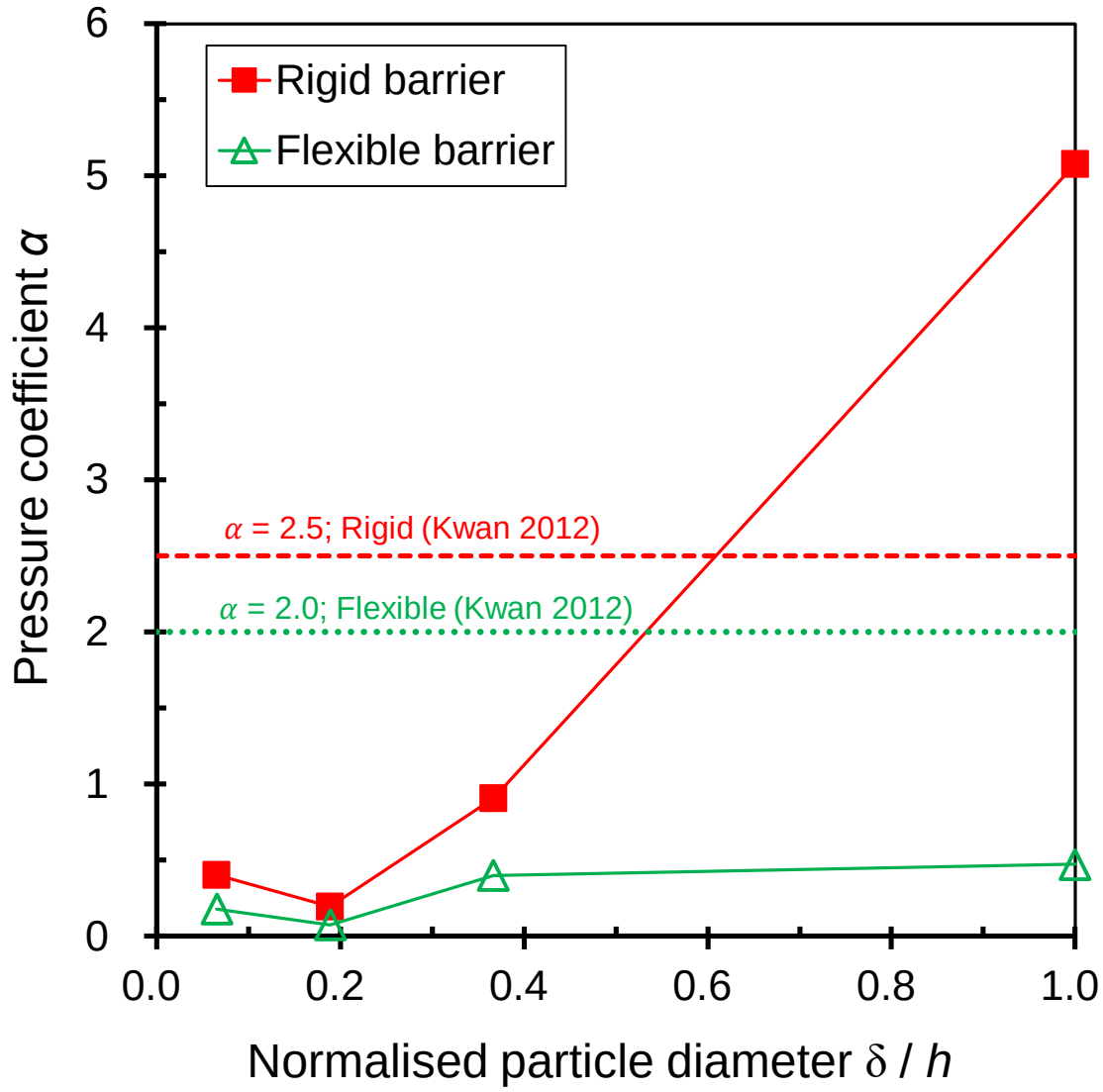

HKUST World-class 172 m Long Debris Flow Flume Facility

Dongchuan Debris Flow Observation and Research Station (DDFORS)

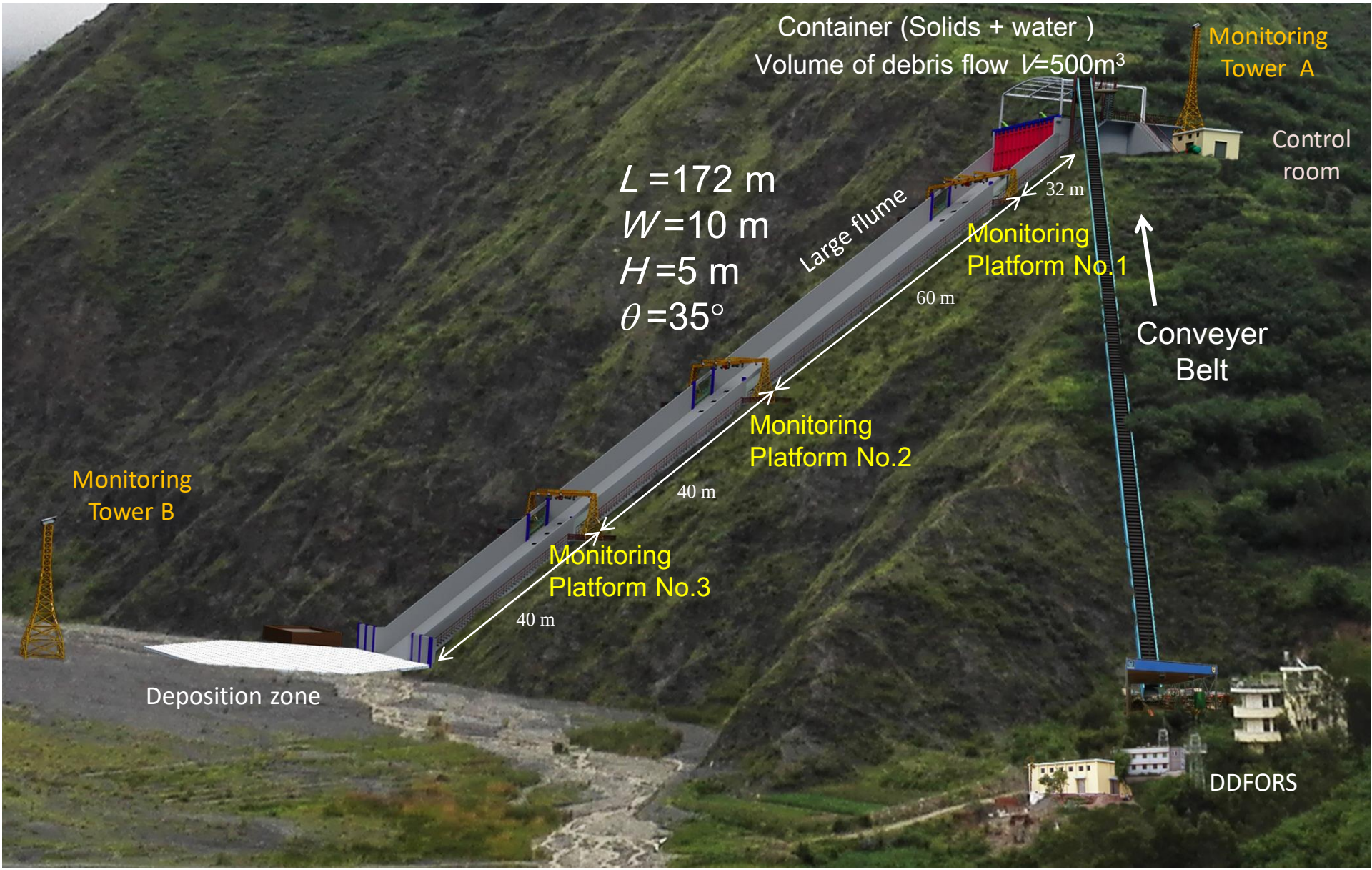

New developments and key findings

1. Ng, C.W.W., Choi, C.E., Cheung, D.K.H. & Cui, Y. (2018). Effects of dynamic fragmentation on the impact force exerted on rigid barrier: centrifuge modelling. *Canadian Geotechnical Journal*, https://doi.org/10.1139/cgj-2018-0092.
2. Ng, C.W.W., Song, D., Choi, C.E., Koo, C. H. & Kwan, J. S. H. (2017). A novel flexible barrier for landslide impact in centrifuge. *Géotechnique Letters*. Vol. 6, No. 3, 221–225.
3. Song, D., Ng, C. W. W., Choi, C. E., Kwan, J. S. H. & Koo, R. C. H. (2017). Influence of debris flow solid fraction on rigid barrier impact. *Canadian Geotechnical Journal.* Vol. 54, No. 10, 1421-1434.
4. Ng, C.W.W., Song, D., Choi, C.E., Liu, L.H.D., Kwan, J. S. H., Koo, R. C. H. & Pun, W. K. (2017). Impact mechanisms of granular and viscous flows on rigid and flexible barriers. *Canadian Geotechnical Journal.* Vol. 54, No. 2, 188-206.
5. Song, D., Choi, C. E. & Ng, C. W. W. (2017). Geophysical flows impacting a flexible barrier: effects of solid-fluid interaction. *Landslides*. Vol. 15, No. 1, 99-110.

(v) The Effects of Root Architecture on Slope Stability

香港科技大學
THE HONG KONG UNIVERSITY OF SCIENCE AND TECHNOLOGY

Contribution of vegetation on slopes

Hydrological behavior

Suction retained by plants

1. Increase shear strength
2. Reduce water permeability

Mechanical behavior

Root reinforcement

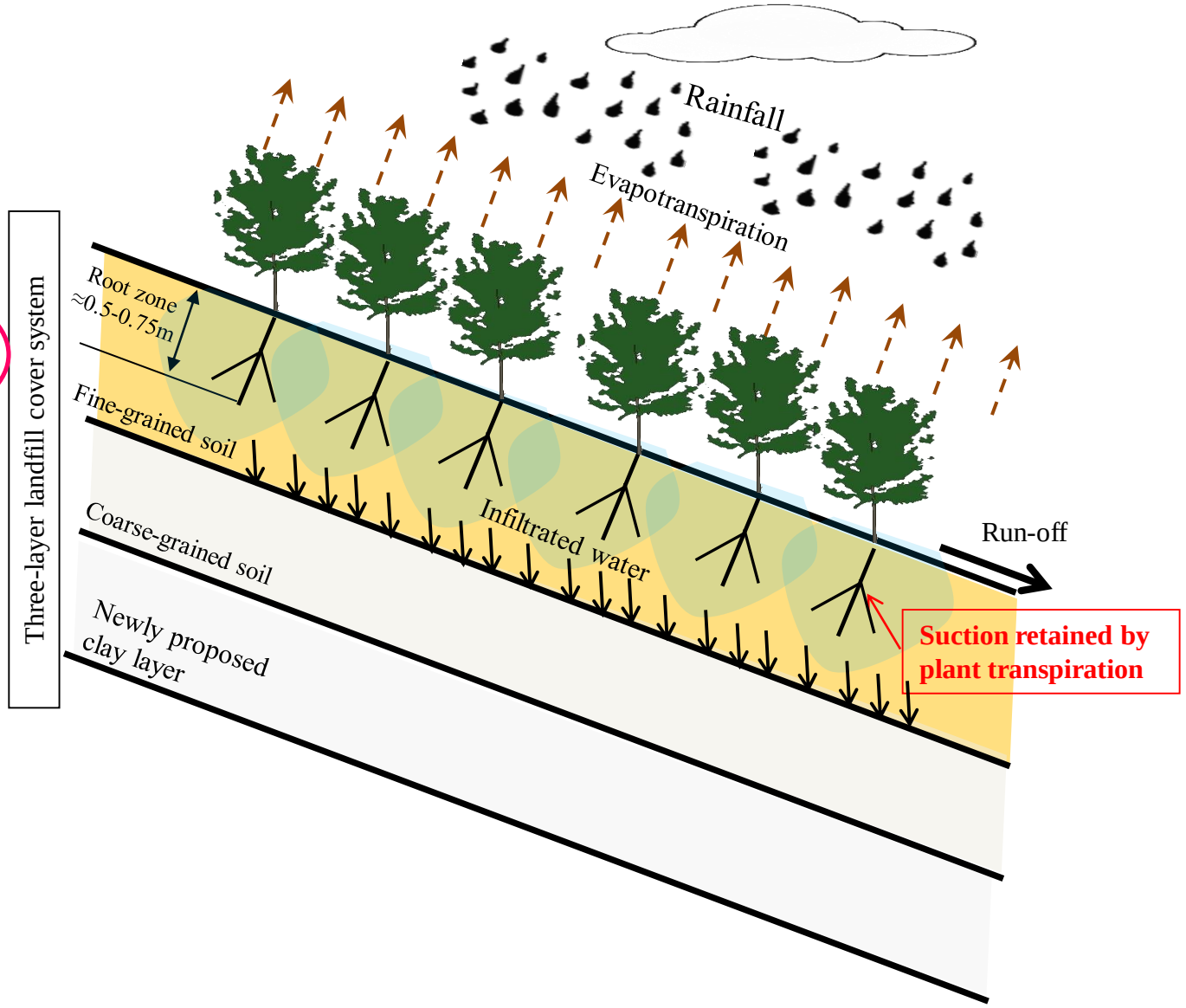

Permeability functions of water in vegetated soils

- Transpiration of plants increases soil suction, resulting in lower water permeability and hence smaller infiltration

Darcy' law

$$v = -k_w i$$

Velocity of water flow | Permeability | Hydraulic gradient

where

Void ratio | Degree of saturation | Water content | Specific gravity

$$k_w = f(e, S_r) \qquad S_r = \frac{wG_s}{e}$$

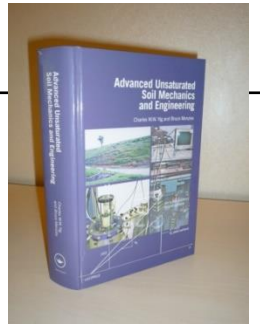

Principle and properties of novel root model

Hydrological effects

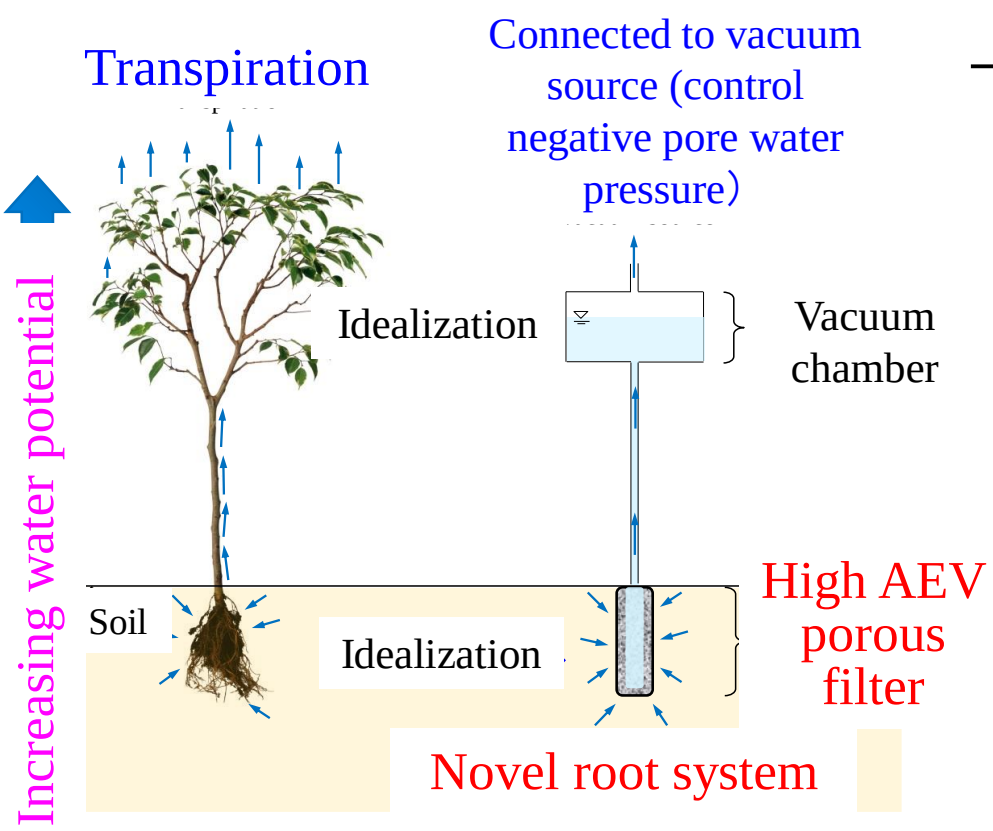

Mechanical reinforcement

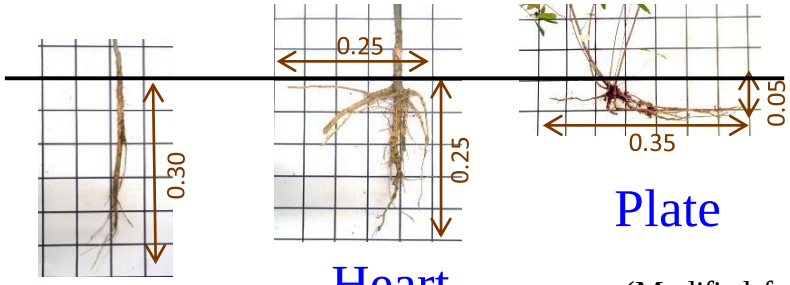

(Modified from Leung, 2014)

Connected to vacuum system

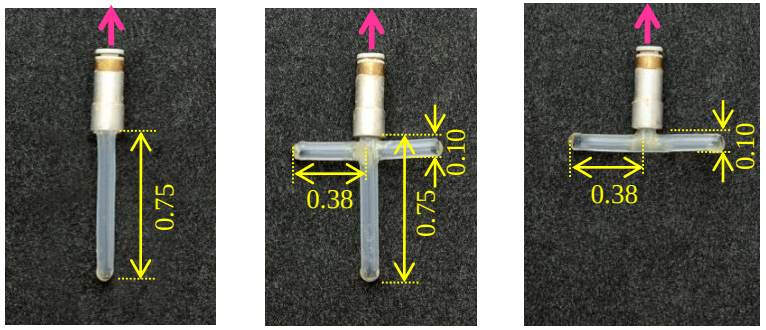

All dimensions are in prototype

References

1. Ng, C. W. W., Kamchoom, V., Leung, A.K. and Jie, Q., Active control of water transport to simulate plant transpiration, CN Patent No. 201310328055.0 (in Chinese)
2. Ng, C.W.W., Leung, A.K., Kamchoom, V., and Garg, A., 2014, "A Novel Root System for Simulating Transpiration-Induced Soil Suction in Centrifuge," Geotechnical Testing Journal, Vol. 37, No. 5, pp. 1–15, doi:10.1520/GTJ20130116. ISSN 0149-6115

Basic properties of the novel root model

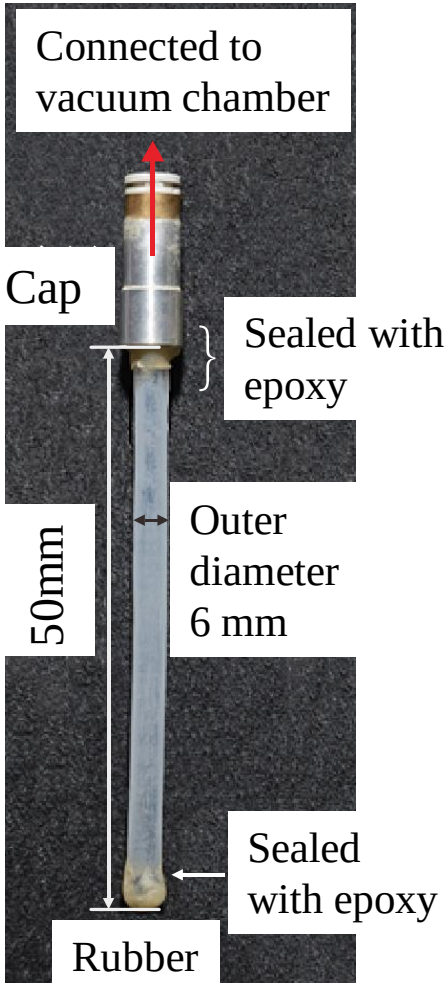

Material: cellulose acetate
（AEV：100 kPa）

Parameters for root model

Variable	Dimensions	Model scale
Geometry of root model		
Length	L	50 mm
Outer diameter	L	6 mm
Inner diameter	L	4 mm
Cross-section area（A）	L^2	1.6×10^{-5} m^2
Inertia（I）	L^4	5.1×10^{-11} m^4
Property of root model		
Tensile strength	M/LT^2	3.1×10^4 kPa
Elastic modulus（E）	M/LT^2	8.3×10^4 kPa
Axial rigidity（EA）	ML/T^2	1.3 kPa·m^2
Flexual rigidity（EI）	ML^3/T^2	4.2×10^{-6} kPa·m^4
AEV of filter	M/LT^2	100 kPa
Permeability of filter	L/T_{diff}	2×10^{-6} m/s

Verification of root water uptake by root model at 1 g

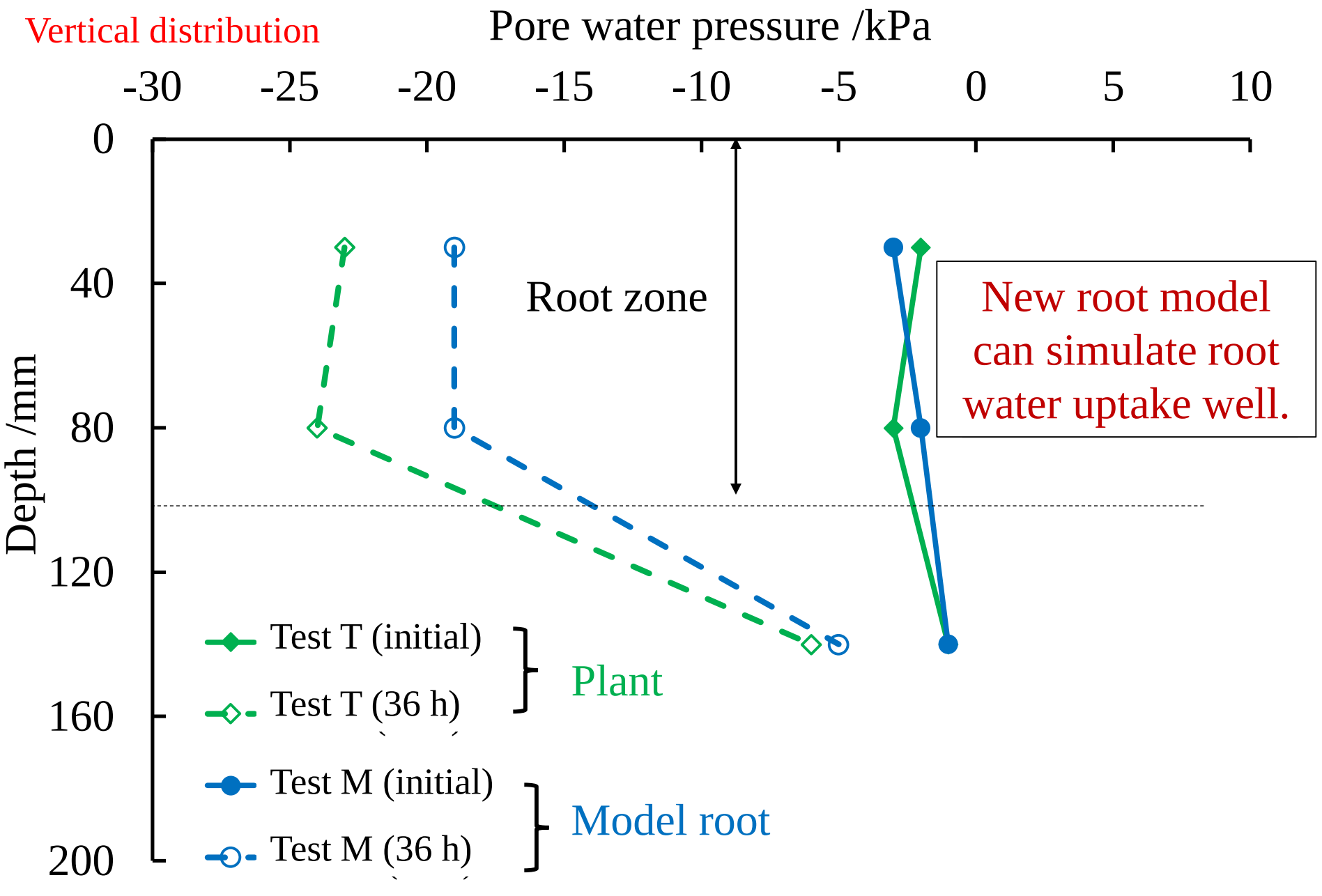

Modelling of root-soil interface property

measured model root-soil interface strength in direct shear box

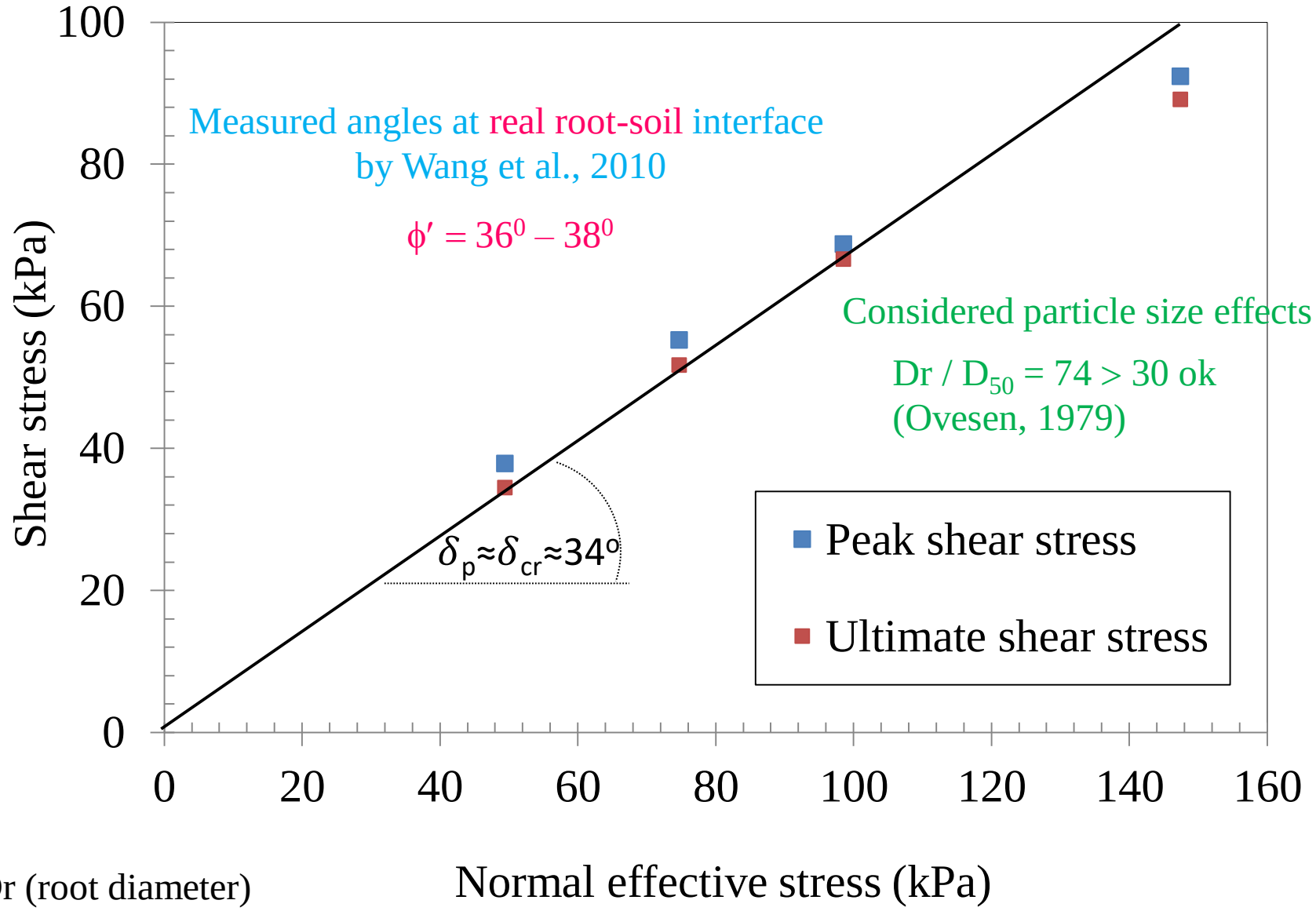

Dr (root diameter)
D_{50} of soil

Effects of root geometry and transpiration on pull-out resistance at 15g

Kamchoom, V., Leung, A.K. & Ng, C.W.W. (2014). Effects of root geometry and transpiration on pull-out resistance. *Géotechnique Letters*. 4, 330-336.

A summary of scaling factors relevant to this study (Ng et al. 2015)

Physical quantity	Dimension	Scaling factor (model/prototype)	Model scale	Prototype scale*
Geometry of artificial root				
Length	L	1/N	50 mm	750 mm
Outer diameter	L	1/N	6 mm	90 mm
Inner diameter	L	1/N	4 mm	60 mm
Cross-section area (A)	L^2	$1/N^2$	$1.6x10^{-5}$ m^2	$3.5x10^{-3}$ m^2
Second moment of inertia (I)	L^4	$1/N^4$	$5.1x10^{-11}$ m^4	$2.6x10^{-6}$ m^4
Material property of artificial root				
Tensile strength of artificial root (s_t)	M/LT^2**	1	$3.1x10^4$ kPa	$3.1x10^4$ kPa
Elastic modulus of artificial root (E)	M/LT^2	1	$8.3 x10^4$ kPa	$8.3 x10^4$ kPa
Axial rigidity (EA) of taproot component	ML/T^2	$1/N^2$	1.3 kPa*m^2	$2.9 x10^2$ kPa*m^2
Flexural rigidity (EI) of horizontal root branch	ML^3/T^2	$1/N^4$	$4.2x10^{-6}$ kPa*m^4	$2.2x10^{-1}$ kPa*m^4
Air-entry value of filter	M/LT^2	1	100 kPa	100 kPa
Hydraulic conductivity of filter	L/T_{diff}**	N	$2 x 10^{-6}$ m/s	$1.3 x 10^{-7}$ m/s
Soil-atmosphere interface				
Rainfall intensity***	L/T_{diff}	N	1050 mm/hr	70 mm/hr
Seepage				
Water flow rate**	L^3/T_{diff}**	1/N	Depend on measurements	
Hydraulic conductivity **	L/T_{diff}**	N		
Hydraulic gradient**	Unitless	1		
Suction****	M/LT^2	1		

* Prototype scale at g-level of 15 (i.e., $N = 15$)

**Time for dynamic condition (T) is scaled by $1/N$, whereas time for diffusion (T_{diff}) is scaled $1/N^2$

*** According to Taylor (1995)

**** According to Dell'Avanzi et al. (2004)

Comparison of RAR between artificial and plant roots

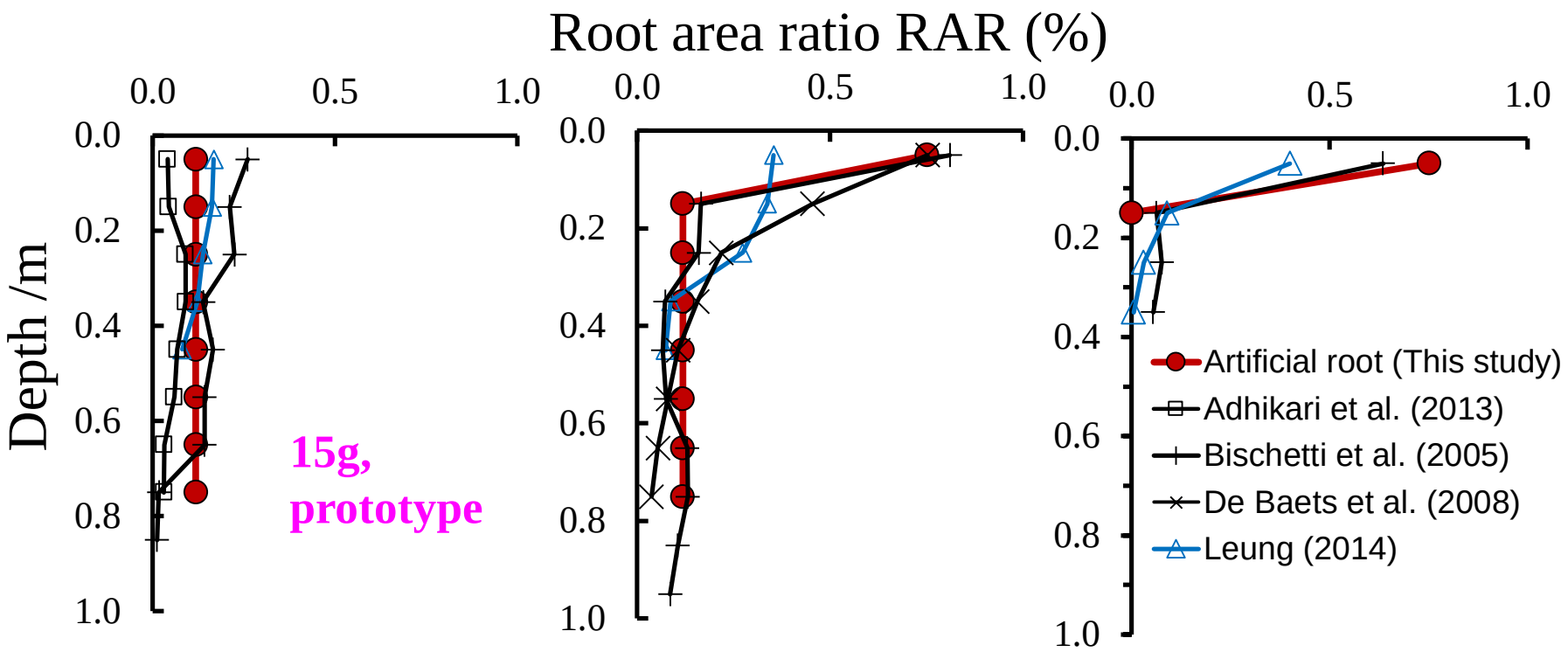

Tap

Heart

Plate

Centrifuge model package and instrumentation

Plan view

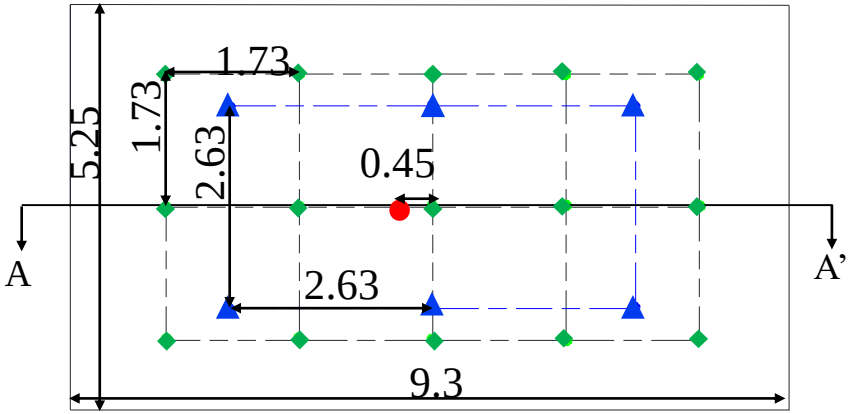

- Artificial root
- Nozzle
- Pore pressure transducer (PPT)
- Load cell

Cross-section view

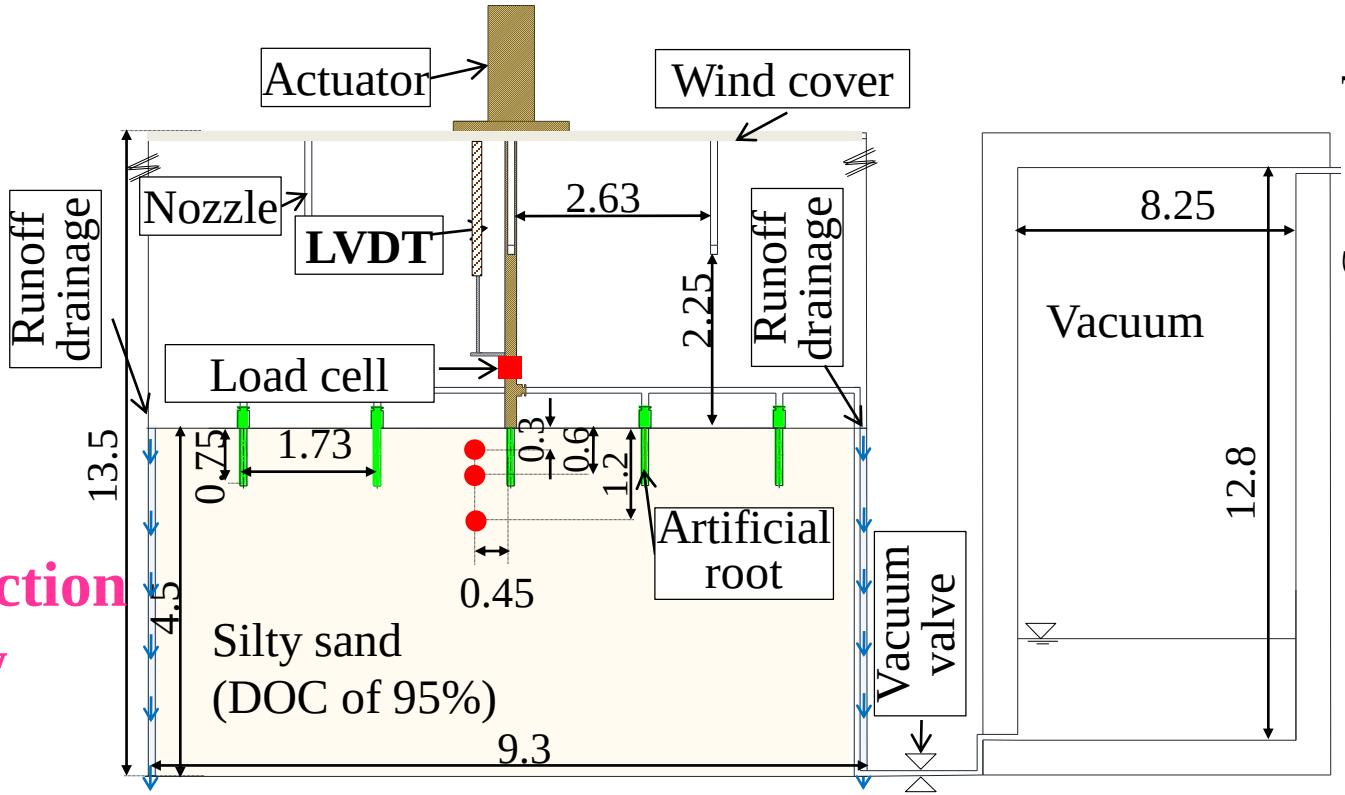

All dimension are in prototype: m

Measured pore water pressure (PWP) after two rainfall events

1. 70mm/hr for 2 hrs - 10 years of return period (T_2)
2. 70mm/hr for 8 hrs - 1000 years of return period (T_8)

At 15g

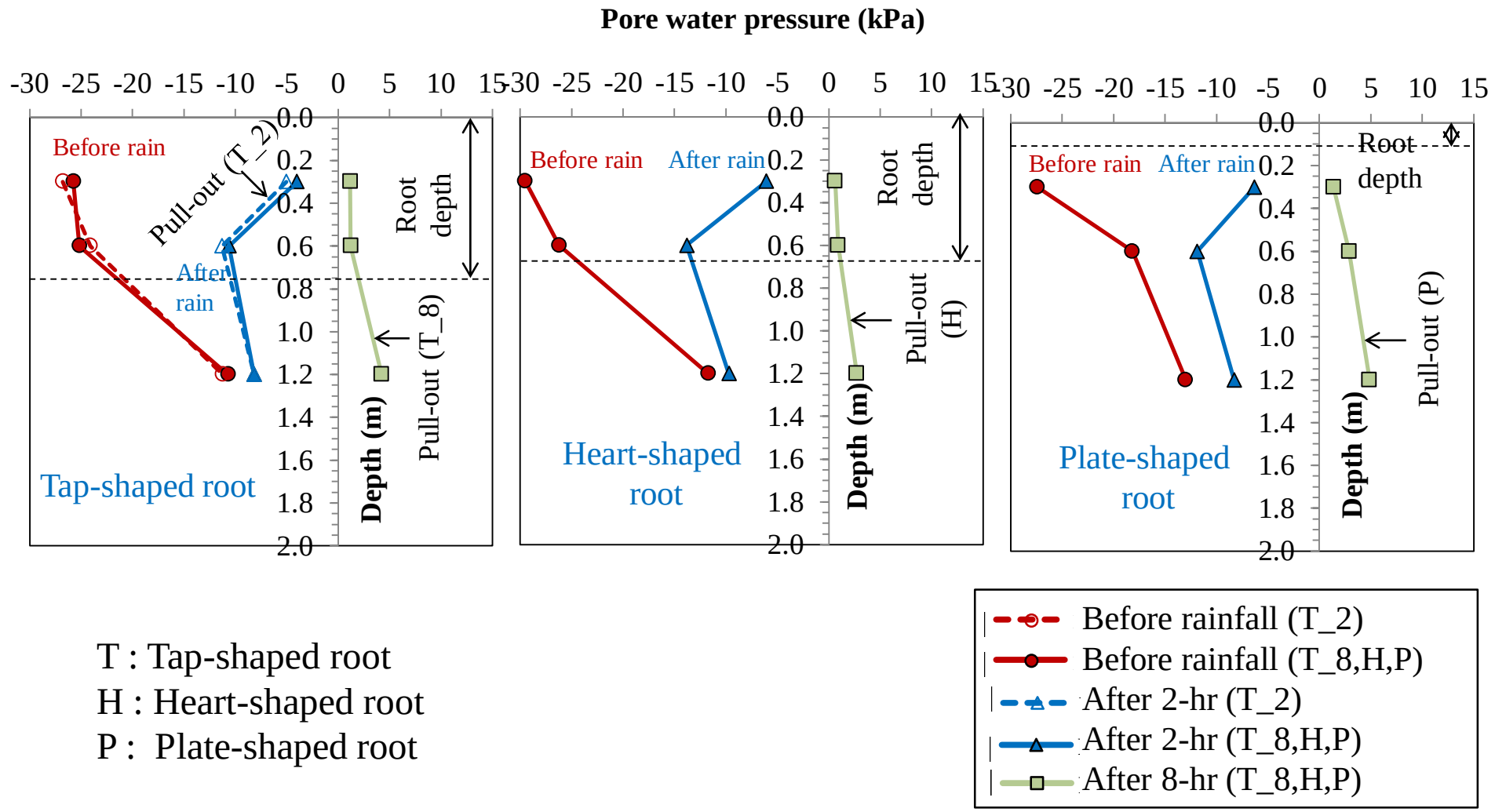

T : Tap-shaped root
H : Heart-shaped root
P : Plate-shaped root

Effects of rainfall duration on pullout resistance for Tap roots roots

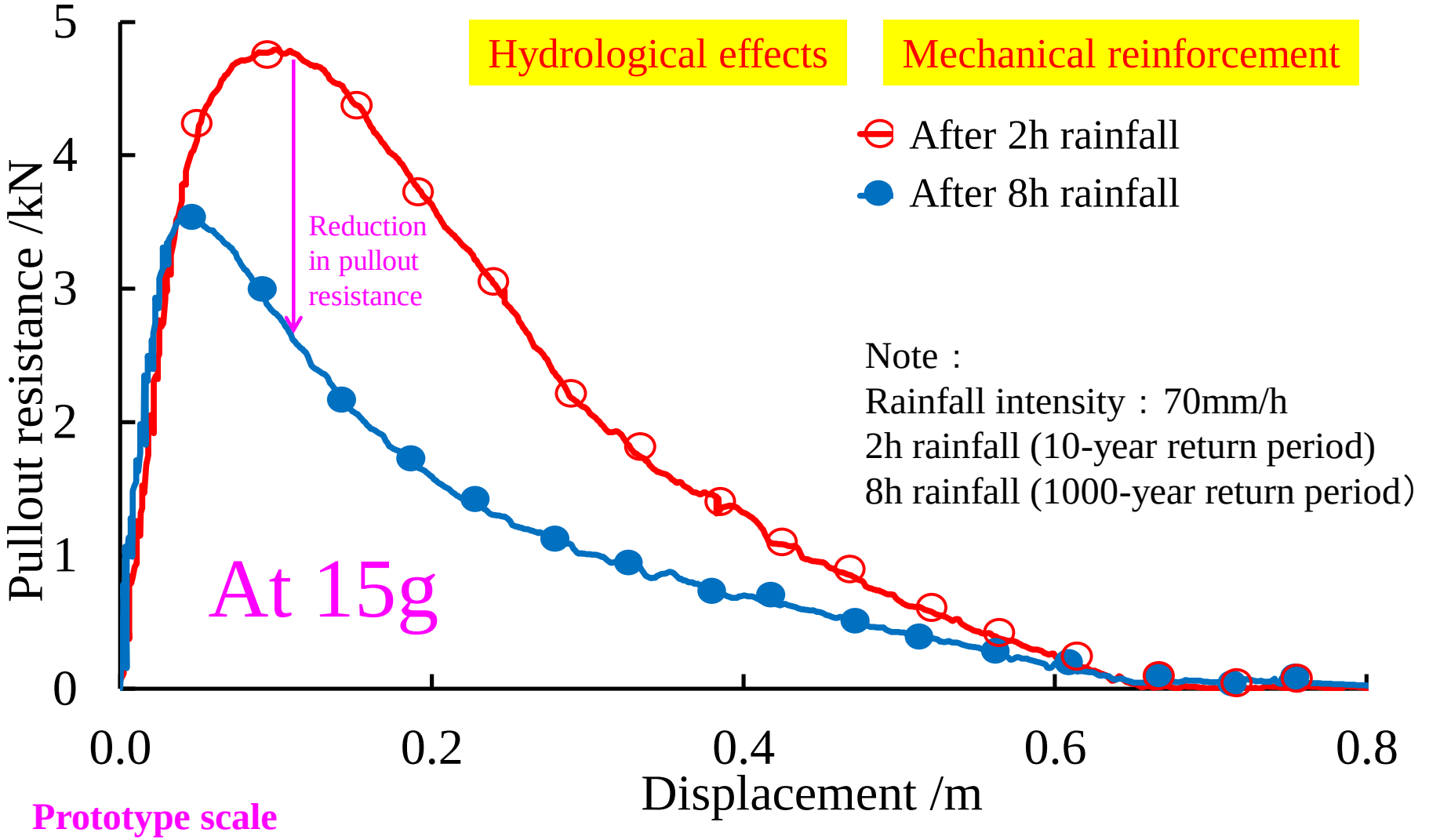

Pullout resistance of tap roots after 2h rainfall is 1.33 times that after 8h rainfall

Effects of root architecture on pullout resistance (after 8h rainfall)

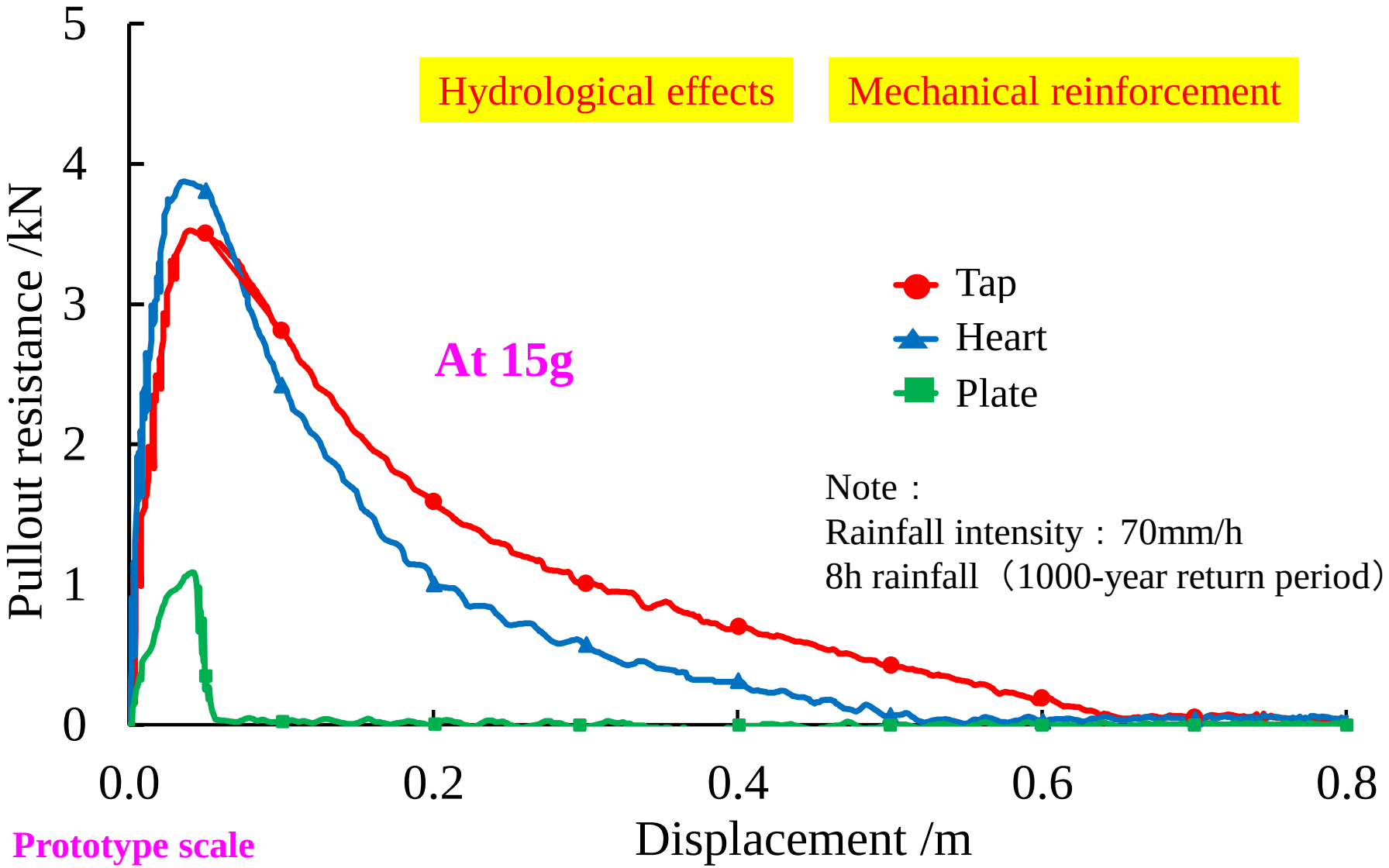

Peak pullout force: Heart（3.9 kN）> Tap (3.5 kN) > Plate（1.0 kN）

Centrifuge modelling of effects of root architecture on pore water pressure and slope stability (45^{o})

- Ng, C.W.W., Leung, A.K., Yu, R. & Kamchoom, V. (2017). Hydrological effects of live poles on transient seepage in an unsaturated soil slope: centrifuge and numerical study. *Journal of Geotechnical and Geoenvironmental Engineering, ASCE*, Vol. 143, No. 3, 04016106.
- Ng, C. W. W., Kamchoom, V. & Leung, A. K. (2016). Centrifuge modelling of the effects of root geometry on the transpiration-induced suction and stability of vegetated slopes. *Landslides*. Vol. 13, No. 5, 1-14.
- Kamchoom, V., Leung, A.K. & Ng, C.W.W. (2014). Effects of root geometry and transpiration on pull-out resistance. *Géotechnique Letters*, Vol. 4, No. 4, 330-336.

Centrifuge model setup and instrumentation

Completely decomposed granite (CDG, silty sand): $\varphi' = 38^{o}$

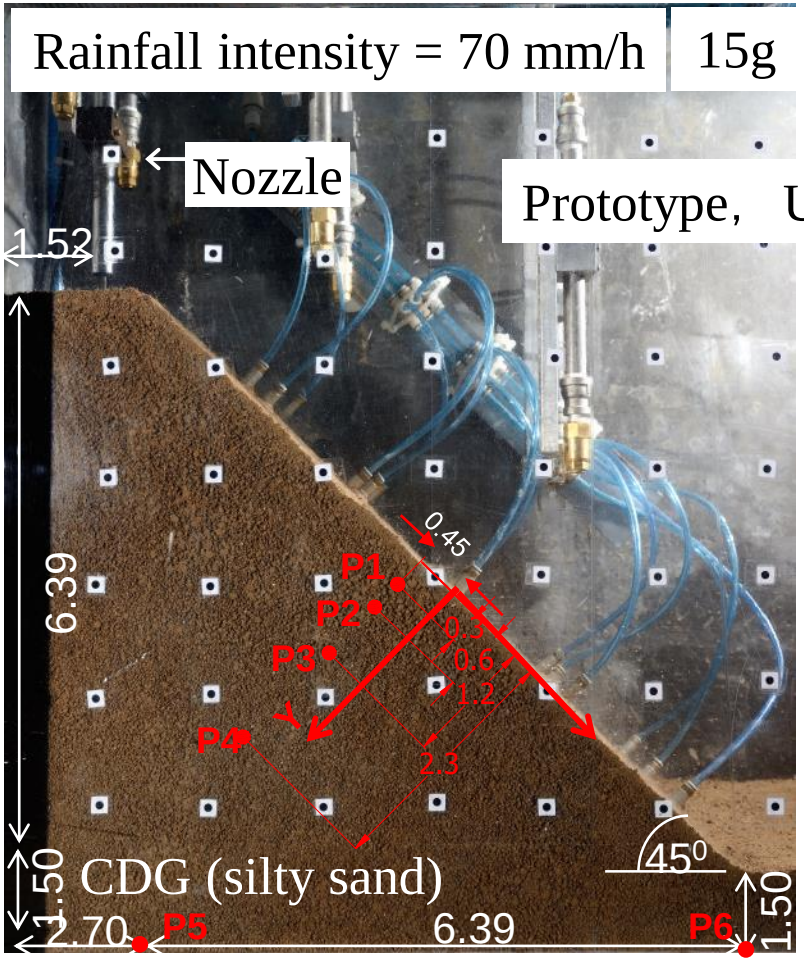

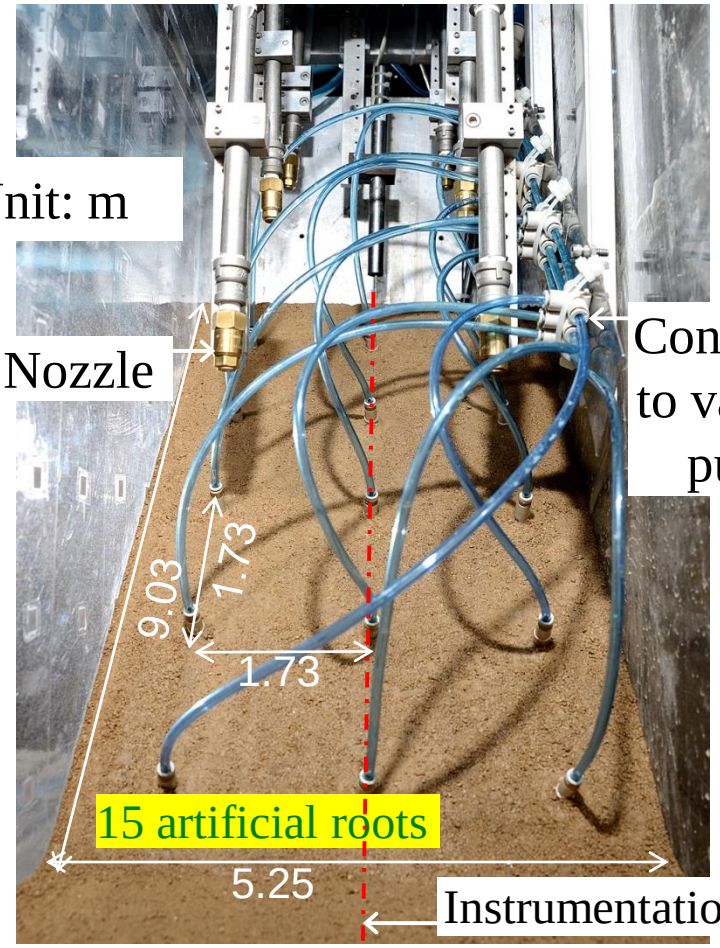

Pore pressure transducer

Side view

Plan view

Typical finite element mesh and boundary conditions (seepage analysis)

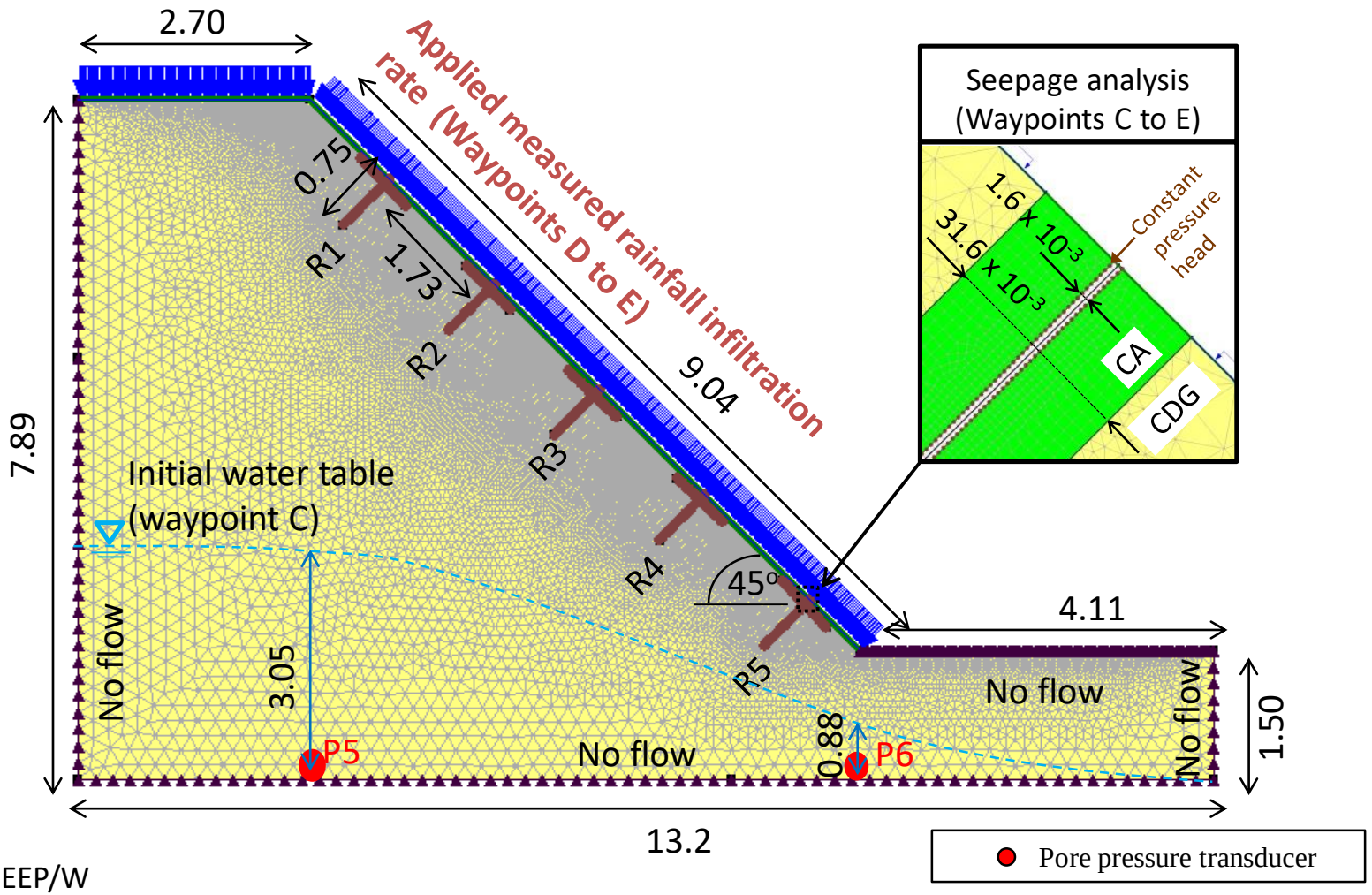

- **Software:** SEEP/W
- **Model geometry and boundary conditions:** identical to that in each centrifuge test
- **Governing equations:** Richard's equation with fitted SWRC & predicted HCF (Van Genuchten 1980)

(all dimensions are in meters and in prototype scale)

Factor of safety (FOS) for slopes with different root architectures

(using the strength reduction method in FE analyses)

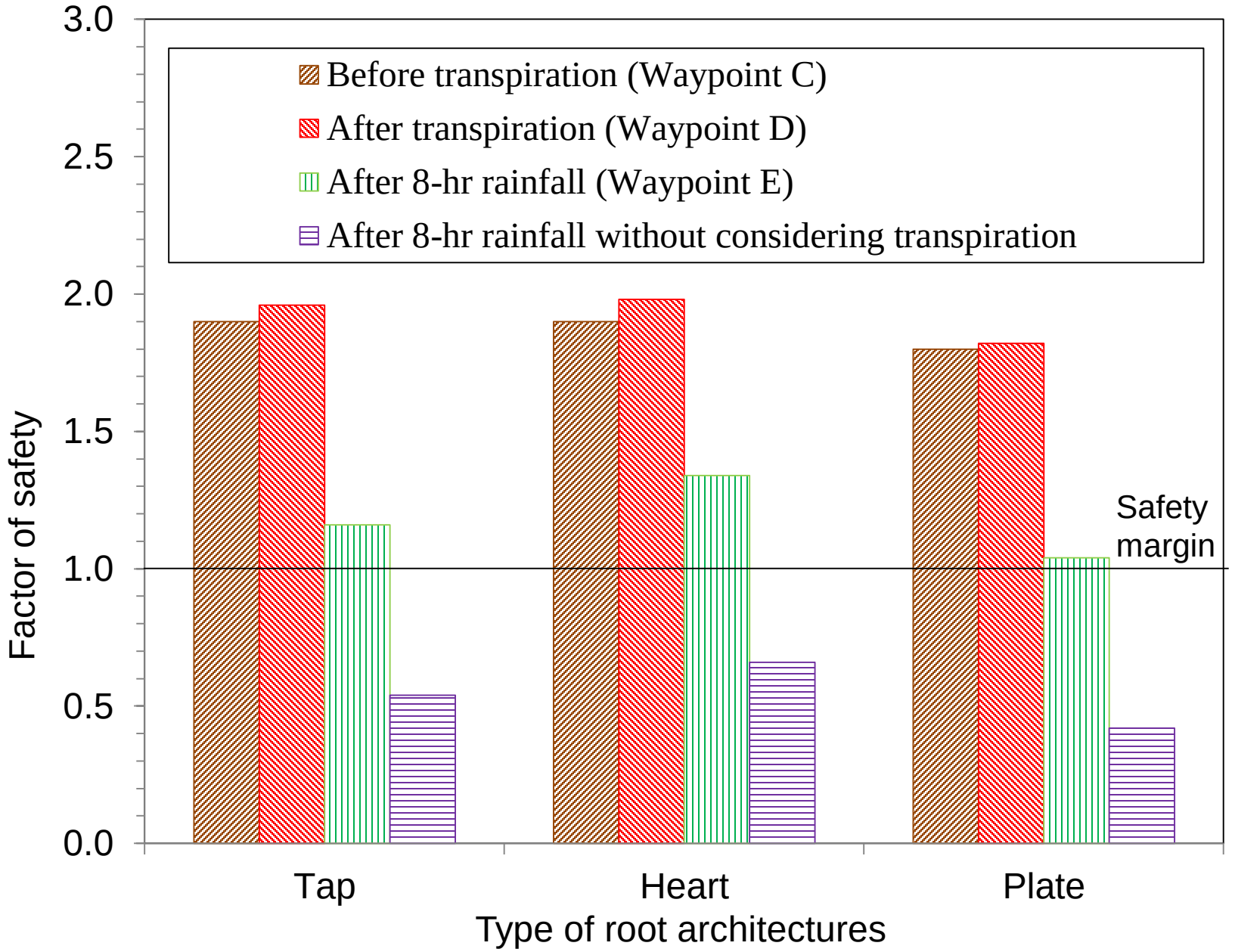

Summary of findings for (45^0 Slope)

1. Mechanical and hydraulic effects of roots can be simulated in centrifuge
2. Root architecture has strong influence on suction distributions
3. Heart-shaped roots create highest suctions within root zone
4. Due to shallow depth (0.1m) of plate-shaped roots, suction cannot be retained after heavy rainfall
5. No failure can be identified from centrifuge tests and numerical simulations in all three vegetated slopes
6. Heart-shaped roots result in the highest FOS, 16% and 28% higher than that reinforced by the tap- and plate-shaped roots, respectively (after 70mm rainfall for 8 hrs or 1 in 1,000 years of return period)

Failure mechanisms of a 60^0 vegetated slope with different root geometries: centrifuge modelling

Failure mechanism during rainfall (60-degree/Tap)

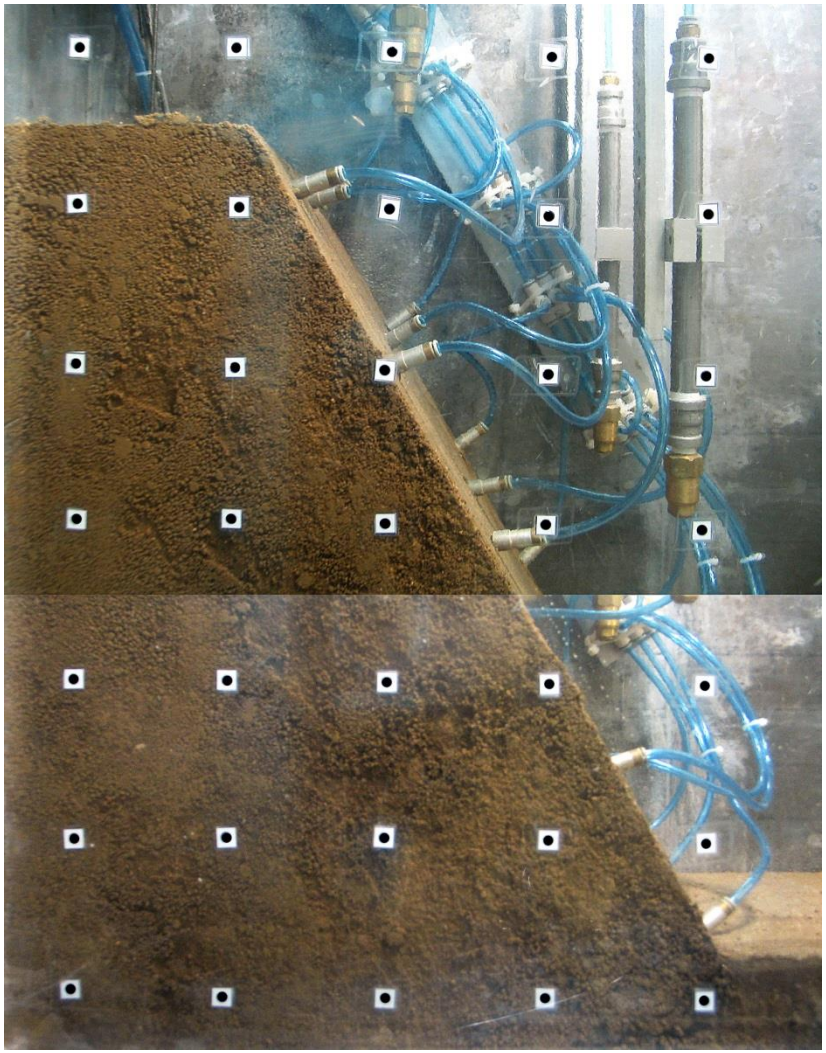

Before rainfall

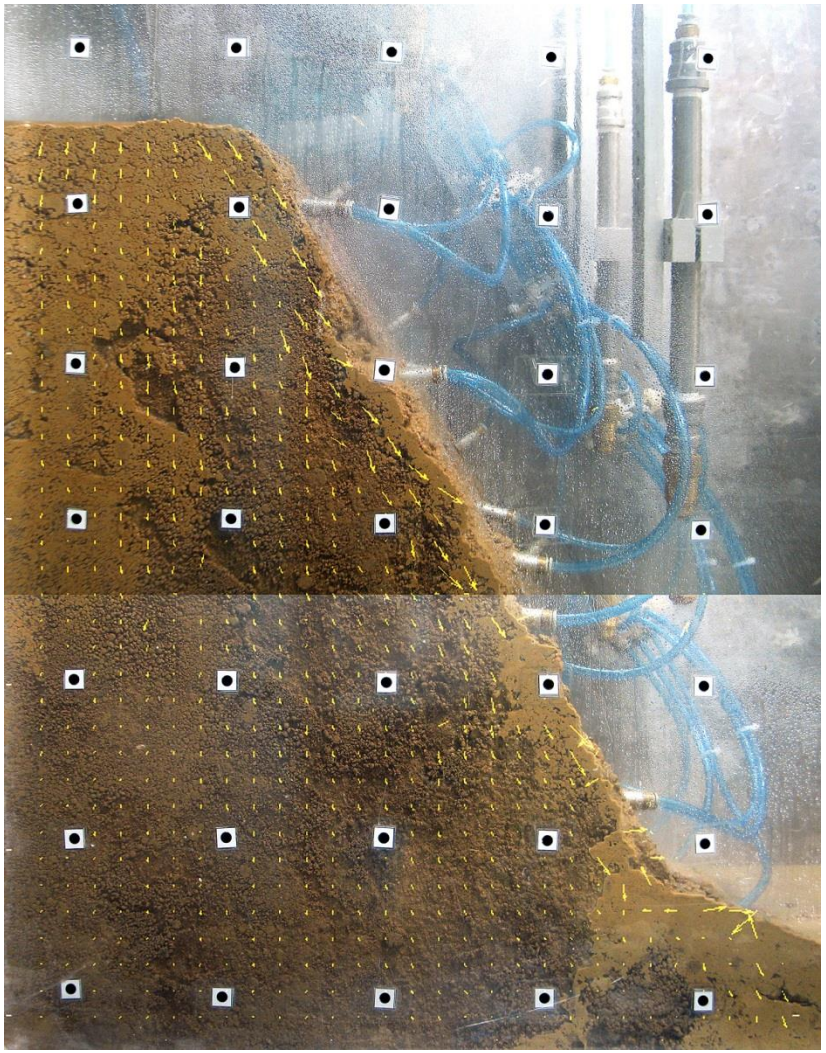

1 hour after rainfall

Failure mechanism during rainfall (60-degree/Tap)

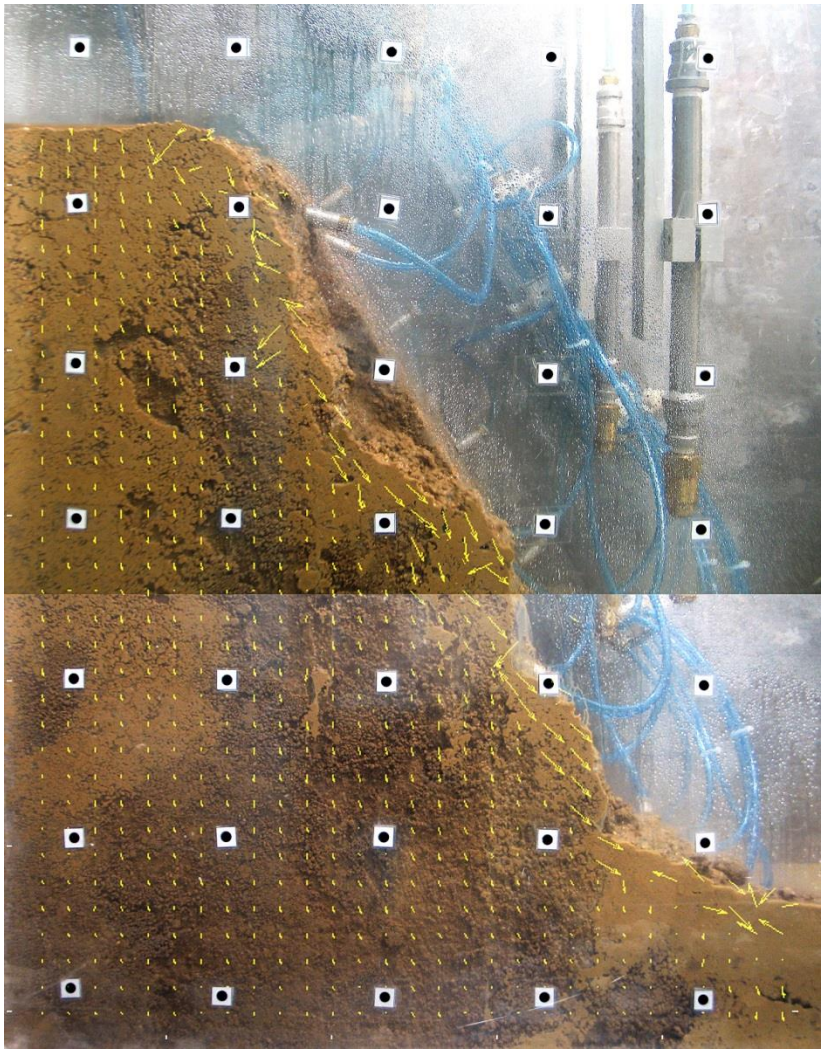

2 hours after rainfall
(equivalent to 10-year return period)

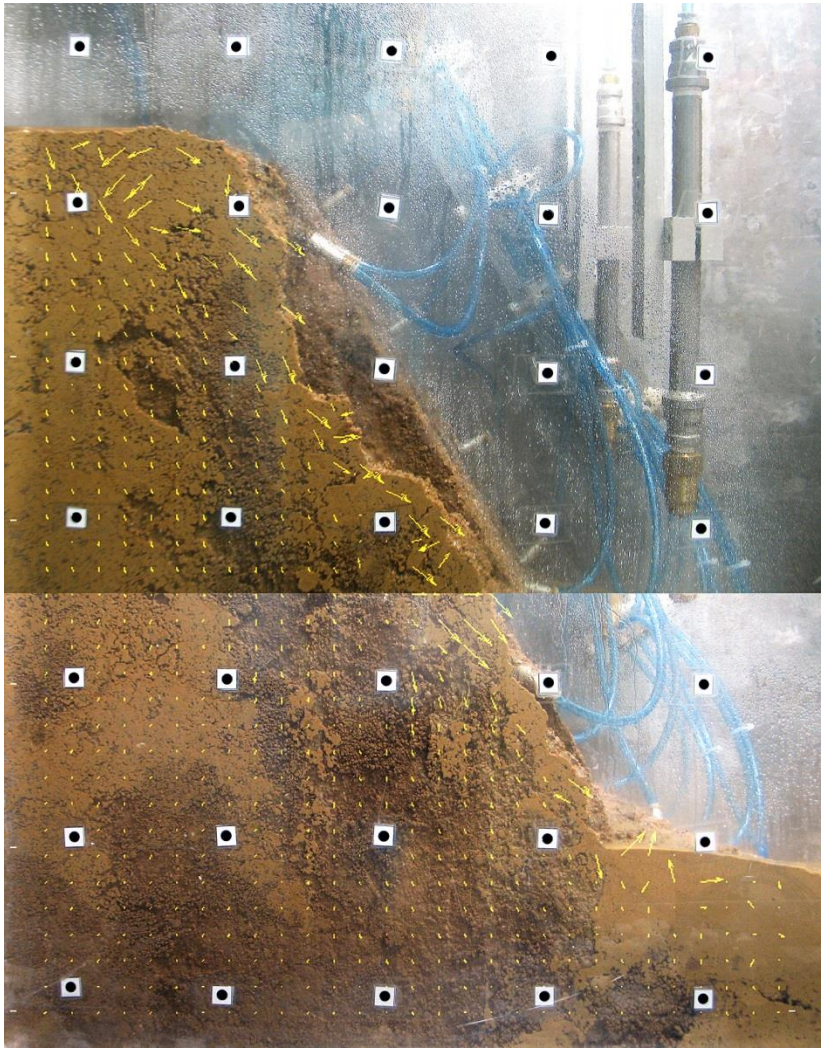

3 hours after rainfall

Failure mechanism during rainfall (60-degree/Tap)

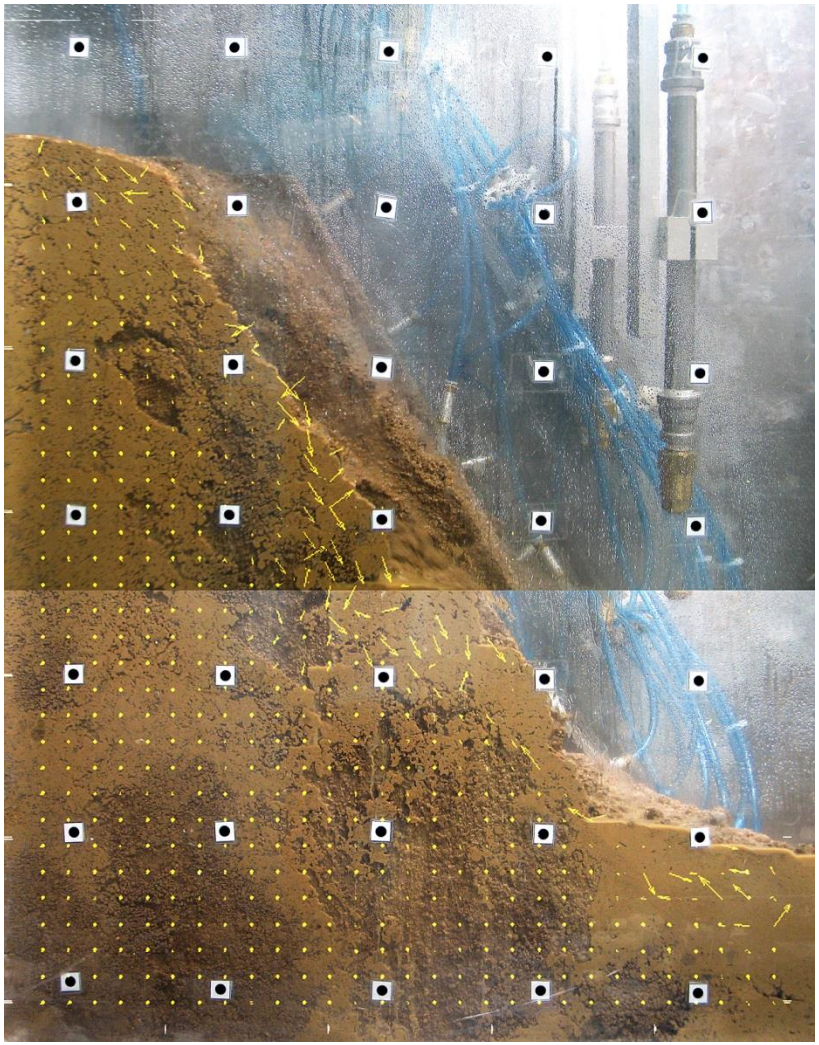

4 hours after rainfall
(equivalent to 100-year return period)

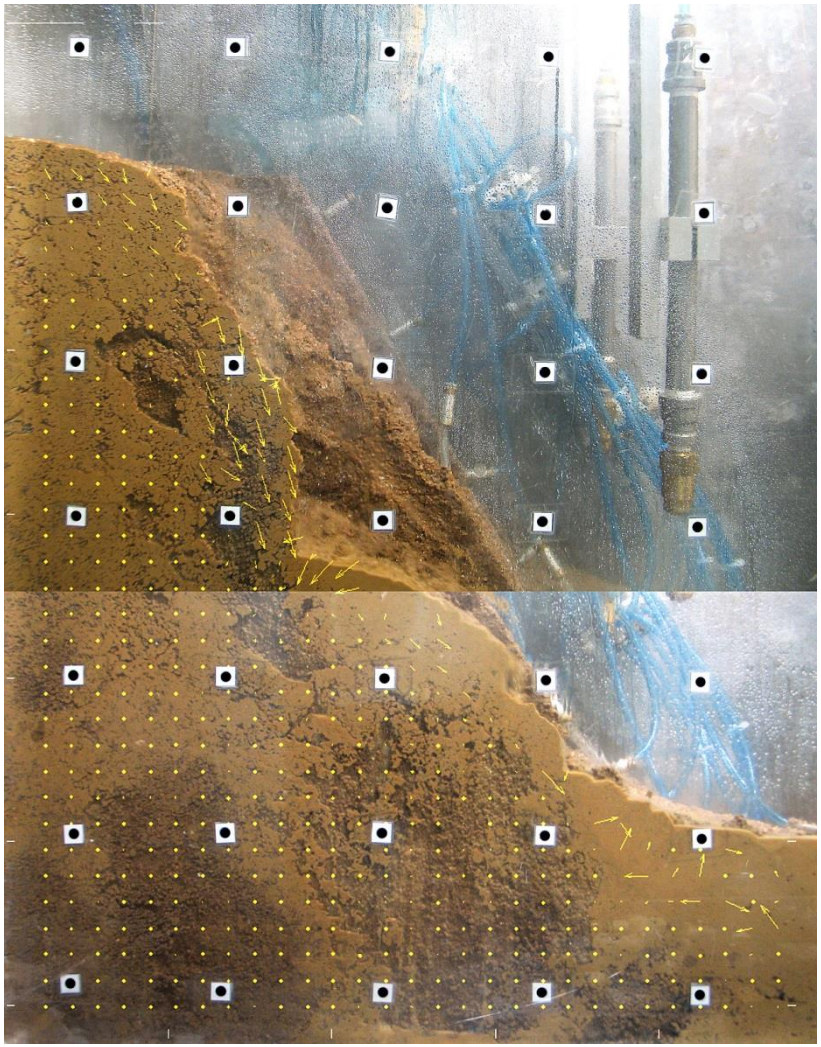

5 hours after rainfall

Failure mechanism during rainfall (60-degree/Tap)

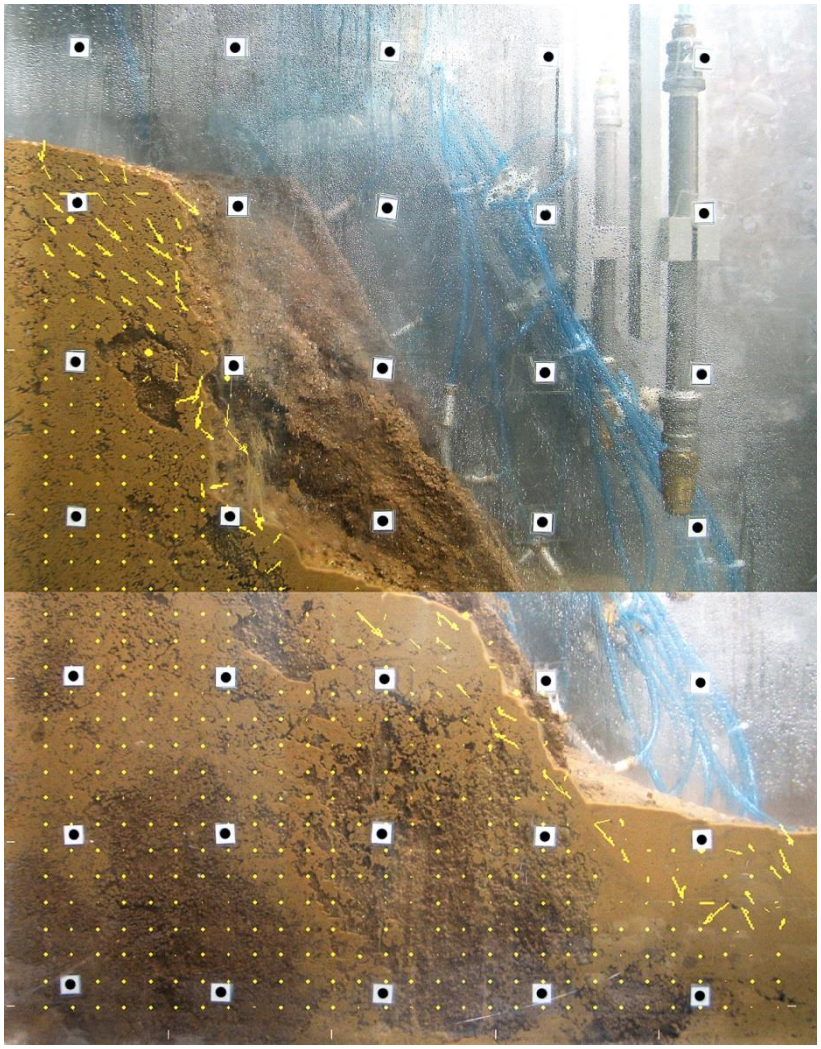

6 hours after rainfall
(equivalent to 200-year return period)

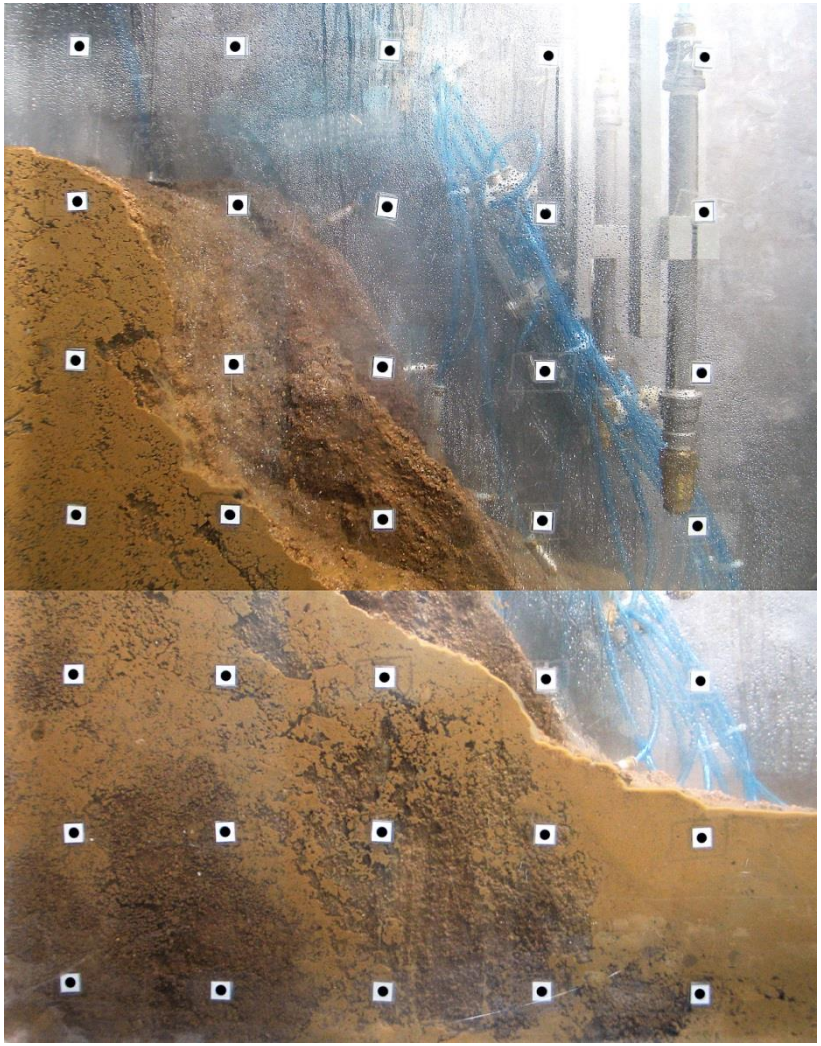

8 hours after rainfall
(equivalent to 1000-year return period)

Comparison of post-failure conditions of 60^0 slope (Tap- vs Heart-shaped roots

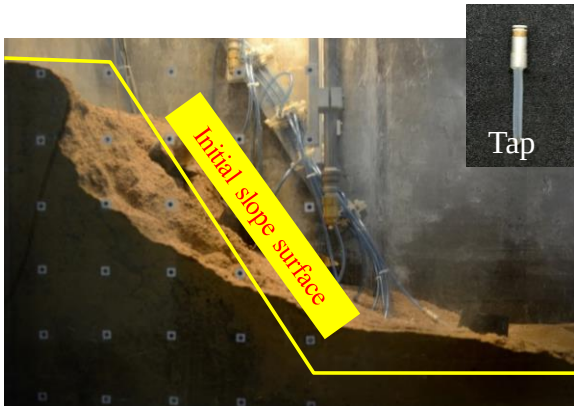

(a)

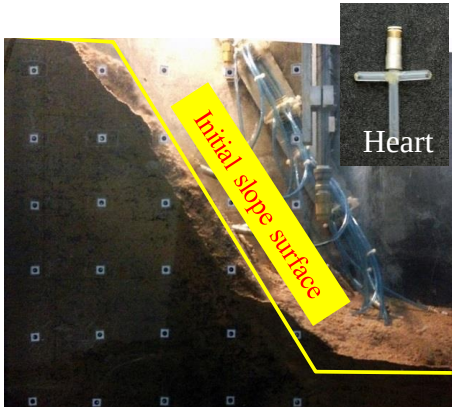

(c)

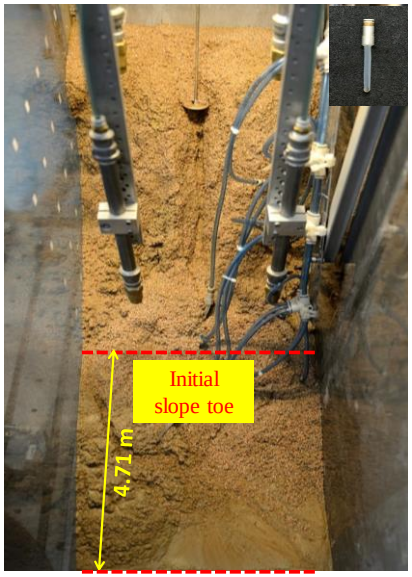

(b)

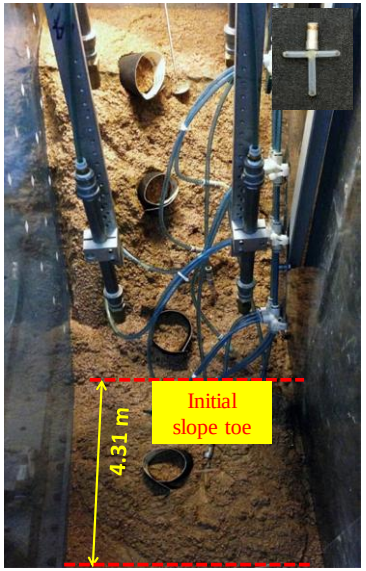

(d)

(a) Side view and (b) plan view of slope reinforced by tap-shaped roots;
(c) side view and (d) plan view of slope reinforced by heart-shaped roots

Summary of findings for (60^0 Slope)

1. Root architecture has strong influence on slope deformations and failure mechanisms
2. Relatively shallow failures occurred in vegetated slope reinforced by heart-shaped roots
3. Heart-shaped roots can minimize run-out distance than tap-shaped ones
4. Engineers should consider root architecture as well as survival rate in their designs

2019
New
book

Plant-Soil slope Interaction

Charles W. W. Ng, Anthony K. Leung & Junjun Ni

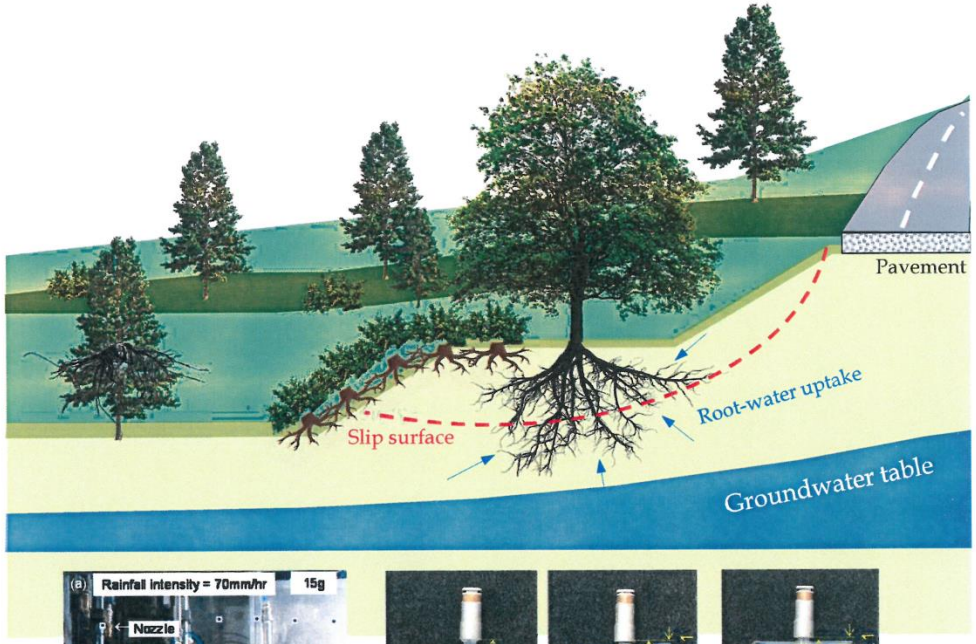

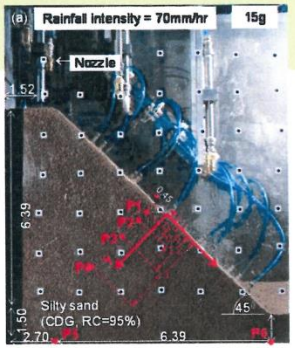

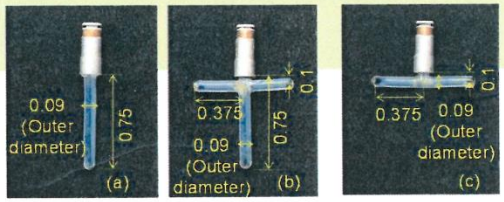

$$u_w = 10\alpha^{-1}\ln\left\{\exp\left[\alpha\left(\psi_0 - z^*\right)\right] + \frac{q_0}{k_s}\left[\exp\left(-\alpha z^*\right) - 1\right] + \frac{\alpha}{k_s\cos^2\varphi}\int_0^{L^*} G(z^*, x^*)\, S\left(\frac{x^*}{\cos\varphi}\right) \mathrm{H}\left(\frac{z^*}{\cos\varphi} - \frac{L^*}{\cos\varphi}\right) dx^*\right\}$$

Publisher: CRC Press of Taylor & Francis Group

Future Developments at HKUST

Novel and State-of-the-Art Environmental Chamber in Centrifuge

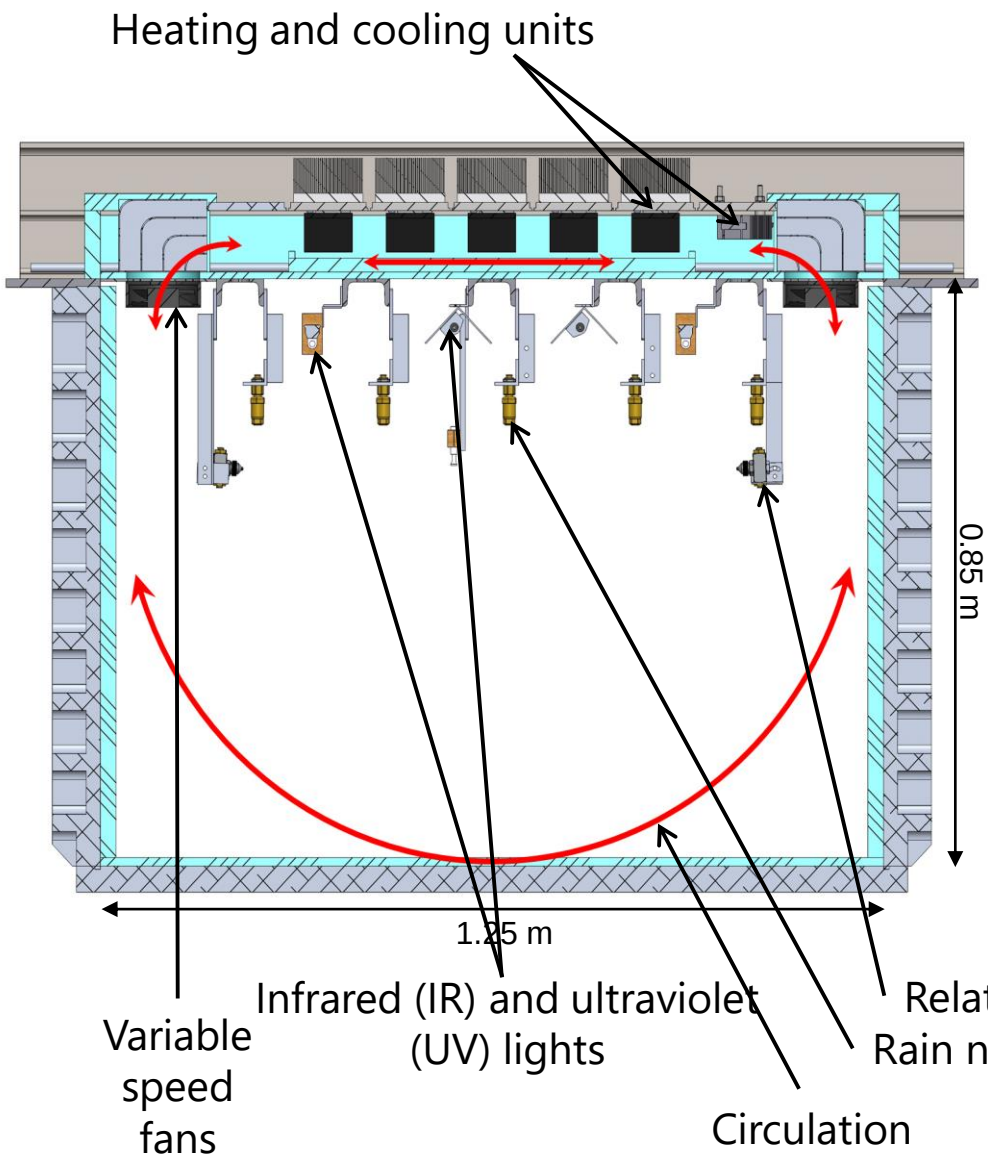

- Convection control concept (Tristancho *et al*. 2012)
- Climate factors considered (separate control):
  1) Relative humidity (30 - 100% model)
  2) Temperature (18 - 60°C model)
  3) Rainfall (5 - 100mm/h prototype)
  4) Variable wind (0.2 – 7 m/s prototype)
  5) Radiation (300 – 1400 W/m^2 model)
- Circulation in two directions – enhanced temperature and relative humidity equalisation
- Can control all variables continuously in-flight

Novel and State-of-the-Art Environmental Chamber

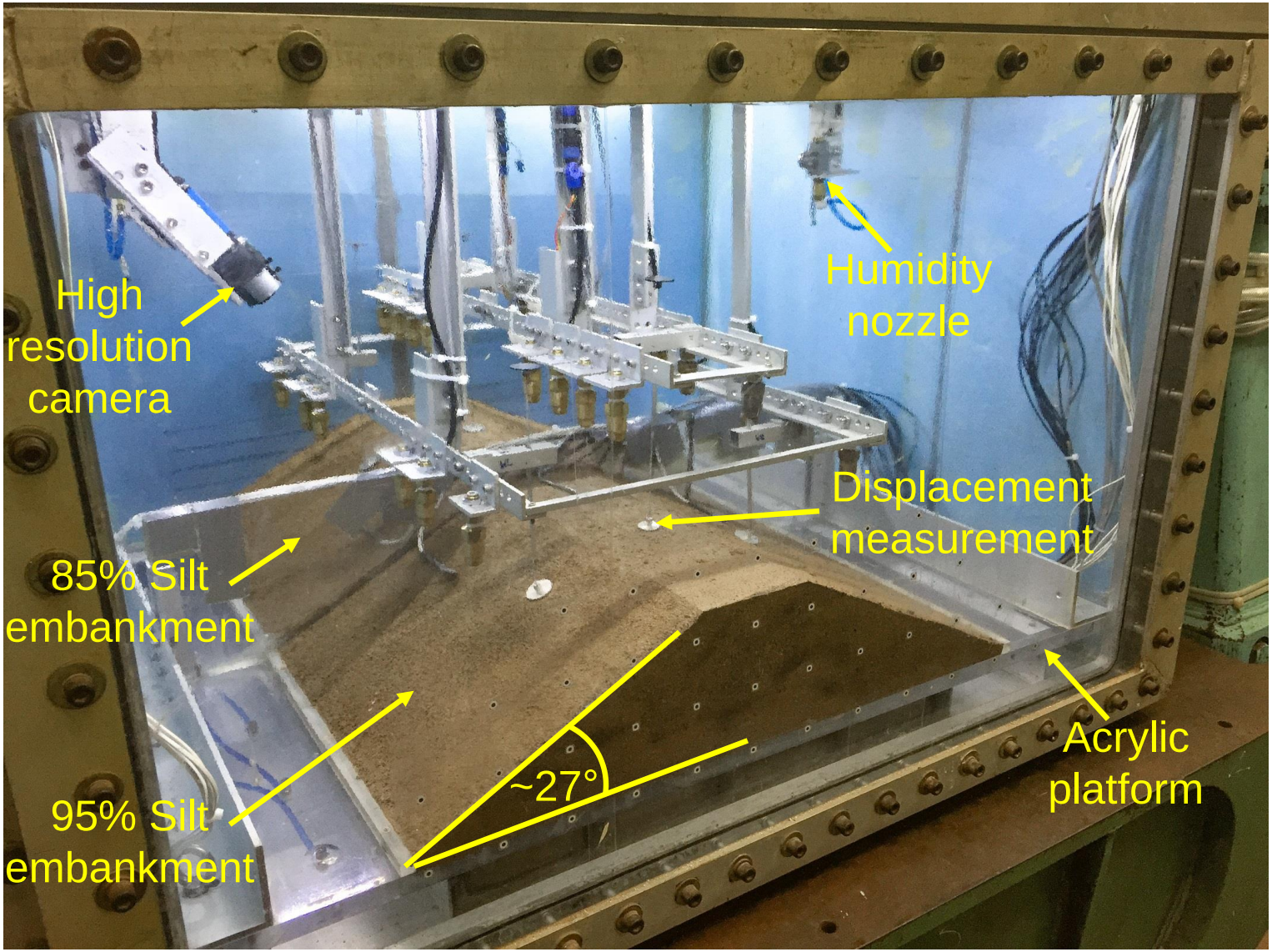

Archer, A. & Ng, C.W.W. (2018). Effects of temperature and relative humidity on a clay embankment: centrifuge modelling. *Géotechnique Letters,* 8, No. 2, 138-143.

Schematic diagram of energy harvesting chamber for centrifuge model tests

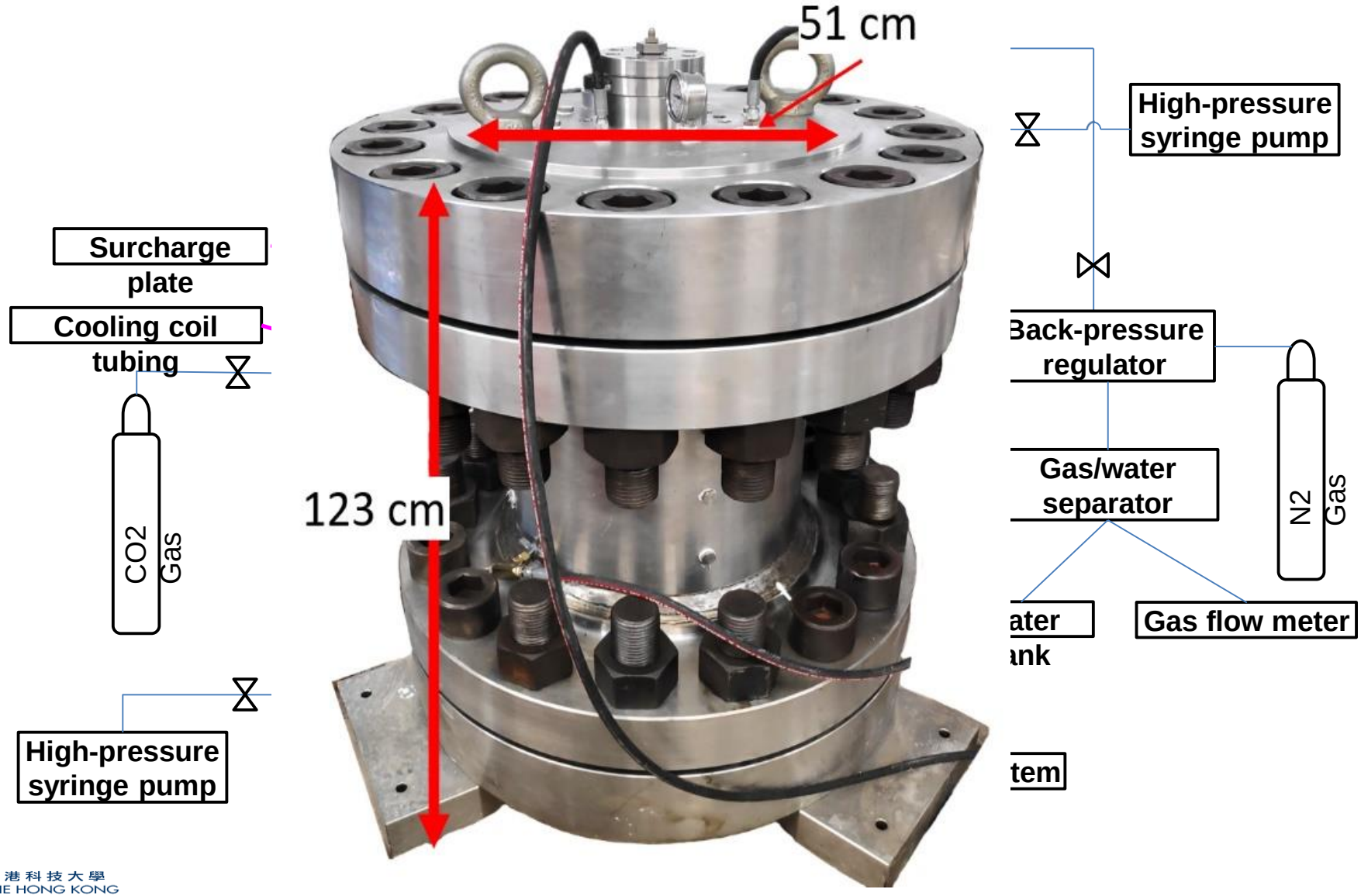

Environmental hydrodynamic wave generator

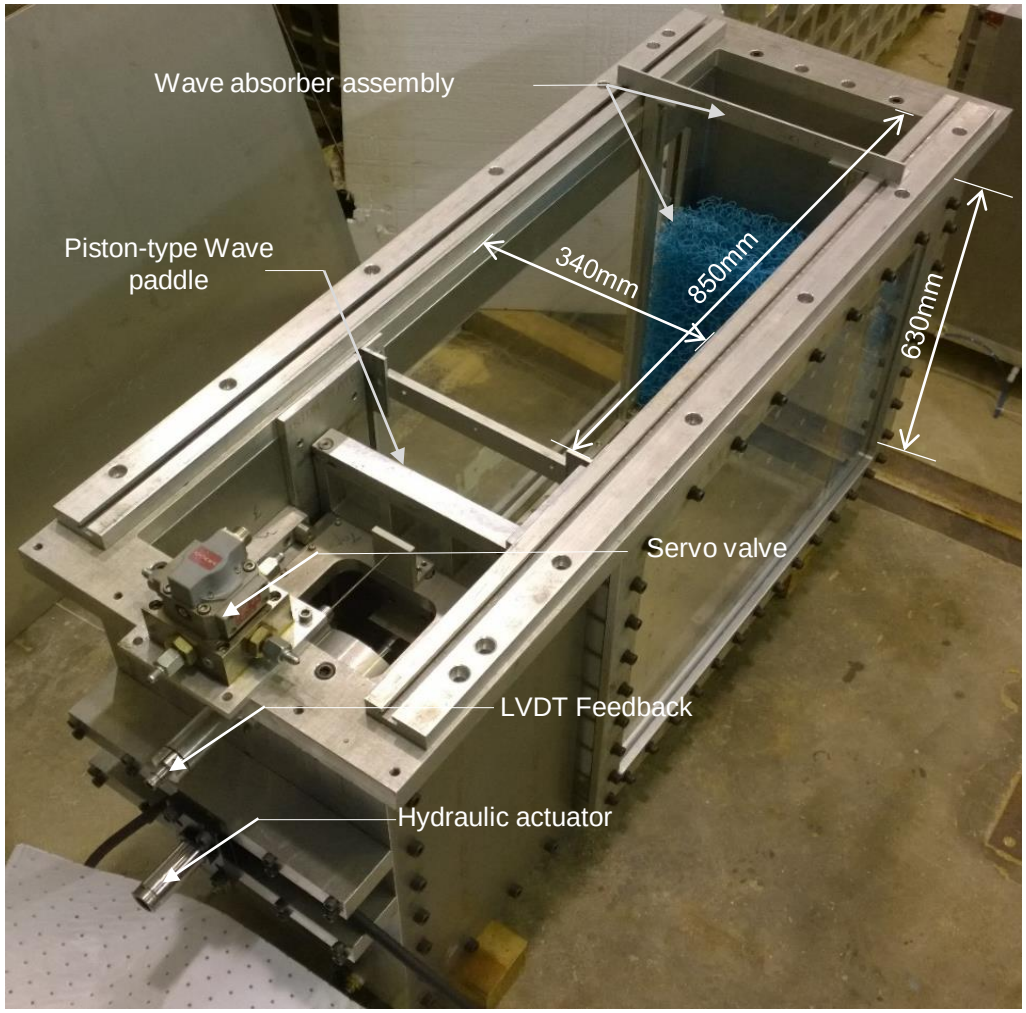

Capabilities:

1) Can produce sinusoidal and cosine waves
2) Wave frequency ranging from 1Hz to 20Hz at 50g.
3) Efficient wave absorption
4) Millions of wave cycles generated at enhanced gravity level
5) Parallel cyclic actuators aids in applying superstructure load/wind loads on model foundation

Thank You